ON IMPROVING CONTROL AND EFFICIENCY OF A PORTABLE PNEUMATICALLY POWERED ANKLE-FOOT ORTHOSIS

BY

YIFAN LI

DISSERTATION

Submitted in partial fulfillment of the requirements
for the degree of Doctor of Philosophy in Mechanical Engineering
in the Graduate College of the
University of Illinois at Urbana-Champaign, 2013

Urbana, Illinois

Doctoral Committee:

Associate Professor Elizabeth Hsiao-Wecksler, Chair
Associate Professor Timothy Bretl
Professor Andrew Alleyne
Professor William Durfee, University of Minnesota

ABSTRACT

Ankle foot orthoses (AFOs) are widely used as assistive and/or rehabilitation devices to correct gait of people with lower leg neuromuscular dysfunction and muscle weakness. An AFO is an external device worn on the lower leg and foot that provides mechanical assistance at the ankle joint. Active AFOs are powered devices that provide assistive torque at the ankle joint. We have previously developed the Portable Powered Ankle-Foot Orthosis (PPAFO), which uses pneumatic power via compressed CO_2 to provide untethered ankle torque assistance. My dissertation work focused on the development of control strategies for the PPAFO that are robust, applicable to different gait patterns, functional in different gait modes, and energy efficient. Three studies addressing these topics are presented in this dissertation: (1) estimation of the system state during the gait cycle for actuation control; (2) gait mode recognition and control (e.g., stair and ramp descent/ascent); and (3) system analysis and improvement of pneumatic energy efficiency.

Study 1 presents the work on estimating the gait state for powered AFO control. The proposed scheme is a state estimator that reliably detects gait events while using only a limited array of sensor data (ankle angle and contact forces at the toe and heel). Our approach uses cross-correlation between a window of past measurements and a learned model to estimate the configuration of the human walker, and detects gait events based on this estimate. The proposed state estimator was experimentally validated on five healthy subjects and with one subject that had neuromuscular impairment. The results highlight that this new approach reduced the root-mean-square error by up to 40% for the impaired subject and up to 49% for the healthy subjects compared to a simplistic

direct event controller. Moreover, this approach was robust to perturbations due to changes in walking speed and control actuation.

Study 2 proposed a gait mode recognition and control solution to identify a change in walking environment such as stair and ramp ascent/descent. Since portability is a key to the success of the PPAFO as a gait assist device, it is critical to recognize and control for multiple gait modes (i.e., level walking, stair ascent/descent and ramp ascent/descent). While manual mode switching is implemented on most devices, we propose an automatic gait mode recognition scheme by tracking the 3D position of the PPAFO from an inertial measurement unit (IMU). Experimental results indicate that the controller was able to identify the position, orientation and gait mode in real time, and properly control the actuation. The overall recognition success rate was over 97%.

Study 3 addressed improving operational runtime by analyzing the system efficiency and proposing an energy harvesting and recycling scheme to save fuel. Through a systematic analysis, the overall system efficiency was determined by deriving both the system operational efficiency and the system component efficiency. An improved pneumatic operation utilized an accumulator to harvest and then recycle the exhaust energy from a previous actuation to power the subsequent actuation. The overall system efficiency was improved from 20.5% to 29.7%, a fuel savings of 31%. Work losses across pneumatic components and solutions to improve them were quantified and discussed.

Future work including reducing delay in recognition, exploring faulty recognition, additional options for harvesting human energy, and learning control were proposed.

To Father and Mother

ACKNOWLEDGEMENTS

This dissertation could not have been completed without generous help from all my friends, colleagues and family members. I am very grateful and thankful for all of you. It is because of your company that my long Ph.D journey has become a memorable chapter in my life.

First and foremost, I would like to express my immense gratitude to my advisor, Prof. Elizabeth Hsiao-Wecksler for bringing me into the intriguing world of Biomechanics, and giving me the freedom to pursue the research that aligned with my interests. She also taught me the importance of systematically conveying an idea, which has had a huge impact on my approach to communicating information. I have always been impressed by her perfectionism and learned through our work together to appreciate the details of my research (even the very small ones). I also want to thank my committee members, Prof. William Durfee, Prof. Andrew Alleyne and Prof. Timothy Bretl for the tremendous help I received during the development of the ideas for my dissertation.

I would really like to thank my HDCL lab mates for their support. Many of them volunteered to be my test subjects and sacrificed their nights and weekends to help me. Some of the best ideas in my dissertation also came from the inspiring conversations I had with all of you Thank you Alex, Louis, Matt, Morgan, Richard, Michael, Iris, Mazhar and Mike.

I would also like to thank all my collaborators: Dan Block, Prof. Young-Hui Chang, Megan Toney, and Jasper Yen from the Comparative Neuromechanics Laboratory at Georgia Tech, Megan Hodgson from Johns Hopkins University, and Jicheng Xia from University of Minnesota.

It was not by chance that I became an engineer. My father, an electrical engineer, worked with me to write my first line of code in BASIC when I was six years old. My mother, a biology professor, taught me how to read and write in English at the age of seven. I love them and am forever indebted to them. Thank you both.

Finally, I am very thankful to my fiancé Jingwei - the best thing that could have ever happen in my life. I met her the week I started my Ph.D, proposed to her as I was completing my proposal for this dissertation, and will marry her in a few weeks after I warp up my Ph.D. Without her support, I would not have been able to accomplish what I did.

This work was supported by the NSF Engineering Research Center for Compact and Efficient Fluid Power grant #0540834, NSF CAREER grant #0955088, and NSF Computer and Network Systems grant #0931871.

TABLE OF CONTENTS

Chapter 1 Introduction 1

Abstract 1

1.1 Motivation 2

1.2 State-of-The-Art Technologies For Human Assist Devices 5

1.2.1 Actuation System Design 6

1.2.2 Gait State Estimation and Terrain Recognition 15

1.2.3 Motion Control Policy Design 18

1.2.4 Energy Harvesting and Redistribution Design 21

1.2.5 Muscle Activation (EMG) Based Solutions 23

1.3 Introduction of the PPAFO 23

1.4 Motivation for Proposed Studies 26

Chapter 2 Estimating System State During Human Walking For a Powered Ankle-Foot Orthosis 29

Abstract 29

2.1 Introduction 30

2.2 Methods 34

2.2.1 Powered Orthosis System 35

2.2.2 Experimental Setup and Pre-Test Procedures 36

2.2.3 Training Data for Estimation Models 37

2.2.4 Experimental Testing Procedure 42

2.2.5 Estimation Comparison Metrics 45

2.3 State Estimation Techniques 46

2.3.1 Estimate Based on Cross-Correlation (CC) 46

2.3.2 Estimate Based on Fractional Time (FT) 47

2.3.3 Estimate Based on *k*-Nearest Neighbor (*k*NN) 48

2.3.4 Reference Estimate (λ^*) 48

2.4 Results 50

2.5 Discussion 55

2.5.1 Performance During Healthy Unperturbed Gait 55

2.5.2 Robustness To Speed and Actuation Disturbances 55

2.5.3 Applications to Control 58
2.5.4 Current Limitations 59
2.6 Conclusion 60
Chapter 3 Gait Mode Recognition and Control for a Portable-Powered Ankle-Foot Orthosis 61
Abstract 61
3.1 Introduction 62
3.2 Methods 66
3.2.1 Ankle Dynamics for Stair Walking Activities 66
3.2.2 Introduction of the PPAFO 67
3.2.3 Current Control Scheme for Level Ground Walking 69
3.2.4 Tracking Motion using an IMU 70
3.2.5 Estimating Orientation 71
3.2.6 Estimating Position 72
3.2.7 Recognizing Stair and Ramp Modes 74
3.2.8 The Optimal Thresholds for Unbiased Recognition 75
3.2.9 Actuation Control for Stair Descent Mode 78
3.2.10 Experimental Protocol 78
3.3 Results and Discussion 80
3.3.1 Experimental Observations 80
3.3.2 Limitations 84
3.4 Summary 90
Chapter 4 System Efficiency Analysis and Energy Recycling of A Portable Pneumatically Powered Ankle-Foot Orthosis 91
Abstract 91
4.1 Introduction 92
4.2 Methods 94
4.2.1 System Description 94
4.2.2 Overall System Efficiency 98
4.2.3 Operational Efficiency 99
4.2.4 Component Efficiency 115
4.2.5 Overall System Efficiency Calculation 119
4.2.6 Calculation of Work Loss Across Different Components 119
4.2.7 Experimental Procedure 125

4.3 Results 126
4.3.1 Fuel Savings and Work Output 126
4.3.2 Operational Efficiency and Component Efficiency 128
4.3.3 Work Losses Breakdown on Components 129
4.4 Discussion 131
4.4.1 Operational Efficiency 131
4.4.2 Fuel Consumption 133
4.4.3 Component Efficiency 134
4.5 Conclusion 135
Chapter 5 Conclusions and Future Work 136
5.1 Gait State Estimation and Actuation Control (Chapter 2) 136
5.1.1 Learning Control 136
5.1.2 Stability Analysis 138
5.2 Gait Mode Recognition (Chapter 3) 139
5.2.1 Reducing the delay in recognition 139
5.2.2 Exploring Faulty Recognition 141
5.3 Energy Efficiency Analysis and Energy Harvesting (Chapter 4) 144
5.3.1 Harvesting Human Energy 144
References 146

Chapter 1 INTRODUCTION

ABSTRACT

Ankle foot orthoses (AFOs) are widely used as assistive/rehabilitation devices to correct gait of people with lower leg neuromuscular dysfunction and muscle weakness. An AFO is essentially an external device worn on the lower leg and foot that provides mechanical assistance at the ankle joint. Active AFOs are powered devices that provide assistive torque at the ankle joint. We have developed on such a device, the portable powered ankle-foot orthosis (PPAFO), which uses a pneumatic rotary actuator powered by compressed CO_2 to provide untethered assistance. My dissertation work is focused on the development of control strategies for the PPAFO that is energy efficient, robust, applicable to different patient groups, and functional in different gait modes. Three studies on this topic will be presented in the dissertation proposal: (1) Estimating of the system state during the gait cycle for actuation control; (2) Gait mode recognition and control (e.g., stair and ramp descent/ascent); (3) Analysis of the PPAFO system efficiency and improved system efficiency through the recycling the exhaust gas from the actuator. This introductory chapter consists of: motivation for this work, a literature review of the state-of-the-art technologies for human assist devices, an introduction to the PPAFO that was previously developed, and an overview of the studies in this dissertation.

1.1 MOTIVATION

Walking is a fundamental part of people's daily routine and an essential component in overall quality of life. Gait can be affected by symptoms resulting from numerous neurological disorders, muscular pathologies and injuries, including trauma, incomplete spinal cord injuries, stroke, multiple sclerosis, muscular dystrophies and cerebral palsy [1]. Powered lower-limb orthoses (e.g. robotic exoskeletons) can be used to assist everyday walking activities, as well as gait rehabilitation therapy. There are several large populations with neuromuscular impairments that can be treated using a powered lower-limb orthoses in the United States alone, and include: stroke (4.7M), polio (1M), multiple sclerosis (400K), spinal cord injury (200K), and cerebral palsy (100K) [2]. As the global population ages, all of the aforementioned populations will continue to grow. This trend is compounded in the US by the baby boomers reaching retirement age. In Japan, it was estimated that 1 in 5 men and women of middle age will experience stroke in their remaining lifetime [3]. Therefore, it is important to develop intelligent, energy efficient and affordable lower-limb orthoses to serve this growing need.

Gait can be divided into multiple phases, in which the ankle dynamics can be described (Figure 1, top). The gait cycle begins with initial contact phase (0 - 20% GC), when the foot strikes the ground (heel strike) and the dorsiflexor muscles decelerate the foot to the ground. No significant ankle torque is needed during the second phase, loading response (20% - 35% GC). The third phase, forward propulsion, occurs during the middle and late stance phase (35% - 60% GC), when the body is propelled forward by the plantarflexor muscles and the leg is accelerated into swing. The fourth phase is limb advancement (60% - 100% GC), in which the foot is advanced to the next

heel strike. We chose the ankle-foot complex as the starting point for powered orthosis development because this complex's muscle-tendons generate half of the power used in normal walking [4, 5], and being able to restore ankle functions is a key to the success of fully restoring gait.

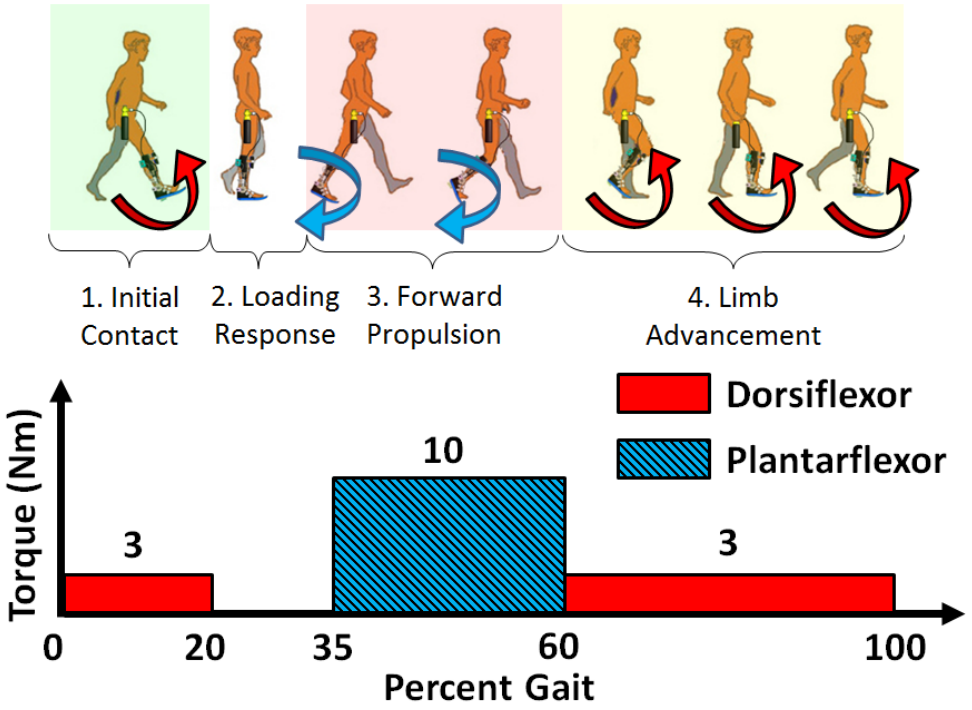

Figure 1 Different phases of a gait cycle (starting with the right heel striking the ground and continuing to the next heel strike) and the needed torque from the ankle joint (red for dorsiflexor direction and blue for plantarflexor direction). The bar plot indicated the assistive torque by the PPAFO in a gait cycle [6].

The required torque at the ankle for these different phases also varies: in initial contact and swing, the ankle generates no more than 5 Nm in dorsiflexion direction, while during forward propulsion phase, the plantarflexor muscles can generate peak torques of up to 100 Nm [1] in plantarflexion.

In this study, due to the limited torque that our actuation system can provide, only partial functional ankle torque could be restored, e.g., 10 Nm (Figure 1, bottom).

Currently, all commercially available AFOs are passive, which are essentially mechanical joints used for motion control without external power input. They can limit the range of motion in phase 1 and phase 4 to prevent foot drop for people with weak dorsiflexors. Passive AFOs have the advantage of low cost and mechanical simplicity [6-15]. However, passive AFOs cannot provide torque assistance during phase 3, where substantial assistive torque is needed. Additionally, the control of passive AFOs is based on the activation of springs in an open loop, in which the robustness and reliability cannot be guaranteed. Due to the inability of passive AFOs to recognize and adapt to the environment and changes in gait, these AFOs usually provide the same type of assistance regardless of functional need.

Alternatively, semi-active AFOs can take advantage of real-time microcontrollers to collect sensor information and determine gait phases (also defined as states) to provide variable assistance. Semi-active AFOs commonly include magneto rheological (MR) dampers [16-18]. The MR dampers are filled with variable-viscosity fluid that is modulated using an electric current. Force and angle sensors are used to determine the state of the system to determine the functional requirement of the user. Depending on the identified state, the damping is used to either decelerate the foot to the ground, or fully restrict the motion of the foot during swing to prevent foot drop. However, while semi-active AFOs are able to adapt to changes of gait and functional needs, they still lack the ability to provide assistive torque to help propulsion.

1.2 State-of-The-Art Technologies For Human Assist Devices

Active AFOs (also referred as powered AFOs) are real-time computer-controlled robotic exoskeletons that have various types of embedded sensors to determine proper actuation control. They combine the advantages of quick gait change adaptation and the ability to provide partial or full assistive torque to meet the functional needs of gait. Because gait itself is not an energy neutral process, an external power source is needed for an active AFO. Currently, almost all active AFOs require a tethered power supply due to the large amount of energy needed by the active AFOs to provide an extended period of actuation [17, 19-21].

In the rest of this section, existing state-of-the-art technologies on powered AFOs will be reviewed and discussed. Additionally, related topics in lower limb and ankle prosthesis design are also reviewed due to the great level of similarities between the design principles of these powered orthoses and prostheses. While the mechanical structure and actuator design of prosthetic devices differs significantly from orthotic devices due to different space and weight constraints, the state estimation, gait recognition and energy harvesting during gait for the two types of devices follow the same guidelines.

Five main topics are be discussed below: actuation, gait recognition, control, energy harvesting, and control based on muscle activation. In the actuation section, where design principles are significantly different between orthoses and prostheses due to space and weight constraints, the

two types of devices will be discussed separately. For the other four topics, their technologies will be discussed together due to the great similarities that they share.

1.2.1 Actuation System Design

Both ankle orthoses and prostheses use actuators to provide assistive torque at the ankle joint. Most existing active orthoses are tethered to a fixed power source due to the high energy consumption of powered assistance. In summary, two types of actuation technologies are utilized to provide actuation: electrical actuators and pneumatic actuators.

1.2.1.1 Electrical Actuators

The most common solution for electrical actuator based actuation is the Series Elastic Actuator (SEA) [19, 22, 23]. It consists of a DC motor powered lead screw mechanism in series with a helical spring. The compliance of the actuator can be adjusted by the computer driven lead screw which varies the length of the spring. The addition of the spring in the actuator allows for better shock absorption, lower reflected inertia, and enhanced force control and torque redistribution within a gait cycle. Compared to direct drive systems, the backdrivability of the SEA significantly improves compliance for locomotion.

1) Actuation System Design for Orthoses

Conventionally, active AFOs use SEA because of its easy impedance modulation and compliance to human dynamics: Blaya and Herr at MIT used a SEA actuator (Figure 2, [19]). The force was modulated by controlling how much the spring was compressed. It had the advantages of low impedance, isolation from motor and shock loads, backlash, and torque ripple. Additionally, the friction was filtered by the spring[19]. Hogan et al. also at MIT developed the Anklebot, using two low impedance brushless DC motors and linear screws without springs to provide backdrivable actuation for rehabilitation (Figure 3). In contrast to most of the orthoses with only one degree-of-freedom in the sagittal plane, the MIT Anklebot can actuate in both sagittal and frontal planes with two DOFs (25˚ dorsiflexion, 45˚ plantarflexion, 25˚ inversion and 20˚ eversion [24, 25]). The Anklebot was able to deliver up to 23 Nm of torque.

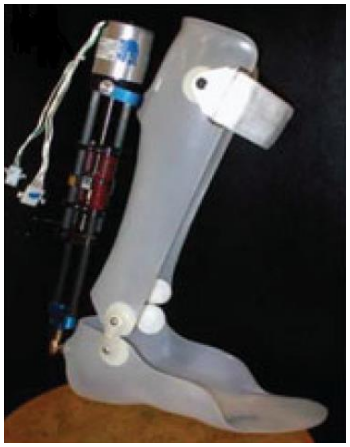

Figure 2 The MIT active AFO (AAFO) using SEA to provide assistive torque at ankle [19]

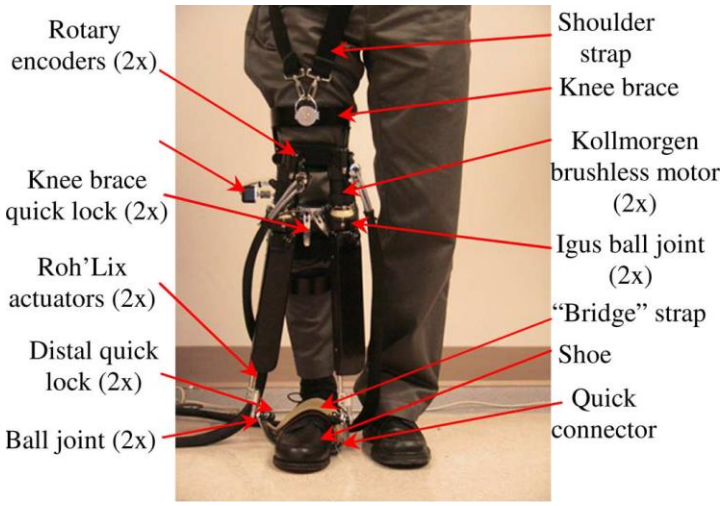

Figure 3 MIT's Anklebot with two degrees of freedom, driven by two DC motors [24]

A variation of the electrical actuator proposed by Sugar et al. at Arizona State University utilizes robotic tendons to achieve the same functionality as the series elastic actuator (Figure 4, [26-29]). The dynamically tuned spring in the robotic tendon system significantly reduced the overall peak power of the system [30]. The increased compliance has the benefits of added safety, increased flexibility to adapt to environment changes, and a reduction to the overall torque output requirement. Recently, they were able to show performance improvements including gait speed, maximum ankle moment and peak power with stroke survivors [31]. It was able to generate up to 60 Nm of peak torque.

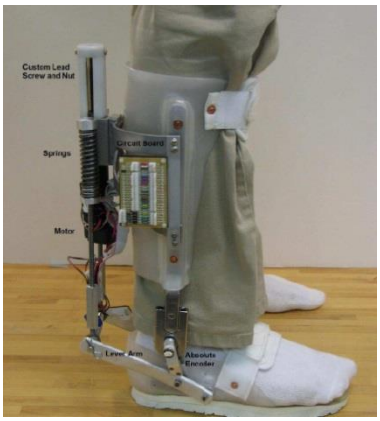

Figure 4 Powered AFO by Sugar et al. with robotic tendon assistive torque at ankle [30]

2) Actuation System Design for Prostheses

One main drawback of the electrical SEA on orthoses is its added size and weight. As a result of its mechanical transmission design, the entire assembly (actuator, lead screw and spring) adds significant weight and packaging size to the orthoses at the ankle joint, which is very undesirable. In contrast, pneumatic systems enjoy the benefit of not needing a transmission nor a spring, which simplifies the system structure and reduces the system weight. Xia and Durfee have demonstrated that high pressure fluid power system (hydraulic) can have advantages over electrical-mechanical systems [32].

However, this size and weight issue is much better tolerated in the design for prostheses, as the mechanism is filling in the missing space and weight for the missing limb. Consequently, SEA can have better applications in prostheses.

Sugar et al. also used their robotic tendon technology to develop the SPARKy ankle prosthesis (transtibial) with two actuated degrees of freedom (plantarflexion/dorsiflexion, inversion/eversion) using regenerative kinetics [33, 34]. Helical springs were used for added compliance (Figure 5). It was able to provide up to 30 Nm of torque at the ankle joint.

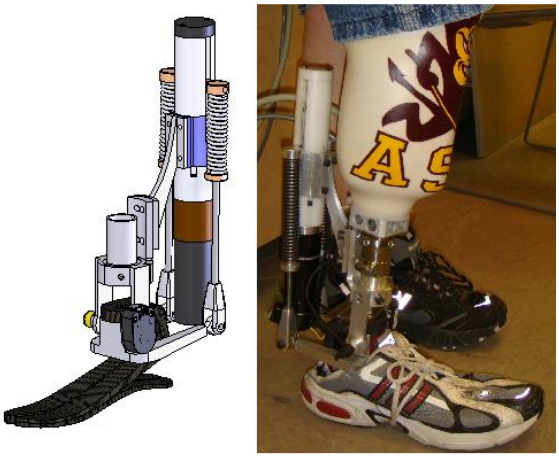

Figure 5 SPARKy 3: two DOF robotic ankle prosthesis with regenerative kinetics [35]

Goldfarb et al. at Vanderbilt University developed a self-contained powered knee and ankle (transfemoral) prosthesis using SEA ([36], Figure 6). The prosthesis was capable of 120˚ of flexion at the knee and 35˚ of plantarflexion and 20˚ of dorsiflexion at the ankle. The motion was strictly limited to the sagittal plane. The peak torque from this actuator was about 119 Nm.

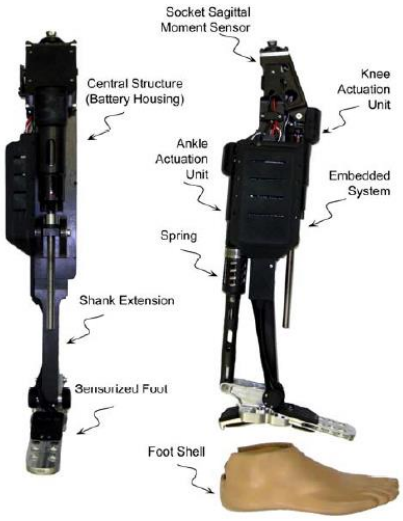

Figure 6 Vanderbilt transfemoral prosthesis [37]

While most researchers use simple series structured SEA actuator, Rahman et al. at Nanyang Technological University had made the effort to build a two-stage SEA actuator, where both linear and torsional springs were used to further increase the compliance of the actuator to human motion on an ankle-foot prosthesis [38], Figure 7. It could generate 60 Nm of torque. As a result, it was able to produce variable impedance based on force ranges without requiring a change in hardware, which may enhance human-friendliness in human assist device applications. Eicholtz et al. at Carnegie Mellon University used a similar cable-transmission-spring structure to achieve impedance control and torque profile tracking (peak torque of 45 Nm) on an AFO [39], Figure 8.

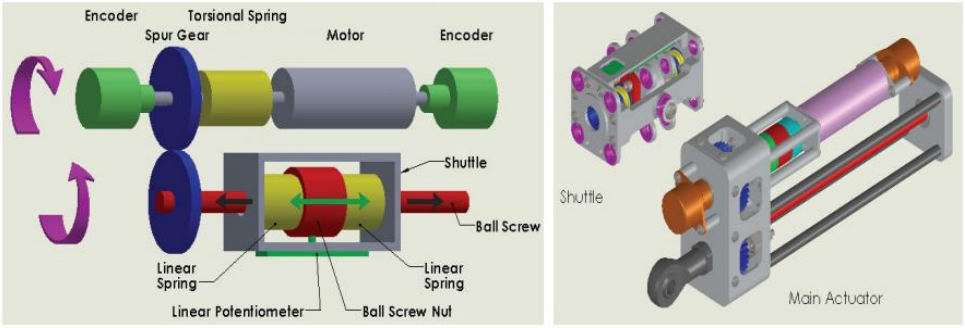

Figure 7 Rahman et al.'s design of an actuator with combined linear and torsional springs[38]

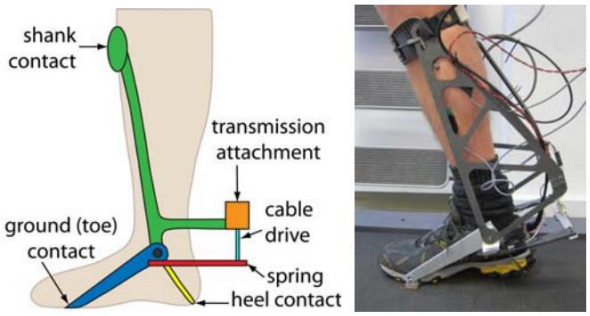

Figure 8 Eicholtz et al.'s cable-transmission-spring structure for ankle impedance control[39]

1.2.1.2 Pneumatic Actuator

Pneumatic alternative solutions for orthotic/prosthetic actuation enjoy advantages over electrical systems such as inherit compliance and backdrivability, no need for a transmission, as well as compact and light-weight actuation assembly (no transmission and series spring needed).

Ferris et al. at the University of Michigan used a set of McKibben style uni-axial artificial pneumatic muscles to generate sagittal plane torque (Figure 9, [40-43]). The use of pneumatic muscles allowed for enhanced compliance, with a peak plantarflexor torque of up to 70 Nm and a peak dorsiflexor torque of up to 38 Nm. Because the McKibben muscles were only capable of generating tension, two pneumatic muscles with different lengths and diameters were chosen to accommodate torque and range of motion requirements in opposite direction of actuations.

Figure 9 Ferris et al's ankle-foot orthosis with artificial pneumatic muscles [44]

Goldfarb et al. also explored the application of a pneumatic cylinder on a transfemoral prosthesis [37]. This pneumatic cylinder replaced the SEA while the rest of the prosthesis design was similar to [36], Figure 6. The resulting design demonstrated the ability to provide requisite joint torque with a minimum volume actuator configuration.

In conclusion, the DC motor based electrical actuators have broad applications in prostheses, but were limited by the size and weight (>2 kg, without batteries) constraints in orthoses design. Pneumatic technologies have promising potentials due to the attractive characteristics such as light weight actuation assembly and compliance to human motion. However, currently all pneumatic applications are limited to linear actuators (cylinders or McKibben muscles [44]), which require further mechanisms for rotary actuation at the ankle joint. The exploration of pneumatic rotary actuators are warranted to pursue the possibilities of a simplified orthosis design.

1.2.1.3 Functional Electrical Stimulation for Actuation

Functional Electrical Stimulation (FES), which uses an electric current to stimulate neuromuscular structures, has been used in conjunction with passive orthoses to assist with gait (e.g., [45-50]). Paralyzed muscles can be reactivated to provide active torque. Passive orthoses are used to stabilize the whole system. Since there is no actuator and power supply needed, significant size and weight reduction is made possible for this hybrid system.

While some believe muscle activation based control schemes are the ultimate solutions for prosthetic/orthotic control, currently these technologies suffer from limited signal-to-noise ratio, significant cross-talk, and intrusiveness to the human body.

1.2.2 Gait State Estimation and Terrain Recognition

Controlling lower-limb powered orthoses and prostheses is a challenging task because the functional needs at different phases of gait are different. A simplistic approach of tracking position or force profiles throughout a gait cycle offers limited help, as it does not account for the specific dynamic situation in each particular phase of gait. For example, simply tracking position during heel strike is undesirable because it is more important to provide impedance at this stage. One major benefit of a computer-controlled powered prosthesis or orthosis could be its ability to collect sensor information and make prompt control decisions in real time, such that the actuation control policies can be designed to accommodate the changes and satisfy the functional needs for the specific conditions. The effort in sensing and adapting to the functional needs to control the actuation can be categorized as follows.

1.2.2.1 Finite State Estimation

Finite state based control schemes have been used widely in the control of both orthoses and prostheses due to its flexibility and robustness [19, 26, 27, 35, 51]. In this scheme, a gait cycle can be divided into several states (typically four, and generally not more than seven), such as 'initial contact', 'terminal stance', 'swing', etc., depending on the specific tasks defined to be associated with each state. For example, Sugar et al. defined seven states in the actuation cycle, and MIT's Anklebot had four states for different functional tasks [25, 33, 35, 52-54].

In a finite state scheme, the system state was identified by examining the measurement from one or more sensors (force, angle, etc.). Once the state was determined, a control task was associated with the state to control the motion. For example, position control was frequently used for swing phase toe clearance and impedance control was often preferred for initial contact landing [30, 31, 35, 55, 56]. The choices of functional tasks and control policy will be further discussed in the following 'Motion Control Policy Design' section (1.2.3).

In conclusion, the finite state scheme gained popularity because it acknowledged and addressed different functional needs in different gait phases, while allowing for user's flexibility. The main drawbacks of this scheme are lack of universal definition of state and a universal means to identify them. These shortcomings limit the performance of devices when gait patterns vary significantly from normative or expected movement behaviors.

1.2.2.2 Model Based State Estimation

Eilenberg et al. [57] proposed a control algorithm of a powered ankle-foot prosthesis based on the neuromuscular model of a Hill-type plantarflexor actuator and a spring-damper dorsiflexor actuator. The assistive torque was controlled in a feedback loop with added adjustment from a real-time neuromuscular model simulation. The study was able to demonstrate the adaptation of actuation control on different speeds and slopes, without the difficulties of sensing the slope [58, 59]. The predicted muscle activation patterns could then be used to determine the control of the ankle-foot prosthesis.

A Gaussian process based human dynamical model was proposed by Wang et al. [60] to use small data sets (1-4 cycles of full body motion) to estimate with low dimensionality different full body movement kinematics (gait cycle or golf swing). These predictions were based data from on a high dimensional 50-DOF model of the human body derived from motion capture data. The approach provided the foundation to use a limited sensor array and a human dynamic model to estimate human kinematic parameters that were not directly measureable. This algorithm could be generalized for prostheses and orthoses, where the overall system state could be estimated from limited sensing information and used to control actuation.

These model-based state estimation schemes have limited applicability because they are computationally expensive and required different neuromuscular or dynamic models for different patient populations.

1.2.2.3 Automated Terrain (or Mode) Recognition

Most powered orthotic/prosthetic designs have focused on level ground walking; however, in order to make a portable assist device that can be used in different walking environments, the device must be able to recognize non-level terrains such as stairs and ramps.

The Goldfarb group's transfemoral prosthesis was equipped with an intent recognition algorithm based on data from mechanical sensors mounted on the powered prosthesis [61]. The intent recognition controller can recognize gait initiation, termination, and transitions between sitting, standing and level ground walking with 100% accuracy. However, it suffered from long delays

(up to 0.5s) when trying to identify other terrains. Further, these modes are limited to sitting, standing and walking. The limited types of recognizable modes were results of limited mechanical sensing information.

Yoon et al. at Gyeongsan National University developed a 6-DOF gait rehabilitation robot, that was capable of real-time updating of walking velocity and could navigate through different terrains in virtual environments [62]. An adaptive learning law was implemented to keep updating the walking velocity as it changed over time. However, it is not known how this device would work in the real world.

In conclusion, there are no reliable terrain recognition schemes that can recognize all types of terrains and gait modes with high reliability.

1.2.3 Motion Control Policy Design

Finite state control and terrain recognition are considered 'high-level' control, in which the type of controller was chosen and the state was identified. Additionally, in each of the identified states, 'low-level' controllers are needed to accomplish the specific motion tasks associated in each of the scenario (e.g., impedance or position control). In the following section, different techniques used for low level motion control will be discussed.

One conventional solution for prosthetic leg control is called 'echo control' or 'master-slave control' [63], in which the prosthetic leg repeated the motion of the sound leg with an appropriate

phase shift. Another approach is ‘stance control’, which locked the knee joint during stance [64] to provide joint stability and let it free during other phases. These simple solutions enjoyed the benefit of easy implementation and robust stability, but suffered from lack of applicability for bilateral amputees, being able to adapt to a changing environment quickly, and not being applicable for all types of targeted populations.

1.2.3.1 Control by Impedance Modulation

For electrical actuators, impedance modulation was crucial to the success of an actuation scheme. MIT’s Anklebot introduced an adaptive algorithm that was able to adjust the parameters on-the-fly, to account for varying walking speeds [24, 25, 65]. Hollander et al.’s ankle-foot orthosis had a two-level control strategy: actuator lever control and ball screw nut control [26]. To further improve the system performance, a robust control scheme was applied for impedance modulation. Those impedance control techniques demonstrated success in resisting motion in some gait states, but could not be applied when assistive torque was needed [26].

1.2.3.2 Control by Optimizing a Cost Function

An alternative approach to modulating the impedance is to optimize a cost function (e.g., position tracking or velocity tracking). A main drawback of using a single metric as the cost function can be lack of ability to accommodate different types of functional needs in different gait phases. HosseinNia et al. implemented a cost function that incorporated both the patient’s muscle power (Illiopsoas, Rectus Femoris, Glutei, Hamstrings, Vasti, Gastrocnemius, Tibialis Anterior and

Soleus) and the error of the angle tracking [66]. This combined cost function allowed for a uniform cost function across different gait phases. Similarly, Zhang et al. combined the LOKOMAT driven-gait robotic hip and knee orthosis with the OpenSim system to compute inverse kinematics, and used gait coordination and real-time gait symmetry as the metric to evaluate for the effectiveness of the LOKOMAT [67].

Other researchers argued that the goal for orthotic/prosthetic control should be minimizing the energy cost of the human during walking. Bregman et al. examined energy cost in a simulation, and varied ankle stiffness [68]. Another study by Wiggins et al. evaluated the metabolic cost and mechanical demands during walking, when the ankle was either locked or let free [69]. These studies provided insight on how assistance at the ankle should be provided if the goal was to optimize the overall energy cost of walking.

Control based on a cost function has the benefit of uniform solution, but is limited by the choice of the cost function that could precisely represent the control objective the device.

1.2.3.3 Learning Control

Learning control has been widely used in the control of manufacturing processes, where a certain motion must be repeated many times [70]. The learning controller learns from past cycles and can apply a feed-forward signal to improve system performance over time. Yang et al. proposed a human-like adaptive learning controller to learn from human gait past performance and make anticipatory compensations in the future. Their learning controller had the unique feature of being

able to deal with unstable situations, by guaranteeing a desirable stability margin [71]. While a learning controller is a great addition to existing control architecture, it cannot operate on its own due to its lack of ability to address uncertainty and unexpected disturbance.

1.2.4 Energy Harvesting and Redistribution Design

The applications for harvesting energy in orthotic or prosthetic control can be categorized into harvesting energy from human gait and regenerating energy from actuations. Existing work mainly focus on the first application.

Human gait in level ground walking is a nearly energy neutral process [72], in the sense that there are no significant differences between total potential and kinetic energy changes. The net work output from the human is turned into heat and dissipated over an extended period of time (as a result, we sweat a lot when we walking or run fast). Although peak force and power provided by the human locomotion system are tremendous, energy is balanced by the efficient energy harvesting system of our bodies, thanks to our ligaments, muscles, and tendons.

The goal of harvesting energy by the body is to harvest the potential and kinetic energy from some part of gait, store it into musculoskeletal soft tissues, and put it back to other parts of gait when needed. In other words, it redistributes energy from certain phases of the gait cycle to another phase to save fuel.

Sugar et al. found that their regenerative robotic tendon AFO was capable of restoring and releasing 16 J of energy per step [73]. The elastic robotic tendon takes advantage of the uneven torque requirement within a gait cycle by harvesting ankle torque generated during mid-stance (second rocker), and uses the energy during late stance to assist plantarflexor propulsion (third rocker) [27, 30, 73].

Collins et al. designed an 'energy-neutral' system, based on the principle of Controlled Energy Storage and Release (CESR), which stores human energy into a gear-spring system, and then release it back [69, 74]. Collins and Kuo designed a CESR foot-ankle powered prosthesis [74]. By recycling the energy and put it back during the push-off phase, the metabolic cost was reduced by 9% compared to walking conventional prosthetic foot. Wiggins et al. created a CESR based AFO [69]. Although the energy harvesting system was implemented on a passive device, the concept can be implemented on active (powered) orthoses and prostheses.

All aforementioned energy harvesting schemes illustrate promising ability to capture energy during gait, but ignored another important part of the energy loss: actuation energy waste. Not all the fuel energy is converted into work output. This difference is especially obvious in pneumatic systems because the energy contained in the compressed exhaust gas is significant.

1.2.5 Muscle Activation (EMG) Based Solutions

Electromyographic (EMG) signals have been used in lower limb orthotic/prosthetic control applications to measure the magnitude of the muscle activation signal, eliminating the need of any type of gait estimation. Ferris et al. used high-pass filtered EMG signals from the soleus and tibialis anterior to establish the relationship between the strength of muscle activation signals and needed force generation in powered orthoses [44, 75, 76]. Similar EMG based volitional control was used by Ha et al. to control the Vanderbilt powered prosthesis [77].

1.3 Introduction of the PPAFO

The portable powered ankle-foot orthosis (PPAFO) has been developed to provide plantarflexor and dorsiflexor torque assistance to an ankle joint [54]. In brief, a bottle of compressed CO_2 with embedded pressure regulator attached to the subject's waist allowed for untethered power assistance. A rotary pneumatic actuator at the ankle joint can generate about 10 Nm of torque at 100 psig pressure (Figure 10). The embedded regulator on the CO_2 bottle controlled the pressure supply for plantarflexor assistance (set to 100 psig). A second regulator could further reduce the pressure (set to 30 psig) for dorsiflexor assistance. Excessive dorsiflexor torque is unnecessary to support the foot during swing and can result in subject discomfort. The compressibility of gas allowed for user compliance and backdrivability for enhanced user-friendliness. Signals from force resistive sensors located at the heel and the toe of the foot plate are processed by a microcontroller to trigger two solenoid valves which control the actuation. Three actuation states could be achieved

through the combinations of the solenoid valves: dorsiflexion, plantarflexion and passive (no actuation).

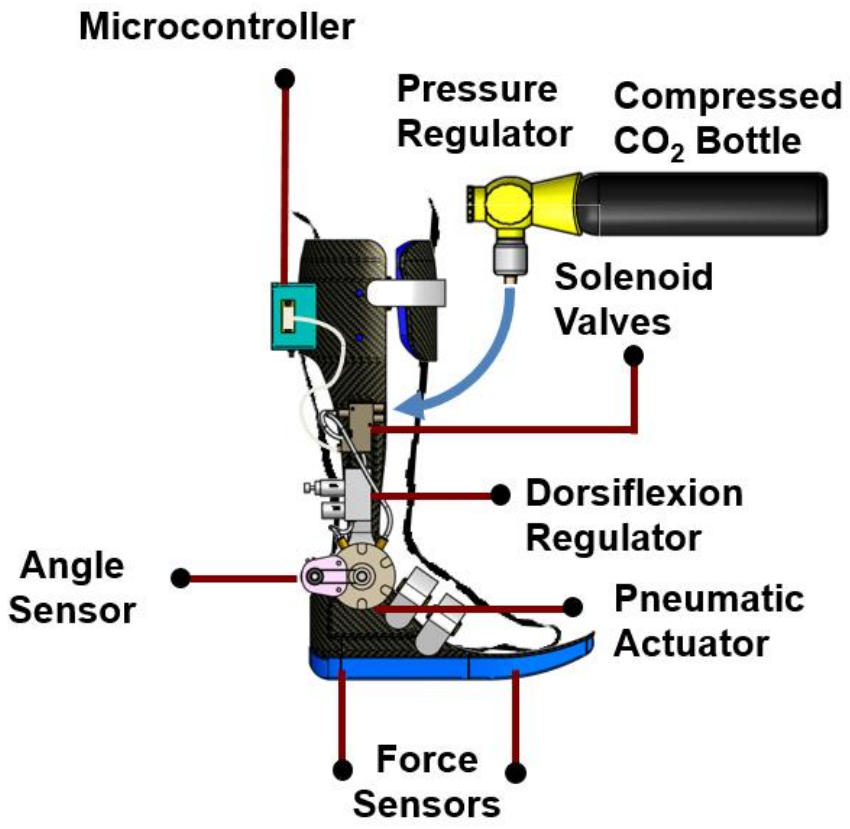

Figure 10 The Portable Powered Ankle-Foot Orthosis (PPAFO). The actuator was driven by a bottle of compressed CO_2, which was worn on the subject's waist [54].

The existing control algorithm before my work was a finite state direct event (DE) controller [54], a common and reliable approach with the benefit of simple implementation [16, 17, 19, 26-28, 78-80], Figure 11. The solenoid valve signals control the rotary actuator in dorsiflexion/plantarflexion directions. The two force sensitive resistors embedded in the sole of the AFO were used to determine gait state. Each on-and-off combination of the two sensors was considered a gait event, which was associated with the start and end of a gait phase (or gait state). Heuristically tuned

thresholds were used to determine the on configuration for each force sensor. The controller was used to switch the actuation direction (or turn it off) based on the combination of the two force sensors. During initial contact, only the heel sensor was compressed and dorsiflexor assistance was provided to prevent foot slapping. During the loading response, when both sensors were compressed, there was no actuation to allow for free range of motion. When only the toe sensor was compressed, plantarflexor actuation was used to assist forward propulsion. The swing phase was identified when both sensors were uncompressed, and dorsiflexor actuation was used to hold the toes up, preventing foot drop.

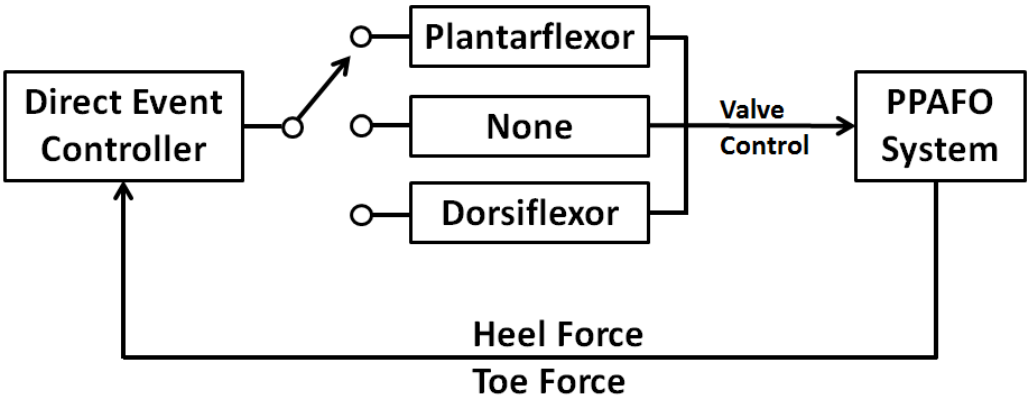

Phase	Heel	Toe	Torque Direction
1. Initial Contact	ON	OFF	Dorsiflexor
2. Loading Response	ON	ON	None
3. Forward Propulsion	OFF	ON	Plantarflexor
4. Swing	OFF	OFF	Dorsiflexor

Figure 11 The PPAFO direct event controller uses heel and toe force sensor data to identify gait events [54]. These gait events indicate the start and end of specific gait phases. In each identified phase, the actuator was controlled by valves to provide actuation in either direction or none.

1.4 MOTIVATION FOR PROPOSED STUDIES

Most of the powered orthotic devices described in section 1.2 require a tethered power supply, because of the high power consumption of the active assistive devices (peak power up to 100W for ankle [1]). Some researchers have attempted to build a self-contained system by fitting other power supplies (e.g., batteries) into a backpack or fanny pack, but they all suffer from being heavy (> 3 kg) and oversized [81-83]. Other existing shortcomings of state-of-the-art technologies include: heavy and bulky design for ankle-foot orthosis, lack of a uniform state estimation scheme for all targeted population, low system efficiency (especially for pneumatic systems), and the inability to recognize and adapt to different terrains. In the rest of this dissertation, many of these problems will be analyzed and solutions will be proposed in different chapters in order to improve the performance of the Portable Powered Ankle-Foot Orthosis (PPAFO) [54].

Specifically, this dissertation aimed to solve existing problems of the current PPAFO actuation control scheme under the original direct-event (DE) controller, as well as to improve the system efficiency for enhanced portability. The DE controller was designed based on two assumptions: the walking pattern was the same as normal healthy walkers, and the AFO would only be used for level ground walking. In this dissertation proposal, Studies 1 and 2 discuss what happens when these two assumptions are relaxed and how to solve the issues that come with it. Study 3 focused on analyzing and improving the system efficiency to increase the system operation time.

In Study 1 (Chapter 2), in level ground walking condition, a state estimation algorithm was proposed as an alternative state estimator because the DE state estimator has limited applicability

to the target population: For example, patients with weak plantarflexors adapt to a 'heel-walking' technique, where little pressure is applied to the forefoot to propel the body forward in late stance. Consequently, the threshold based DE state controller failed to trigger the actuation in proper sequence because the requisite toe sensor activation and therefore plantarflexion were not observed. Instead of trying the map out the force distribution for every group of targeted population as in [84], the proposed least-square-estimator (LSE) state estimator generalized the gait cycle to a series of finite states, and estimated a given state using a model that depended on previously collected time-history data. Other state estimators were also compared. The performances of the new estimators were examined in different speed/actuation conditions. A journal paper and a conference proceeding were published from this work [85, 86].

Study 2 (Chapter 3) focused on relaxing the assumption of level ground walking. In order for the PPAFO or any powered orthotic or prosthetic device to be widely used as an assistance/rehabilitation device for daily activities, it is very important that the device can recognize various gait modes (i.e. level ground walking, stair ascent/descent and ramp ascent/descent) and adopt to mode changes promptly. There were two critical aspects to this problem. First, the original sensor array on the PPAFO had limited sensing ability (it only measured heel and toe contact forces and ankle joint angle), which did not contain enough information to reliably detect all gait modes. Second, a new gait mode had to be recognized at the earliest possible time to prevent potential misfiring. Failing to adjust actuation for the current gait mode could increase the fall risk for the user. In this study, an Inertial Measurement Unit (IMU) based gait mode recognition scheme was proposed and validated by experimental trials. Additionally, how to evaluate the outcomes of the success rate of the recognition scheme was discussed and a

generalized procedure to justify the results from a recognition task were proposed. Three conference abstracts/proceedings were published from this work [87-89].

Study 3 (Chapter 4) tackled another major limitation of the current system, energy efficiency. Currently, the portable system could run continuously for about 20 minutes. The goal was to analyze the system efficiency and find solutions to improve the system operation time. For the PPAFO, long operation time without increasing the size of the power source will be a key to its success as a rehabilitation device. In this study, the overall system efficiency was separated into operational efficiency and component efficiency. The two types of efficiency were derived and experimentally tested. Solutions to enhance the efficiency were proposed and experimentally implemented. Additionally, work loss across different components were identified. A journal paper is in preparation and two conference proceeding were published from this work [90, 91].

Chapter 2 ESTIMATING SYSTEM STATE DURING HUMAN WALKING FOR A POWERED ANKLE-FOOT ORTHOSIS [1]

ABSTRACT

This paper presents a state estimator that reliably detects gait events during human walking with a portable powered ankle-foot orthosis (AFO), based only on measurements of the ankle angle and of contact forces at the toe and heel. Effective control of the AFO critically depends on detecting these gait events. A common approach detects gait events simply by checking if each measurement exceeds a given threshold. Our approach uses cross-correlation between a window of past measurements and a learned model to estimate the configuration of the human walker, and detects gait events based on this estimate. We tested our approach in experiments with five healthy subjects and with one subject that had neuromuscular impairment. Using motion capture data for reference, we compared our approach to one based on thresholding and to another common one based on *k*-nearest neighbors. The results showed that our approach reduced the RMS error by up to 40% for the impaired subject and up to 49% for the healthy subjects. Moreover, our approach was robust to perturbations due to changes in walking speed and to control actuation.

[1] This work has been published in [85].

2.1 INTRODUCTION

Gait is a cyclic task characterized by repetitive events, and is defined from the initial ground contact of the foot to the subsequent contact of the same foot. Gait events are used to divide the cycle into phases and sub-phases each with a functional objective that contributes to one of three main functional tasks during gait: weight acceptance (stance), support and propulsion (stance), and limb advancement (swing) [1, 72, 92]. Gait can be impaired by conditions including trauma, incomplete spinal cord injuries, stroke, multiple sclerosis, muscular dystrophies, polio or cerebral palsy [1]. These deficiencies create impairments because they prevent or hinder the functional tasks required for gait.

Ankle-foot orthoses (AFOs) are orthotic devices used to correct gait deficiencies created by impairments to the lower limbs. In the United States alone, sizable populations exist with symptoms that can be treated with an AFO: stroke (4M, [93]), polio (1.4M, [94]), multiple sclerosis (300K, [95]), spinal cord injuries (200K, [96]) and cerebral palsy (100K, [97]). Clinically prescribed AFO systems assist impaired individuals by providing support for the lower leg and foot while restricting unwanted motion of the foot in a predetermined and fixed manner [8, 9, 98, 99]. Unfortunately, these fixed motion control properties can impede gait and cannot adapt to a changing environment [17]. Powered AFO systems address the limitations of passive devices by using computer control to vary the compliance, damping, or net power of the device for motion control and torque assistance at the ankle joint [16, 17, 19, 20].

The performance of a powered AFO depends critically on the ability to do two things: first, detect gait events based on measurements from onboard sensors (e.g., accelerometers, potentiometers,

and force sensors), and second, control applied torque to meet the functional objective determined by each gait event. Our focus in this paper is on the first of these things, reliable detection of gait events.

Many state-of-the-art AFOs detect gait events simply by checking if each sensor measurement at a particular time exceeds a given threshold [16, 17, 19, 20, 26, 54, 78, 80, 100, 101]. This approach has been used to provide appropriately timed motion control and torque assistance both for level walking and for stair climbing. However, this approach becomes less reliable when the individual's gait pattern changes, for example as the result of impairment, fatigue, preference, or functional assistance from the orthosis. Moreover, this approach may not even be possible when there exists no unambiguous mapping from sensor measurements to a gait event of interest, in particular an event other than "heel-strike" or "toe-off." These situations limit the number and reliability of gait events that can be used for control.

In this paper we consider an alternative approach that uses the time history of sensor measurements to compute an estimate of body configuration and then detects gait events based on this estimate. It is well known that body configuration during cyclic gait can be approximated by a single state variable, the "percent gait cycle," and that gait events are associated with particular values of this state variable [1]. Recent work has shown that it is possible to compute an estimate of this state variable by comparing motion capture data (producing measurements of lower-limb joint angles and joint velocities) to a learned model [102]. We will do the same, but must address the fact that a powered AFO typically does not have access to motion capture data, nor to similarly rich sensor measurements.

In particular, our approach computes a state estimate (i.e., an estimate of where an individual is in the gait cycle) based only on measurements of the ankle angle and of contact forces at the toe and heel. These measurements are taken only from sensors mounted on the portable powered AFO (PPAFO) that we use in our experiments [54]. This sensor package is comparable to what is found on other AFOs, including those of Blaya and Herr [19] with joint angle and ground reaction force sensors, Svensson and Holmberg [17] with a joint angle sensor, and Hollander et al. [26] with a joint angle sensor and foot switches. None of these sensor packages are sufficient to compute a state estimate based only on one set of measurements. However, due to the cyclic nature of gait, sensor measurements from different gait cycles exhibit a high degree of correlation. We take advantage of this fact to compute a state estimate based on maximizing the cross-correlation between a window of past sensor measurements and a reference model learned from training data. When tested in experiments with human subjects, our approach to event detection was more accurate and more robust to changes in gait than other approaches previously reported in the literature.

Throughout this paper, we will denote time by $t \in \mathbb{R}$, the state variable describing percent gait cycle by $\lambda \in [0,100)$, and the vector of sensor measurements by $\mathbf{y} \in \mathbb{R}^3$. Since the mapping from λ to gait events is well known [1], our goal is to compute an estimate $\hat{\lambda}(t)$ of the state $\lambda(t)$ at the current time t based on all sensor measurements $\{\boldsymbol{y}(s)|s \in [0,t]\}$ up to this time. In our experiments, we use the method of [102] to compute a reference estimate $\lambda^*(t)$ based on motion capture data, and define the error in our own estimate by $\lambda_{err}(t) = \hat{\lambda}(t) - \lambda^*(t)$.

To examine the performance of our proposed cross-correlation estimator, we compare it to two other estimators and to a direct event detector. All three estimators that we consider are based on a pre-computed model $\overline{\boldsymbol{y}}(\lambda)$ that tells us what sensor measurements to expect at a given state λ. This model is given by regression analysis of training data (λ^*,$\boldsymbol{y}$). We also derive the average cycle period T from this model.

The estimators and direct event detector are as follows:

A. **Cross-Correlation (CC)** The estimate $\hat{\lambda}_{CC}$ minimizes the sum-squared-error between sensor readings from the last T seconds and training data with a phase shift of $\hat{\lambda}_{CC}$.

B. ***k*-Nearest-Neighbors (*k*NN)** The estimate $\hat{\lambda}_{kNN}$ minimizes the squared-error between the current sensor reading and training data at $\hat{\lambda}_{kNN}$.

C. **Fractional-Time (FT)** The estimate $\hat{\lambda}_{FT}$ is the time since the last heel strike (determined by thresholding the heel sensor) normalized by T.

D. **Direct Event (DE)** DE uses thresholds on heel and toe sensors to determine heel strike and toe off events. Because DE is limited to these two events, it is not a state estimator.

FT is similar to what is found in the AFO literature [16, 17, 19, 20, 26, 54, 78, 80, 100, 101], *k*NN is similar to [102] but applied to AFO sensor data rather than motion capture data, and CC is the approach that we present here. We emphasize that cross-correlation is a classical method of signal

processing (e.g., [103]) that has been used previously for gait analysis (e.g., [104, 105]). Our contribution is the application of this approach to state estimation for a powered AFO and the analysis of experiments with human subjects necessary to demonstrate its performance.

The remainder of our paper proceeds as follows. The Method section describes the metrics and methodology used to quantify the performance of each state estimator. The following section presents the details of our CC state estimator and two others used as a basis for comparison. The Results section provides the results of experiments with five healthy subjects and one subject that had neuromuscular impairment. The Discussion section considers the implications of these results in the context of AFO control. The last section gives concluding remarks.

2.2 METHODS

Three state estimators (CC, *k*NN, and FT) and DE were implemented on a powered AFO capable of operation in real-world environments outside of the laboratory or clinic. A reference estimate λ^* was also derived using kinematic data from a motion capture system and kinetic data from an instrumented treadmill. Experimental trials with five healthy subjects and one subject with a neuromuscular impairment were performed to assess the three AFO estimators on their performance relative to the reference state model λ^*, ability to identify relevant gait events during the cycle, and robustness to speed and actuation perturbations. This section describes the PPAFO system, the gait lab data collection procedure, and the experimental setup.

2.2.1 POWERED ORTHOSIS SYSTEM

The PPAFO in this work used a pneumatic power supply and a rotary actuator at the AFO ankle joint for motion control and propulsion assistance, Figure 12, [54]. The PPAFO control loop and estimators ran at 66 Hz, using sensor feedback sampled at the same rate from two force sensors (0.5 in circle, Interlink Electronics, Camarillo, CA) mounted underneath the heel and toe between the carbon fiber shell and the sole of the PPAFO and a potentiometer (53 Series, Honeywell, Golden Valley, MN) that measured the angle between the shank and foot sections.

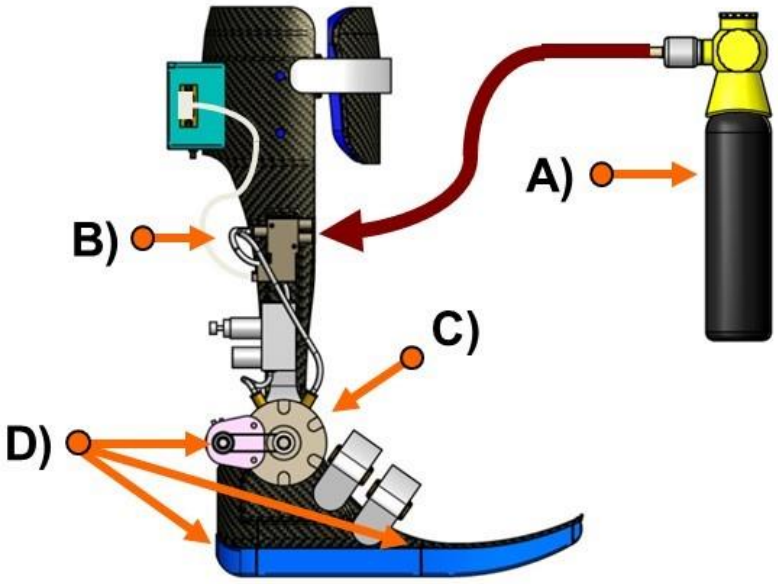

Figure 12 PPAFO system components: A) Power supply: a compressed CO_2 bottle with regulator provides up to 120 psi for the system; B) Valves: two 3-2 solenoid valves control the flow of CO_2 to the actuator; C) Actuator: a pneumatic rotary actuator provides up to 12 Nm at 120 psi; D) Sensors: two force sensors under the heel and toe, and a potentiometer at the ankle joint.

2.2.2 Experimental Setup and Pre-Test Procedures

2.2.2.1 Experimental Setup

Subjects walked with the PPAFO on an instrumented treadmill. For each trial, the subject wore sleeveless top and snug-fitting shorts. Thirty-two reflective markers were attached to the body, including torso, thighs, shanks, feet and the PPAFO. Data from the healthy subject were collected at the University of Illinois. Kinematic data were collected using a 6-camera motion capture system sampled at 150 Hz (Model 460; Vicon, Oxford, UK). Ground reaction force (GRF) data for each foot was collected on a splitbelt treadmill with embedded force plates sampled at 1500 Hz (Bertec, Columbus, OH, USA). Data from the impaired subject were collected at Georgia Institute of Technology. Kinematic data were collected using a 6-camera system sampled at 120 Hz (Model 460; Vicon, Oxford, UK). The kinetic data were collected on a custom force-sensing instrumented split-belt treadmill sampled at 1080 Hz [106]. Joint angles were calculated from kinematic data. Joint angles and GRF were filtered by a low-pass, fourth-order, zero-lag, Butterworth filter with cutoff frequency of 10 Hz. All procedures were approved by the institutional review boards of the University of Illinois and Georgia Institute of Technology, and all participants gave informed consent.

2.2.2.2 Subject Information

Healthy Subjects The five healthy male subjects (28 ± 4 yrs; height 186 ± 5 cm; mass 72 ± 8kg) had no gait impairments and no history of significant trauma to the lower extremities or joints.

Impaired Subject The impaired male subject (51 yrs; height 175 cm; mass 86kg) has a diagnosis of cauda equina syndrome (CES) caused by a spinal disc rupture. This gait deficit does not allow him to generate plantarflexor torque to push his toes down. The subject walks without the use of walking aids (i.e., cane or walker), but usually wears AFOs bilaterally. For our testing, he wore his own pre-fabricated carbon composite AFO (Blue RockerTM, Allard, NJ, USA) on his left leg while walking with the PPAFO on his right leg.

2.2.2.3 Determining Self-Selected Speed

A self-selected walking speed for each subject was determined prior to testing. For the healthy subjects, comfortable treadmill walking speed was determined by averaging three self-selected speeds chosen while wearing the PPAFO with no actuation. Average walking speed for the five healthy subjects was 1.18 ± 0.11 m/s with an average gait period of 1.16 ± 0.09 s over 30 seconds of walking. The impaired subject's comfortable walking speed was determined while in his running shoes on the treadmill with no assistive devices on either leg. This walking condition was used because it was the impaired subject's most difficult condition. Walking speed for the impaired subject was 0.7 m/s with an average gait period of 1.09 ± 0.04 s over 30 seconds of walking.

2.2.3 Training Data for Estimation Models

The PPAFO state estimators require a model derived from data collected during a preliminary training process. Each model is unique to each subject, and is not varied between experimental trials. During this process, a subject walked with the unactuated PPAFO on the treadmill for 30s at his comfortable walking speed.

GRF_Z data from the force-sensing treadmill were compared to a threshold to identify heel strikes. The average period of the gait cycle, *T*, was calculated from these data.

The data were also used to create regression models for each of the PPAFO sensor measurements during gait cycles. Models for different sensors were computed separately. Each model is a function of cycle state λ, where $\lambda \in [0,100)$, and describes the expected reading for a given sensor $\overline{\boldsymbol{y}}(\lambda)$. The regression models were formulated in the following manner.

For each sensor, we use locally weighted regression (LWR) analysis [107] to establish the functional relationship between the normalized input/output pairs of state λ and sensor measurement *y*.

$$(\lambda_1, y_1), \ldots, (\lambda_N, y_N) \tag{1}$$

where *N* is the number of measurements collected from training, and λ is the percent gait cycle found by normalizing time between heel strikes.

Regression evaluates $\overline{\boldsymbol{y}}$ at the point λ. This evaluation depends on the signed distance

$$x_i = \text{dist}(\lambda_i - \lambda) \tag{2}$$

between λ_i and the query point λ. Because λ_i and $\lambda \in [0,100)$, the distance is defined as

$$\text{dist}(\lambda_i - \lambda) = \begin{cases} (\lambda_i - \lambda) - 100 & \text{if } \lambda_i - \lambda > 50 \\ \lambda_i - \lambda & \text{if } -50 \leq \lambda_i - \lambda \leq 50 \\ (\lambda_i - \lambda) + 100 & \text{if } \lambda_i - \lambda < -50 \end{cases} \quad (3)$$

First, we select a fixed set of M polynomial basis functions

$$\phi(x_i) = [1, x_i, \dots, {x_i}^{M-1}]^T, \quad (4)$$

and denote

$$\Phi = \begin{bmatrix} \phi(x_i)^T \\ \vdots \\ \phi(x_N)^T \end{bmatrix}, \quad (5)$$

We also define

$$Y = \begin{bmatrix} y_1 \\ \vdots \\ y_N \end{bmatrix} \quad (6)$$

by concatenating the data associated with each output. We select the row vector $v \in \mathbb{R}^M$ of parameters that minimizes the weighted sum-squared error e

$$e = \sum_{i=1}^{N} \omega_i (y_i - v^T \phi(x_i))^2 \quad (7)$$

where

$$\omega_i = \exp\left(-\frac{{x_i}^2}{2r^2}\right) \text{for each } i = 1, \dots, N \tag{8}$$

and r is a design parameter. Because ω_i depends explicitly on λ, we must store and use the entire set of training data $(\lambda_1, y_1), \dots, (\lambda_N, y_N)$ to make predictions. Let

$$W = \text{diag}(\omega_i, \dots, \omega_N) \tag{9}$$

then the cost function can be rewritten in matrix form

$$e = (\Phi v - Y)^T W (\Phi v - Y), \tag{10}$$

In order to minimize e, v can be solved as,

$$v(\lambda) = (\Phi^T W \Phi)^{-1} \Phi^T W Y, \tag{11}$$

Now we can obtain the regression model for a given sensor over one gait cycle as

$$\overline{\boldsymbol{y}}(\lambda) = v(\lambda)^T \phi(0) \tag{12}$$

For each subject, we precompute $\overline{\boldsymbol{y}}(\lambda)$ at $\lambda = \{0,1, \dots, 99\}$ for all three sensors, and they will form the sensors regression model matrix $\overline{\boldsymbol{y}}(\lambda)$. The results of applying this form of regression analysis to multiple gait cycles of healthy subject #3 are shown in Figure 13.

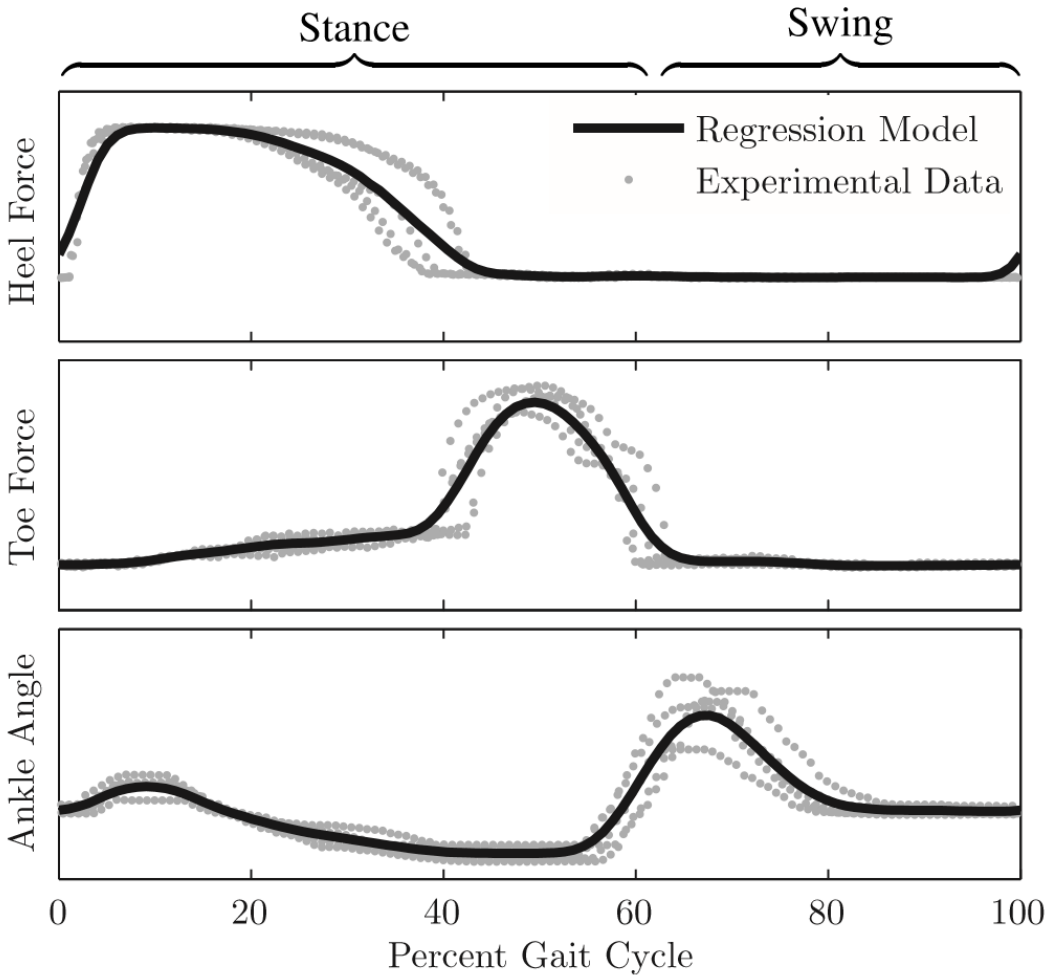

Figure 13 Locally-weighted linear regression analysis with $M = 2$ polynomial basis functions and a weighting bandwidth of $r = 0.02$ applied to heel force, toe force and ankle angle sensor measurements as a function of percent gait cycle. 5 cycles of sensor measurements (gray dots) from healthy subject #3 walking at steady-state, self-selected speed were used to create a regression model $\overline{\boldsymbol{y}}(\lambda)$, shown in black, for each sensor.

2.2.4 Experimental Testing Procedure

Tests were conducted with two possible disturbances: actuation and slow speed. The actuation disturbance modeled the effect of providing assistive torque with the PPAFO. During each gait cycle, a plantarflexor (toes down) disturbance torque was applied if both the toe and heel sensors were loaded, and a dorsiflexor (toes up) disturbance torque was applied if both sensors were unloaded—otherwise, no disturbance torque was applied. State estimates (from CC, *k*NN, or FT) could also have been used to trigger the application of torque in these experiments, but the use of a simple decision rule allowed for a less biased comparison between estimators. Figure 14 shows the resulting change in gait kinematics as a consequence of actuation. The slow speed disturbance modeled the effect of variable walking speed, which is a common gait perturbation. It was created by slowing the treadmill.

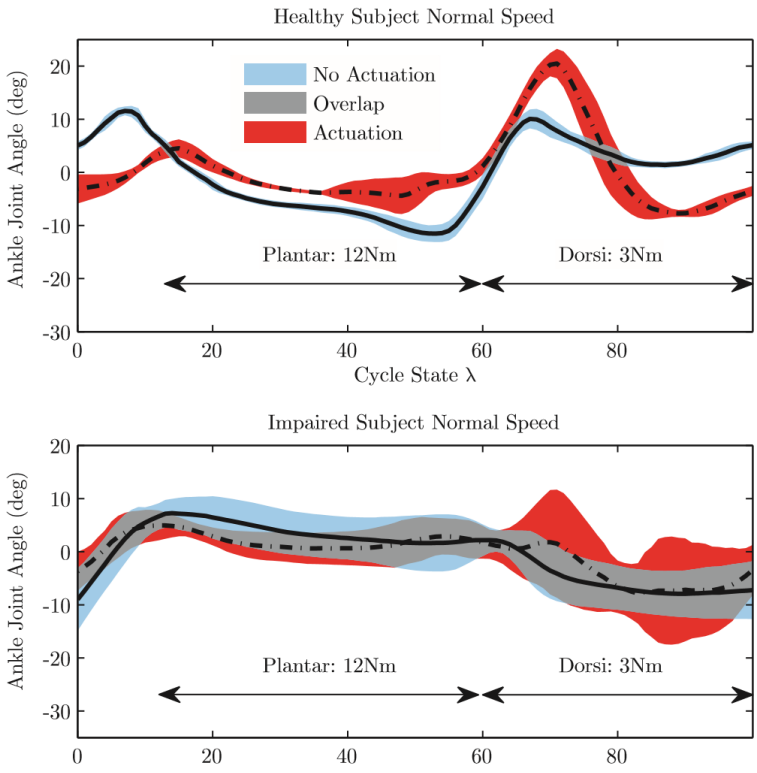

Figure 14 Ankle joint angle for healthy subject #3 (top) and the impaired subject (bottom) with and without actuation at normal speed. The PPAFO was able to generate a modest plantarflexor torque (12 Nm) compared to a healthy walker (105 Nm for a 70kg individual). Only 3 Nm of dorsiflexor torque was required to support the foot during swing. Sensor readings without actuation and with actuation are significantly different. Because the sensor regression model was generated without actuation, these differences resulted in worse correlation between current measurements and the model. For the impaired subject, excessive dorsiflexion actuation during swing may have caused the large variability of ankle joint position.

Five experimental trials were used to evaluate the performance of the PPAFO estimators under these two disturbances. For each test, the subjects were given time to reach a steady walking speed on the treadmill before data collection began. Thirty seconds of data were recorded during steady-state walking for trials 1-4.

1) **Normal Speed – No Actuation (Healthy and Impaired)**

This test compares the PPAFO estimators under nominal conditions. Each subject walked at his self-selected speed (normal speed) with no actuation from the PPAFO.

2) **Normal Speed – Actuation (Healthy and Impaired)**

Torque applied by the PPAFO can affect gait timing and sensor readings, adversely impacting estimation. The PPAFO was supplied with pneumatic power at 110psi and actuated by the simple threshold rule described above.

3) **Slow Speed – No Actuation (Healthy and Impaired)**

The treadmill was set to 75% of the subject's self-selected speed, with no PPAFO actuation.

4) **Slow Speed – Actuation (Healthy and Impaired)**

This trial examined the effects of slow walking (75% of self-selected speed) along with actuation. The actuation was in the same manner as trial 2 above.

5) Change in Speed (Healthy)

Changing speed is a common gait perturbation. A speed change was introduced to examine the effect of this perturbation on the accuracy of the PPAFO estimators. Each healthy subject began walking at his self-selected speed. After 20s, the treadmill was gradually slowed to 75% of self-selected speed in approximately 5s. The speed remained 75% of self-selected speed for the rest of the trial. Sixty seconds of data were recorded during the trial.

2.2.5 Estimation Comparison Metrics

Two metrics were used to evaluate and compare the performance of the PPAFO estimators for the tests in section 0:

1) Event Detection

Temporal errors were compared between gait event times identified using gait lab data, event times predicted by the three PPAFO estimators, the direct event detector, and the reference state estimator λ^*. The gait events selected for comparison were right heel strike, left toe off, left heel strike and right toe off.

2) State Estimation

Errors were compared between reference state estimate λ^* and the three PPAFO state estimates throughout the cycle.

2.3 STATE ESTIMATION TECHNIQUES

The experiments described in the previous section tested three state estimators (CC, FT, and *k*NN) and the direct event detector (DE), all based on PPAFO sensor measurements in comparison to a reference estimate (λ^*) based on motion capture and treadmill data. In this section we will describe how each state estimator was implemented.

2.3.1 ESTIMATE BASED ON CROSS-CORRELATION (CC)

The CC estimator slides a window of actual sensor data across the regression model of the sensor data, and finds the point where the mean-square-error is minimized (i.e., where the data and model best align). Given the regression model $\overline{\boldsymbol{y}}$ and the average period *T*, we can apply the CC approach to estimate λ at each time *t*. We do this in the following way. We have pre-computed $\overline{\boldsymbol{y}}(\lambda)$ at $\lambda = \{0,1,\ldots,99\}$ using the locally weighted linear regression approach mentioned above. We take a time-history of sensor data $\boldsymbol{y}_1, \ldots, \boldsymbol{y}_m$ sampled at m particular times $t_1, \ldots, t_m \in [t-T, t]$. For all $j = 1,\ldots,m$, we normalize these times according to

$$\lambda_j = 100\frac{t_j - (t - T)}{T} \tag{13}$$

then generate an index set $I = I_1, \ldots, I_m$ according to

$$I_j = round(\lambda_j) \tag{14}$$

so that each *Ij* will be an integer index between 0 and 100. We denote the measurements by $\boldsymbol{y}[j] = \boldsymbol{y}_j$. We wrap the regression model around periodic borders by setting $\overline{\boldsymbol{y}}[i] = \overline{\boldsymbol{y}}[i \pm 100]$ for all i. The state estimate $\hat{\lambda}_{CC}$ is the integer k $\in\{0,1, \ldots, 99\}$ that minimizes

$$\sum_{j=1}^{\boldsymbol{m}} \left(\overline{\boldsymbol{y}}[I_j + k] - \boldsymbol{y}[j]\right)^{\boldsymbol{T}} \left(\overline{\boldsymbol{y}}[I_j + k] - \boldsymbol{y}[j]\right) \tag{15}$$

2.3.2 Estimate Based on Fractional Time (FT)

The fractional time (FT) estimator assumes that the state estimate $\hat{\lambda}$ increases linearly with time from heel-strike:

$$\hat{\lambda}_{FT} = 100(t - t_{hs})/T \tag{16}$$

where ths is the time of last heel strike as determined by thresholding $\mathbf{y}(t_{\mathrm{hs}})$, and *T* is the average cycle period.

2.3.3 ESTIMATE BASED ON *K*-NEAREST NEIGHBOR (*K*NN)

Another common way to estimate state is to compute the best match between current sensor measurements y and the regression model learned from training data $\bar{\boldsymbol{y}}$:

$$\hat{\lambda}_{k\mathrm{NN}} = \underset{\lambda\in[0,100)}{\arg min} \|\boldsymbol{y}(t) - \bar{\boldsymbol{y}}(\lambda)\|_2 \tag{17}$$

This approach can be improved by averaging the *k* best matches ("*k* nearest neighbors" [108]). We chose $k = 3$.

2.3.4 REFERENCE ESTIMATE (Λ^*)

We use an estimator generated from motion capture and treadmill data as a reference for comparing the PPAFO estimators. The joint angle information expands 8 variables (vertical ground reaction forces, and bilateral hip, knee, and ankle angles) and their derivatives to a 16-dimension state space. We build a linearly weighted regression model, $\bar{\boldsymbol{q}}$, using data from multiple cycles to form a closed curve in this 16D state space. This curve is divided into 100 sections and labeled linearly with time. λ^* is the label of the nearest neighbor on the curve to the current measurement vector, as in [102].

At time *t* the sensors return an 16-element vector $\boldsymbol{q}(t)$. We compare this vector to the regression model $\overline{\boldsymbol{q}}$. The state λ^* at time *t* is defined as

$$\lambda^*(t) = \underset{\lambda \in [0,100)}{\arg min} \|\boldsymbol{q}(t) - \overline{\boldsymbol{q}}(\lambda)\|_2 \tag{18}$$

Figure 15 illustrates how normalizing the data by λ^* aligns sensor measurements across different trials better than by time or percent gait cycle.

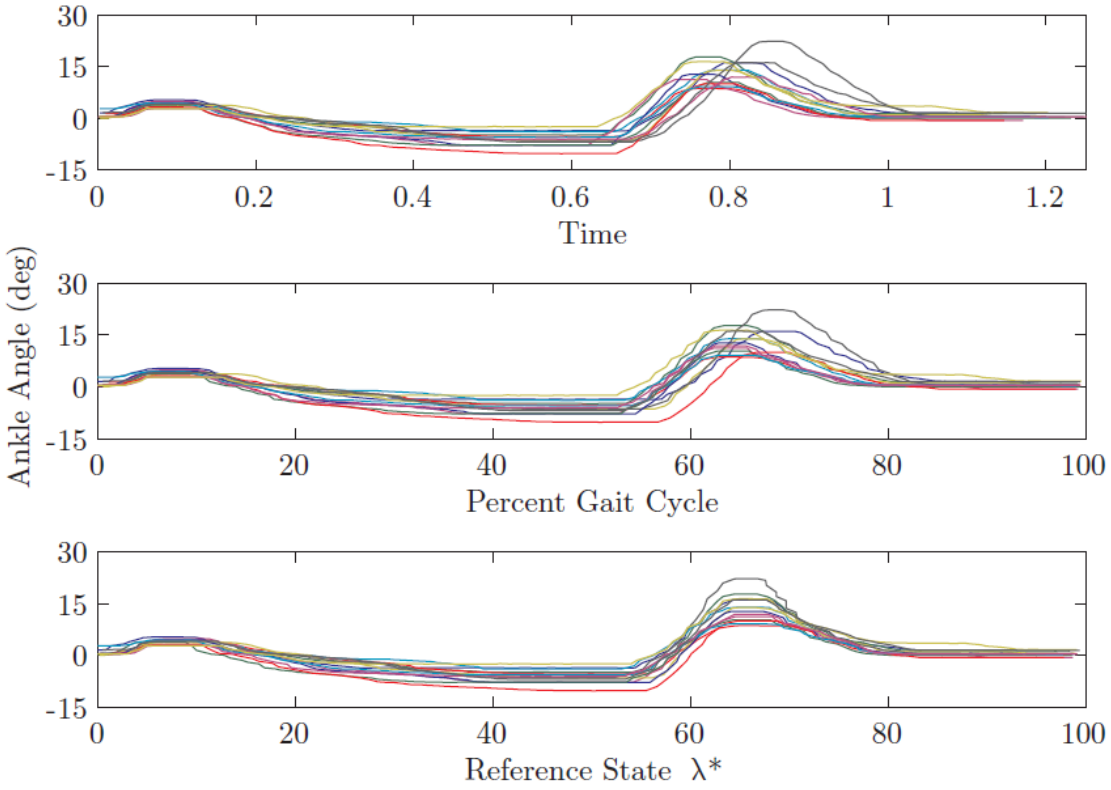

Figure 15 The ankle angles of healthy subject #3 aligned at heel strike for ten cycles. The angle is plotted with respect to time, percent gait cycle, and reference estimate λ^*.

2.4 RESULTS

CC and FT outperformed *k*NN for all tests. For the impaired subject, CC demonstrated the best accuracy for all tests, reducing event detection RMS error by up to 40% compared to FT. For the healthy subjects, FT and CC performed comparably during normal speed walking, but CC was more accurate during slow walking tests (Table 1 and Table 2).

1) Normal Speed – No Actuation (Healthy and Impaired)

   For the healthy subject, both CC and FT worked well for event detection and state estimation, while *k*NN did not. FT had low state estimate error around heel strike, but the error increased as time progressed in the gait cycle (Figure 16) while CC stayed relatively low. For the impaired walker, the CC technique had a smaller average error (Figure 16 and Figure 17). The FT estimate diverged more during swing (Figure 16).

2) Normal Speed – Actuation (Healthy and Impaired)

   This task verified that FT and CC can successfully track the system state, even when actuated. The RMS error for state estimate is under 4% for the healthy subjects and around 10% for the impaired subject. For the healthy subjects, FT and CC have similar performance, with FT having slightly higher accuracy. CC for the impaired subject has 23% lower RMS error than FT, a decrease in RMS state error from 12.4 to 8.0 (Table 2).

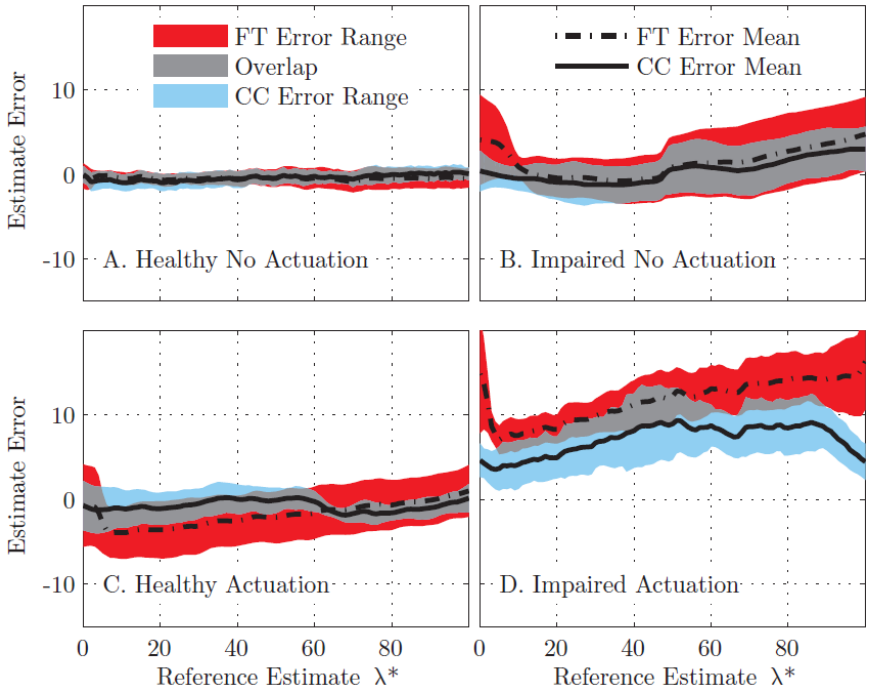

Figure 16 Continuous state estimate error (mean and ± standard deviation) of FT and CC estimators and the overlap of the two behaviors for healthy subject #3 and the impaired subject, with and without actuation

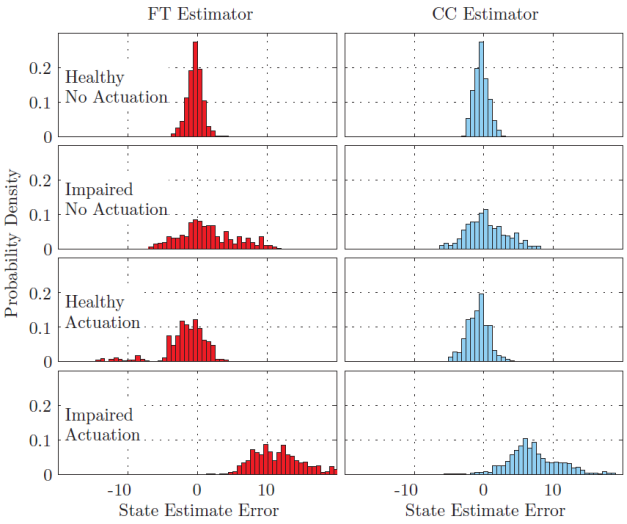

Figure 17 Histograms of errors from FT and CC estimators for healthy subject #3 and the impaired subject, with and without actuation. The CC estimator demonstrates higher precision and often lower error, i.e., tighter distributions.

Table 1 Event Detection Error Results for Each Technique due To Speed and Actuation Perturbation Effects for Healthy and Impaired Subjects

5 Healthy Subjects						*Impaired Subject*					
Actuation	Speed	Method	RMS Error (ms)	Ave. Error (ms)	Worst (ms)	Actuation	Speed	Method	RMS Error (ms)	Ave. Error (ms)	Worst (ms)
0psi	Normal	CC	**14.8±4.8**	-1.7±2.9	35.5±19.1	0psi	Normal	CC	**36.8**	-3.6	**76.7**
		FT	14.8±5.6	**1.7±1.5**	**30.5±9.7**			FT	53.2	-1.4	138.2
		*k*NN	65.0±29.0	-14.8±9.6	208.1±194.3			*k*NN	104.6	**-1.4**	441.6
		λ^*	6.4±1.2	-1.2±2.0	14.7±3.0			λ^*	19.0	-6.2	33.3
		DE†	5.8±2.8	2.3±2.0	13.2±6.8			DE†	39.1	3.0	78.2
110psi	Normal	CC	45.9±15.0	17.0±36.7	113.8±54.8	110psi	Normal	CC	**87.6**	-64.2	**23.4**
		FT	**41.9±11.8**	27.6±15.3	**106.5±52.4**			FT	113.4	-86.0	44.1
		*k*NN	93.6±38.0	**1.2±26.4**	307.0±184.2			*k*NN	353.2	**-25.1**	762.9
		λ^*	7.6±1.4	-0.9±2.6	18.7±5.6			λ^*	15.5	0.5	57.4
		DE†	31.3±13.2	13.3±11.9	77.2±66.4			DE†	51.3	-25.8	19.2
0psi	Slow	CC	**49.4±23.9**	-29.0±25.2	**37.7±26.1**	0psi	Slow	CC	**74.8**	-47.2	**62.3**
		FT	69.6±15.7	-41.8±15.9	49.7±32.2			FT	108.8	-33.8	157.9
		*k*NN	77.8±32.4	**10.8±18.9**	289.7±199.0			*k*NN	110.9	**-5.3**	576.3
		λ^*	9.5±4.2	0.3±2.7	30.4±28.5			λ^*	18.4	-0.5	30.6
		DE†	14.2±5.1	-0.9±5.2	25.3±28.6			DE†	47.9	-8.6	78.0
110psi	Slow	CC	84.0±53.2	-51.5±52.9	**47.7±24.6**	110psi	Slow	CC	**105.5**	-81.1	**21.5**
		FT	**82.9±20.9**	-35.0±24.0	81.2±30.1			FT	175.7	-103.5	167.6
		*k*NN	112.7±88.7	**3.9±27.2**	272.0±190.9			*k*NN	214.8	**17.2**	681.9
		λ^*	16.0±18.5	7.3±13.4	33.3±29.8			λ^*	14.2	2.3	59.3
		DE†	37.9±12.6	5.9±15.5	59.8±22.4			DE†	50.2	-19.4	67.6

†The direct event detector (DE) can only detect toe off and heel strike on the right foot.
True event times for left and right heel strike and toe off events are detected using treadmill force sensors. Gait period $T = 1.16 \pm 0.09$s for healthy and 1.09±0.04s for impaired. For the healthy subjects, errors are reported as mean±1 standard deviation. The best PPAFO estimator for each case is bolded and highlighted in dark gray. DE and the reference estimate λ^* are highlighted in light gray and were not included in this comparison between estimators.

Table 2 State Estimation Error Results for Each Technique Due to Speed and Actuation Perturbation Effects for Healthy and Impaired Subjects

5 Healthy Subjects						*Impaired Subject*					
Actuation	Speed	Method	RMS Error (λ)	Ave. Error (λ)	Worst (λ)	Actuation	Speed	Method	RMS Error (λ)	Ave. Error (λ)	Worst (λ)
0psi	Normal	CC	1.3±0.4	-0.1±0.1	4.5±1.2	0psi	Normal	CC	2.9	0.4	7.7
		FT	1.3±0.5	-0.0±0.3	4.7±1.7			FT	4.3	1.5	11.4
		*k*NN	6.2±1.0	0.2±0.5	34.4±9.1			*k*NN	12.9	-2.4	49.4
110psi	Normal	CC	3.5±1.6	-1.1±3.5	7.9±1.9	110psi	Normal	CC	8.0	7.1	18.9
		FT	3.2±0.8	-1.5±1.6	9.7±2.4			FT	12.4	11.8	25.8
		*k*NN	8.9±2.0	0.2±2.2	41.3±9.4			*k*NN	21.6	6.1	49.0
0psi	Slow	CC	3.9±1.8	2.8±2.1	13.2±8.3	0psi	Slow	CC	7.1	6.2	14.6
		FT	7.7±1.7	6.4±1.5	18.1±3.6			FT	10.0	8.2	26.4
		*k*NN	8.5±1.1	-2.6±1.5	37.8±7.3			*k*NN	10.8	-0.5	48.0
110psi	Slow	CC	7.1±3.7	5.6±4.3	13.9±5.6	110psi	Slow	CC	9.6	8.4	19.9
		FT	9.3±3.6	7.4±3.2	21.3±6.3			FT	15.7	13.7	32.0
		*k*NN	8.2±3.5	-0.0±1.3	25.7±13.8			*k*NN	15.6	-1.9	51.5

For the healthy subjects, errors are reported as mean±1 standard deviation. The best estimator for each case is highlighted. Errors are the difference between PPAFO estimators and reference estimation λ^*.

3) Slow Speed – No Actuation (Healthy and Impaired)

For the healthy subjects, this test shows the largest improvements of CC over FT in both event detection and state estimate error. For both healthy and impaired subjects, the CC reduced the state estimate error by at least 29%, from 10 to 7.1 and the event detection error by at least 30%, from 69.6 to 49.4ms (Table 1 and Table 2).

4) Slow Speed – Actuation (Healthy and Impaired)

The combined speed and actuation perturbations make this the only test where *k*NN becomes competitive with other estimators. The healthy subjects were best estimated using CC. For the healthy subjects the state estimate RMS error was reduced 25% from FT to CC. For the impaired subject the results are striking: a 40% reduction in state estimate error from FT to CC, from 15.7 to 9.6 (Table 2).

5) Change in Speed (Healthy)

This test reduced the walking speed by 25% midway through the trial. Figure 18 shows the errors from the three estimators as a function of overall time for this test. The error variance for FT illustrates unreliability at the slower walking speed, while CC maintains accuracy. The RMS and worst case for FT were all reduced by a factor of 2 by the CC estimate.

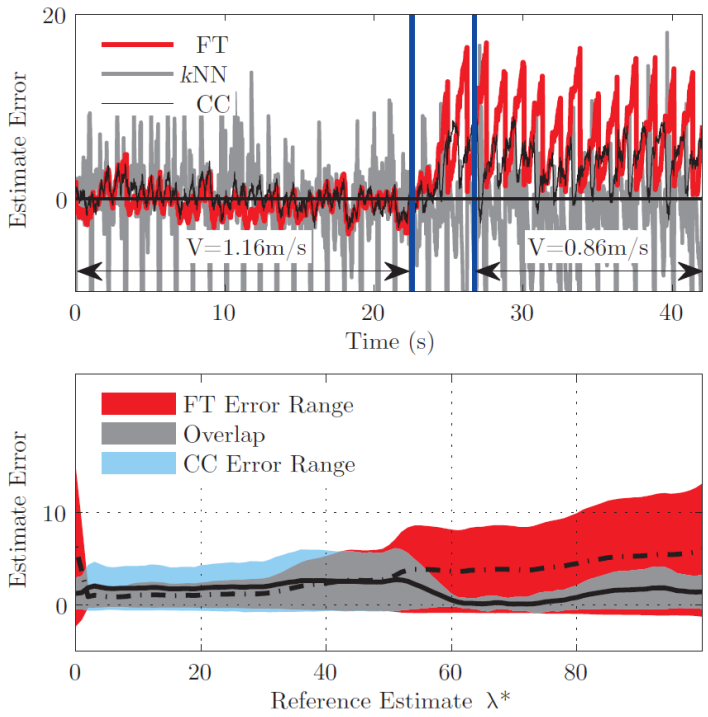

Figure 18 Estimation error of healthy subject #3 during the change in speed test. The walking speed changed from 1.16 m/s to 0.86 m/s. Top: estimate error as a function of time. Bottom: overall estimate error as a function of state during the slow speed section. Note the high variance in the FT error at the slower speed caused by the cycle period T increasing from 1.16 ± 0.09s to 1.32 ± 0.09 s.

2.5 DISCUSSION

2.5.1 PERFORMANCE DURING HEALTHY UNPERTURBED GAIT

The CC and FT estimators performed comparably during the healthy subject normal speed walking trials. The CC estimator correlates a window of past sensor readings to a regression model of normative sensor data to estimate the state. The FT estimator is an extension of the direct event (DE) estimator using thresholds, and only requires a model of the subject's gait period. The FT has the advantage of simple implementation, but as we will discuss below, the CC estimator was more robust to disturbances.

The *k*NN estimator performed poorly during all subject trials. This estimator is based on [102], but uses PPAFO sensor data rather than motion capture data as in [102]. The poor performance of *k*NN was due to the limited data used to construct the subject's state configuration, and that *k*NN only makes use of the current sensor measurements. This shortcoming is compounded because the PPAFO sensor data contain large sections with nearly identical readings (Figure 13, e.g., 70-100% gait cycle). As a result, *k*NN cannot reliably compute gait state during these periods.

2.5.2 ROBUSTNESS TO SPEED AND ACTUATION DISTURBANCES

The robustness of the estimators was evaluated during trials with speed and actuation disturbances. A decrease in speed was used to perturb gait because preliminary experimentation demonstrated greater estimation errors after a decrease rather than an increase in speed. Future work could

examine the robustness of the CC estimator by applying time varying disturbances such as sinusoidal speed variations, accelerations/decelerations and gait initiation/cessation. A simple decision rule, rather than using the state estimators, was used to determine the timing of the actuation disturbance to allow for an unbiased comparison. This approach enabled the performance of the individual estimation schemes to be evaluated in the presence of the same disturbances. Our use of the term "actuation disturbance" may seem unusual, since the nominal purpose of the PPAFO is to provide assistance with applied torque. However, by choosing to view applied torque as a disturbance, we are hoping to ensure that estimators perform well regardless of the control policy used.

On average, the speed disturbance increased estimation error by a factor of 2.4 for healthy subjects and 1.9 for the impaired subject, and the actuation disturbance increased error by a factor of 2.6 for healthy subjects and 1.6 for the impaired subject.

The CC estimator was more robust to the speed perturbation and performed better during the impaired walking trials (both with and without actuation) as compared to the FT and *k*NN estimator (Table 1 and Table 2). The performance of FT and CC estimators were comparable during healthy walking trials perturbed by actuation. The *k*NN estimator was not robust to either of the disturbances.

The CC estimator performed well during all of the perturbed walking trials. The results from the impaired subject are particularly noteworthy because these results are representative of the intended population for this assistive device. During both perturbed and unperturbed gait of the

impaired subject, the CC estimator outperformed the FT estimator by a minimum state estimation RMS error of 29% and a minimum event detection error of 23% (Table 1 and Table 2). The benefits of the CC estimator are also highlighted by the healthy walking trials with the speed perturbation, where the state estimate RMS error and event detection RMS error were up to 49% and 29% smaller than the errors resulting from the FT estimation. During the healthy walking trials with the actuation perturbation, the performance of the CC estimator was comparable to the FT estimator. Actuation perturbation introduced differences to the sensor readings with little change to the cycle period (T for 0 psi Normal: 1.16 ± 0.09 s vs. 110 psi Normal: 1.18 ± 0.04 s). As a result, the FT estimator maintained accuracy, while the CC estimator was adversely affected by the weaker correlation between sensor measurements and the sensor regression models (Figure 14, Figure 16).

While the FT estimate performed well with the healthy walkers during normal speed walking and with actuation perturbation, this estimator was not robust to the speed perturbation. Figure 18 clearly shows the degradation in performance of the estimator following the decrease in speed. The speed perturbation changed the cycle period, leading to a reduction in FT estimator performance because FT was dependent on a predetermined cycle period. The FT estimator did not outperform the CC estimator during any impaired walking trials. Table 1 shows that direct event detection (DE) RMS error was up to 6 times larger for the impaired subject than the healthy subjects during the normal walking trials. The increased event detection error is a significant component in the degradation of FT estimator performance for all impaired walking trials. Certain impaired walking patterns make event detection difficult, causing the DE estimator and any estimator relying on DE to perform poorly. In contrast, CC bases its estimate on the raw sensor measurements, not an assumed model of gait and thus is more robust to gait impairments.

2.5.3 APPLICATIONS TO CONTROL

As we have emphasized throughout this paper, many powered AFOs rely on gait events to determine control objectives [16, 17, 19, 20, 26, 54, 78, 80, 100, 101], and so reliable event detection is required for system control. Notable exceptions are powered orthotic systems that use surface EMG to directly control actuation [109]. That approach eliminates the necessity of gait event detection, but is limited by surface EMG signal reliability and availability.

In the current study, we have demonstrated that the CC estimator is able to accurately and robustly determine events during the gait cycle using data from PPAFO sensors. However, the CC estimator has broader applicability than just the PPAFO. In particular, a similar approach could be applied to provide state estimates for the control of any other assistive device (e.g., another orthosis or prosthesis) that has quasi-periodic inputs and outputs.

As we discussed in Section I, the control problem for an AFO has two parts, gait event detection and the controlled application of torque to meet the functional objective determined by each gait event. Our experiments showed the results (Table 1 and Table 2) of using state estimators to detect gait events but did not use these detected events as the basis for controlling torque. Future work will evaluate PPAFO performance during walking trials when state estimates (in particular, those provided by CC or FT) are used to control the actuation timing.

2.5.4 CURRENT LIMITATIONS

The key limitation of our current approach to state estimation is that it requires a preliminary training process. This process was necessary to construct models used for state estimation. Inaccuracies in the CC estimate were created by mismatched training and actual testing conditions. One approach to reduce these inaccuracies would be to parameterize the models with respect to other gait variables such as gait period *T*. In this scenario, gait period would be measured directly from one of the sensors (e.g., heel sensor) and used to select the appropriate model from a library of predetermined models in real time. The training process was also time consuming and could serve as an impediment for use in a clinical setting. This issue could be addressed by continuously updating the regression model during gait. Such an approach could allow the system to adapt to changing environments, reduce the amount of training required to build the models, and improve session to session robustness since the models would be constructed as the subject walked.

The key limitation of our experimental study was that we only examined estimator performance during steady state, level walking on a treadmill in the gait lab. In order to successfully implement the estimation techniques outside of the lab, modes such as overground walking, stair ascent/descent and ramp ascent/descent must also be addressed. One approach would be to generate individual models for each mode and apply a methodology to switch between them. We will address these issues in future work.

2.6 CONCLUSION

Accurate state estimates allow a powered AFO to adapt to changing environmental and functional needs. In contrast to previous methods of state estimation that rely largely on thresholding sensor measurements, this paper presented a method of state estimation based on cross-correlation between a window of past sensor measurements and a learned model. This approach—along with three others for comparison—was implemented on a powered AFO. Experiments with healthy and impaired subjects suggested that our cross-correlation state estimator provided the best overall performance.

Chapter 3 GAIT MODE RECOGNITION AND CONTROL FOR A PORTABLE-POWERED ANKLE-FOOT ORTHOSIS[2]

ABSTRACT

Ankle foot orthoses (AFOs) are widely used as assistive/rehabilitation devices to correct the gait of people with lower leg neuromuscular dysfunction and muscle weakness. We have developed a portable powered ankle-foot orthosis (PPAFO), which uses a pneumatic bi-directional rotary actuator powered by compressed CO_2 to provide untethered dorsiflexor and plantarflexor assistance at the ankle joint. Since portability is a key to the success of the PPAFO as an assist device, it is critical to recognize and control for gait modes (i.e. level walking, stair ascent/descent and ramp ascent/descent). While manual mode switching is implemented in most powered orthotic/prosthetic device control algorithms, we propose an automatic gait mode recognition scheme by tracking the 3D position of the PPAFO from an inertial measurement unit (IMU). The control scheme was designed to match the torque profile of physiological gait data during different gait modes. Experimental results indicate that, with an optimized threshold, the controller was able to identify the position, orientation and gait mode in real time, and properly control the actuation. It was also illustrated that during stair descent, a mode-specific actuation control scheme could better restore gait kinematic and kinetic patterns, compared to using the level ground controller.

[2] This work has been presented at conferences [87-89].

3.1 INTRODUCTION

Walking is a fundamental part of people's daily routine and an essential component in overall quality of life. Normal gait can be affected by symptoms resulting from numerous neurological disorders, muscular pathologies and injuries, including trauma, incomplete spinal cord injuries, stroke, multiple sclerosis, muscular dystrophies and cerebral palsy [1]. Powered lower-limb orthoses (e.g. robotic exoskeletons) can be used to assist everyday walking activities, as well as gait rehabilitation therapy. There are large populations with neuromuscular impairments that can be treated using a powered lower-limb orthoses. In the United States alone, these include: stroke (4M, [93]), polio (1.4M, [94]), multiple sclerosis (300K, [95]), spinal cord injuries (200K, [96]) and cerebral palsy (100K, [97]). These populations will continue to grow due to the aging Baby Boomer generation. Therefore, it is important to develop intelligent, energy efficient and affordable lower-limb orthoses to serve these growing needs. Recently, we have developed a portable powered ankle-foot orthosis (PPAFO) at University of Illinois at Urbana Champaign, which can provide modest dorsiflexor or plantarflexor ankle torque at different phases of gait for functional assistance, using a portable pneumatic power system [54]. The untethered design can allow power-assisted walking outside of the laboratory or clinic. Force contact sensors under the heel and toe and an ankle angle sensor allowed an embedded microcontroller to estimate gait state in real time [85].

One of the challenges that can prevent the PPAFO, or any powered orthotic/prosthetic device, from being widely used as an assistance/rehabilitation device for daily activities is the ability to recognize various gait modes (i.e. level ground walking, stair ascent/descent and ramp ascent/descent) and adapt to mode changes promptly. For the PPAFO, there were two critical aspects to this problem.

First, the original sensor array on the PPAFO had limited sensing ability (it only measured heel and toe contact forces and ankle joint angle), which cannot contain enough information to reliably detect all gait modes (e.g., during stair ascent and level ground walking, the force and angle readings were almost the same). Second, a new gait mode must be recognized at the earliest possible instant to prevent potential misfiring. Failing to adjust actuation for the current gait mode could increase fall risk for the user. Subsequently, with gait mode recognized in real time, the actuation control during each gait mode can be adjusted quickly to match the expected normative gait kinematics and kinetics of the recognized mode.

Currently, manual mode switching schemes are implemented in many applications due to simplicity and reliability. For example, Au et al. [110] required the user to flex the knee before switching modes, and applied a pattern-recognition technique on the EMG signal to recognize this intent. Similar approaches were used by Jin [111] and Wang [112] for transfemoral prostheses, as well as for other types of prostheses (hand and arm prostheses) by other researchers to recognize the user's intent [36, 113-117]. While the EMG approach had the benefit of high robustness and reliability, it had a major limitation that additional EMG electrodes had to be attached to the human body all the time, which would result in increased system complexity and affect the user experience. Additionally, the number of recognized modes was limited by the number of EMG patterns that a user could successfully trigger without misfire or getting confused. Huang et al. used the combination of EMG and mechanical sensors to detect multiple gait modes including ramps and stairs with high reliability [118], but required extended sensor array. Alternatively, Ottobock's C-Leg could switch modes by tapping the heel multiple times continuously [119]. The knee prosthesis could then be locked for better stability. These two schemes were not considered ideal solutions for

intent recognition, as additional user intervention was needed. Goldfarb et al. [61, 120-122] used mechanical sensors mounted on the powered prosthesis for intent recognition, which was able to successfully detect stand, sit, stumble, different walking speeds and different upward ramps on a transfemoral prosthesis. Their recent ramp walking study also demonstrated that recognizing ramp ascent and controlling the prosthesis differently to adapt to the functional needs can reproduce several kinematic characteristics of healthy ramp ascent that passive prosthesis does not. But they had not yet shown the ability to detect stair activities.

Multiple efforts had been made to develop an autonomous system for gait mode recognition. Zhang et al. [123] used an inertial-measurement-unit (IMU) fixed to the torso and a laser distance sensor to map out the terrain in front of the user to predict gait mode; the shortcoming of this method was the need of a sensor attached to the user's body and intense computer computation cost of combining the IMU with laser data. Although it showed promise in its ability to observe, predict and respond to the terrains in front of the user, the lack of accuracy and reliability in current technology had prevented it from being broadly used. Coley et al. [124] proposed a recognition algorithm that used only a gyroscope attached to the torso, but the detectable mode was limited to stair ascent. Furthermore, that strategy was dependent on future information, thus it was not a causal algorithm that can be implemented in real time.

To sum, there is currently no available automatic gait mode recognition scheme that is capable of reliably detecting multiple modes including ramps and stairs.

We propose tracking body motion using inertial sensors (IMU) and recognizing gait modes based on tracked position and orientation. IMU based motion tracking has been an emerging topic and attracted much attention thanks to the advantage of not depending on an external reference source. Recently, the availability of low-cost and small-size, micro-electro-mechanical systems (MEMS) sensors has made it possible to implement it on compact devices that need orientation and position estimates, including powered prostheses and orthoses.

In this study, an IMU based motion tracking algorithm was implemented and five modes were recognized. Different actuation control schemes were applied based on recognized gait modes and the experimental results of kinematic and kinetic data in the scenarios of with and without gait mode recognition were compared and analyzed.

3.2 METHODS

3.2.1 ANKLE DYNAMICS FOR STAIR WALKING ACTIVITIES

Previous studies had shown that for healthy individuals, ankle dynamics of stair ascent/descent vary significantly from level walking [110, 125-129]. Therefore, it was important to recognize changes in gait mode in real-time, so that the actuation would be provided at the proper time and in the right direction.

To better illustrate the necessity for a mode recognition scheme, we discuss normative ankle moment characteristics during stair descent compared to level walking based on the results from [125] and illustrated in Figure 19. During normal level walking, ankle moment gradually increases and peaks at late stance (50% Gait Cycle) to propel the body forward. In contrast, for stair descent, the first peak moment is at the beginning of the gait cycle (about 10% GC, as a toe strike, opposed to heel strike). Energy is absorbed during stair descent (or the weight acceptance phase). The ankle joint is also plantarflexed to prepare for the landing. The second moment peak (at 50% GC) shares similar timing as level walking, but with a substantially smaller magnitude. Thus a smaller plantarflexor torque, compared to level walking, should be applied at this portion of the gait cycle. It can be concluded that the functional assistance for different gait modes differs significantly and it is necessary to develop a real-time gait mode recognition scheme. On the other hand, the ankle moment for stair ascent and level walking share similar trends that they do not have to be treated differently.

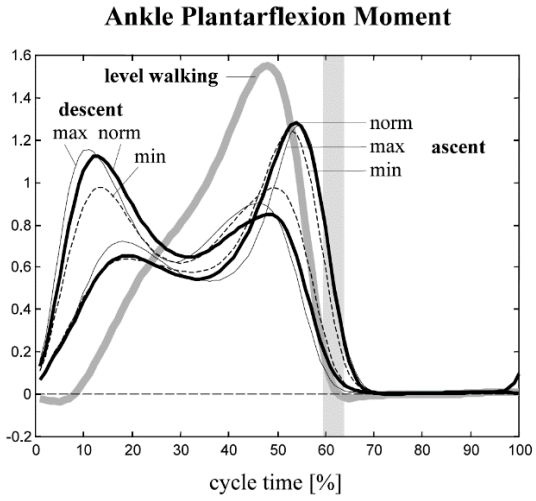

Figure 19 Normal healthy ankle joint moment as a function of percent gait cycle in three gait modes: level walking, stair descent and stair ascent. (From [125], reproduced with approval.)

3.2.2 INTRODUCTION OF THE PPAFO

The portable powered ankle-foot orthosis (PPAFO) was developed from mainly off-the-shelf components to provide powered assistance to an ankle joint (Figure 20) [54]. A compressed CO_2 bottle with embedded pressure regulator (JacPac J-6901-91, 20 oz capacity; Pipeline Inc., Waterloo, ON, Canada) attached to the subject's waist allowed for untethered power assistance. The rotary actuator at the ankle joint is a dual-vane, bidirectional pneumatic actuator (PRN30D-90-45, Parker Hannifin, Cleveland, OH) that was rated for 150 psig and could generate about 12 Nm of torque at 100 psig pressure in both dorsiflexion (toes up) and plantarflexion (toes down) directions. The embedded regulator on the CO_2 bottle controlled the pressure supply for plantarflexor assistance (set to 100 psig), while the additional regulator (LRMA-QS-4; Festo Corp-US, Hauppauge, NY) further reduced the pressure (set to 30 psig) for dorsiflexor assistance based on the needed torque to lift the foot so that this muscle group was not overpowered. Excessive dorsiflexor torque is

unnecessary to support the foot during swing and can result in subject discomfort. Two solenoid valves (VOVG 5V; Festo Corp-US, Hauppauge, NY) were used to control the actuation. Three actuation states could be achieved through the combinations of the solenoid valves: dorsiflexion, plantarflexion and passive (no actuation). Actuation was controlled by embedded micro-controller (MCU). The MCU (TMS320F28335, CPU:150 MHz, Sampling Rate for forces and angle: 1 kHz. Texas Instruments, Dallas, TX) read two force resistive sensors located at the heel and the toe of the foot plate (#403, 2" square; Interlink Electronics Inc., Camarillo, CA, USA) and a rotary potentiometer at the ankle joint (53 Series, Honeywell, Golden Valley, MN).

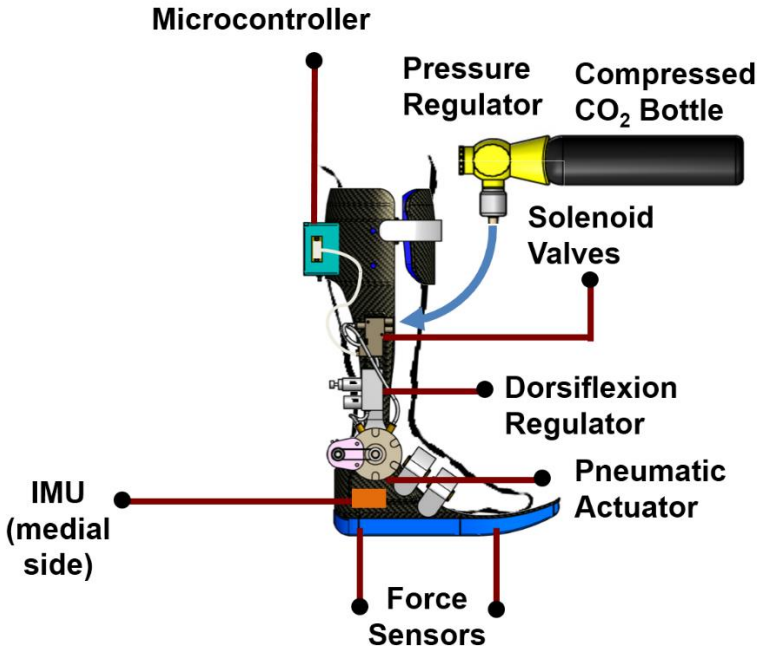

Figure 20 The Portable Powered Ankle-Foot Orthosis (PPAFO). The pneumatic rotary actuator at the ankle is driven by a bottle of compressed CO2, which is worn on the subject's waist.

3.2.3 Current Control Scheme for Level Ground Walking

In previous studies, we have demonstrated the PPAFO system's ability to provide torque assistance during typical level ground walking [54]. Four functional tasks are defined by different regions of gait (Figure 21): (1) initial contact, (2) loading response, (3) forward propulsion and (4) swing. Each task was determined using a state estimation algorithm that we had previously developed. This algorithm compared the sensor history data (contact forces and ankle angle) to a pre-computed training model to determine the current state and task [85]. During each task, full actuation in one direction was provided.

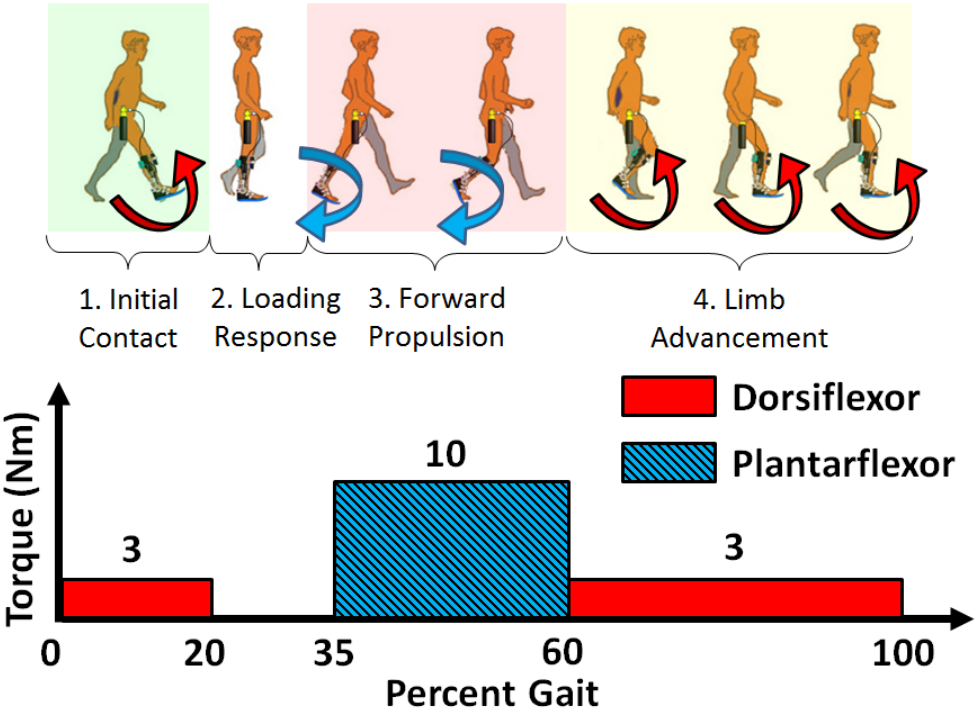

Figure 21 Assistive torque at different times in a gait cycle during level ground walking: dorsiflexor assistance from 0% to 20%, plantarflexor assistance from 35%-60%, and dorsiflexor assistance from 60% to 100%.

3.2.4 TRACKING MOTION USING AN IMU

We used an IMU (XSens MTi-28A53G35, XSens Technologies. Enschede, The Netherlands) to track the orientation and position of the PPAFO's foot piece, because they could be directly used to identify gait modes. The stair modes were recognized by comparing the vertical position difference of each step to a threshold (Figure 22), and the ramps modes were detected by examining foot orientation via foot pitch angle when the foot was in full contact with ground.

Only 3-DOF acceleration and 3-DOF angular rate were measured by the IMU at 200Hz. Although the IMU had an embedded magnetometer, due to the complex environment that we have targeted including indoors, outdoors, or inside a clinic or lab while working with other electronic rehabilitation devices, the magnetometer was not used, as it demonstrated very poor reliability and lack of consistency during indoor activities. Instead, the orientation drift was compensated by identifying certain gait phases in which the relative orientation was known, as described below.

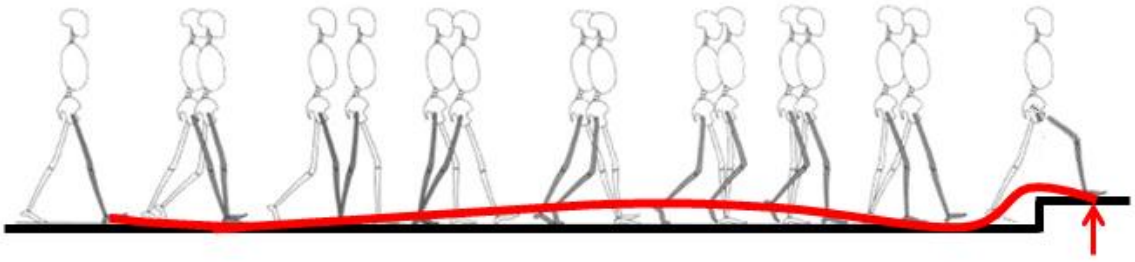

Figure 22 Illustration of tracking position to recognize stair walking mode. Ground surface and stairs were indicated by black lines. The tracked vertical position (red line) was compared at each step heel strike to recognize gait modes.

3.2.5 ESTIMATING ORIENTATION

In order to track the real-time position, the accelerations had to be rotated into Earth coordinates, which requires pitch and roll angle of the IMU. Thus, the orientation of the IMU had to be estimated first. The orientation was also used to determine the foot pitch angle for ramp recognition. Data from the gyroscopes are used to track the orientation. A quaternion based coordinate system was used to avoid gimbal lock problem.

The initial orientation was inversely estimated [130] by the gravity vector measured during 5 seconds of static calibration at the beginning of the experiment when the subject wore the AFO and stood upright without moving. The yaw angle was ignored because it could not be estimated without a magnetometer. Additionally, yaw angle is irrelevant to measuring vertical position.

With an initial estimate of the orientation, the real-time orientation was tracked from the angular rates. Simply double integrating the angular rate usually does not provide an accurate orientation estimate, due to long-term drift errors. A common approach to avoid drift is to use complementary sensors such as a magnetometer. The magnetometer is often added to the same package of 3-axis accelerometer and 3-axis gyroscope, and the package is referred as a MARG sensor [131]. The 9-DOF data can be fused using a Kalman or complementary filtering algorithm [132-134].

However, in this study, due to reliability concerns, the magnetometer was not used. Instead, the calibration was achieved by combining the accelerometer and rate gyro with the heel and toe contact force sensors that already existed on the PPAFO to detect calibration instants, similar to [135].

Zero-rate instants were used for orientation recalibration, while zero-acceleration instants were used for velocity recalibration.

A zero-rate instant was defined as when the PPAFO was in full contact with the ground (with both force sensors compressed). At this time instant, the IMU itself was assumed to be static relative to Earth coordinates, which was equivalent to zero readings from the gyroscope, as in

$$\|\omega\| < \varepsilon_1 \tag{19}$$

where ω was the angular rate from the gyroscope, and ε_1 was a heuristically tuned threshold for determining the zero-rate instant. ε_1 was tuned such that the zero-rate instant would only happen when the controller was certain that the AFO was flat on the ground and not rotating. From the experiment, usually it happened when the subject was standing still before the start of walking, which was sufficient to correct the gyroscope drift.

3.2.6 Estimating Position

Once the orientation was known, the real-time position could be tracked. Yun et al. [136] proposed an algorithm for self-contained position tracking for human motion. The cumulative error in tracked velocity due to long-term drift was recalibrated, and the position was compensated at every zero-acceleration instant. A zero-acceleration instant usually happened at every step (Figure 23), but it could be skipped if the criterion was not satisfied. The criterion for determining zero-acceleration was,

$$\|a - g\| < \varepsilon_2 \tag{20}$$

where a was the acceleration from the accelerometer converted to Earth coordinates, g was the gravitational vector, and ε_2 was a heuristically tuned threshold for determining the zero-acceleration instant. The threshold was chosen such that zero-acceleration instant would occur at almost every step, with the exception when the foot was not static enough during stance, where (20) would not be met.

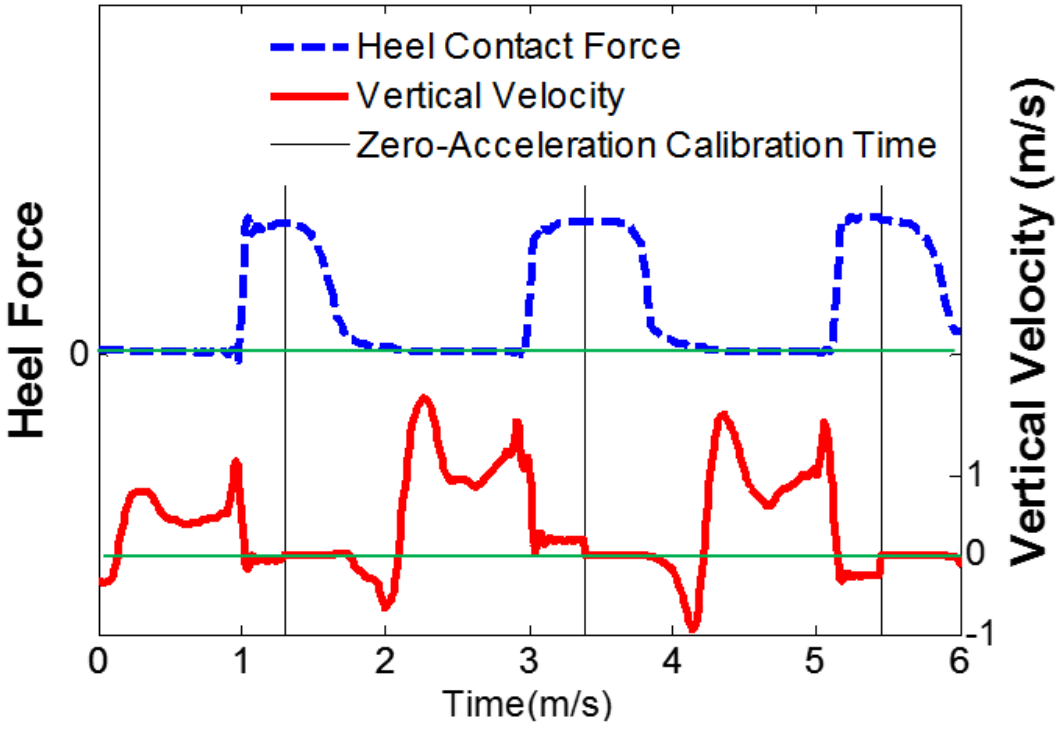

Figure 23 Vertical velocity profiles are re-zeroed based on accelerations and heel force.

The zero-acceleration instants were identified when (20) is met and the AFO is in full contact with the ground (both force sensors compressed). At each zero-acceleration instant, the tracked velocities were recalibrated to zero, and the tracked positions were compensated,

$$\Delta P_z = -\frac{1}{2} V_z T \tag{21}$$

where ΔPz was the vertical position compensation based on tracked vertical velocity V_Z. T was the elapsed time from the last zero-acceleration recalibration. The vertical position compensation was derived based on the assumption that there was a constant offset in measured acceleration, which resulted in drifted V_Z. The acceleration drift constant and elapsed time since last zero-acceleration recalibration is used to find the appropriate value based on this theory [136].

3.2.7 Recognizing Stair and Ramp Modes

Next, the vertical position was sampled by the microcontroller at each time of heel strike (or toe strike), and compared to the vertical position from the previous step to calculate the change. The vertical position change at the n^{t}h step Z(n) was defined as,

$$Z(n) = P_Z(t_{HS}(n)) - P_Z(t_{HS}(n-1)) \tag{22}$$

where tHS (n) is the nth heel strike time and t_{HS} (n-1) is the one before.

Now the gait mode $M(n)$ can be recognized by applying thresholds on Z(n) each time after heel strike

$$M(n) = \begin{cases} \text{Stair Ascent}, & \text{if } Z(n) > T_A \\ \text{Stair Descent}, & \text{if } Z(n) < T_D \\ \text{Level or Ramp}, & \text{otherwise} \end{cases} \tag{23}$$

where T_A and T_D were the thresholds for ascent and descent vertical position, and $M(n)$ represented the gait mode between the n-1th and n^{th} heel strike.

To distinguish whether a change in vertical position associated with a stair or ramp ascent/descent, the foot pitch angle was also examined. Foot pitch angle was tracked by the IMU orientation at the first instant when both heel and toe force sensors were simultaneously in contact with the ground (roughly about 25% of gait cycle). In the cases when the subject could not activate both force sensors, percent gait state (25% GC) could be used to help identify the timing to sample the foot pitch angle.

The pitch angle was offset to 0 at flat ground during the 5 second calibration trial. Pre-defined thresholds were used to examine the pitch angle to check whether the foot was in contact with an inclined or declined surface, which was considered as a ramp,

$$M(n) = \begin{cases} \text{Ramp Ascent}, & \text{if } C(n) > R_A \\ \text{Ramp Descent}, & \text{if } C(n) < R_D \\ \text{Level or Stair}, & \text{otherwise} \end{cases} \quad (24)$$

where C(n) was the foot pitch angle sampled each step when the foot was in full contact with ground, and R_A and R_D (5˚ grade used in the experiment) were the pre-defined threshold for ramp ascent and descent. They remained the same values for all trials and subjects.

3.2.8 THE OPTIMAL THRESHOLDS FOR UNBIASED RECOGNITION

Thresholds were used in both stair and ramp recognition schemes. The choice of threshold values for mode recognition was crucial for reliably detecting a new gait mode and reducing the inaccuracies introduced by the IMU. Intuitively, if the threshold value for level walking to stair ascent transition (T_A) was too high, it was likely that the microcontroller would falsely detect an

actual stair ascent as level mode. Likewise, if the choice of T_A was too low, the microcontroller would interpret actual level walking as stair ascent mode. In addition, the choice of thresholds have to do with the accuracy of tracking at different modes (i.e., if we had better accuracy in level mode, the threshold could be chosen to be closer to zero, which would better tolerate the potential errors in ascent mode). Therefore, we derived theoretical optimal threshold values to maximize the reliability of the mode recognition scheme.

A preliminary training session was used to collect vertical position change data and foot pitch angle data in different walking modes. Based on the training data, an optimal threshold was found for unbiased mode recognition.

Vertical position changes in the same mode were assumed to be a Gaussian distributed random variable with fixed mean and standard deviation. Therefore, for level walking mode,

$$Z(n) \sim N(0, \sigma_L^2) \tag{25}$$

where σL was the standard deviation for $Z(n)$ in level ground walking mode. Similarly, for stair ascent mode,

$$Z(n) \sim N(h, \sigma_A^2) \tag{26}$$

where σA was the standard deviation for Z(n) in stair ascent mode and h is the stair rise for the stairs, assuming one stair traverse for stair walking. Note that technically the mean of the distribution could deviate from their expected values. Nevertheless the expected values are used for ease of derivation.

Two types of error could be described in a null hypothesis: the actual gait mode is level ground mode (Figure 24)

Type I error (false negative) B_A: Mistaking level mode as ascent mode

Type II error (false positive) B_L: Mistaking ascent mode as level mode

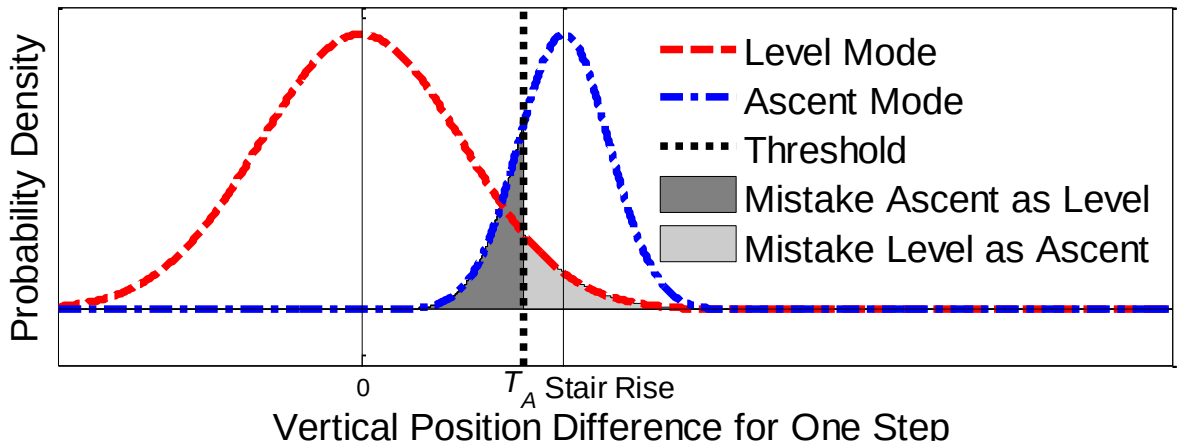

Figure 24 Impact on two types of error from the choice of threshold.

Define the cost function as the bigger value of the two types of error,

$$C = \max(B_A, B_L) \tag{27}$$

Therefore, the optimal threshold can be found as,

$$T_A = \frac{h\sigma_L}{\sigma_L + \sigma_A} \tag{28}$$

3.2.9 Actuation Control for Stair Descent Mode

As discussed in the previous section, the actuation control for stair descent mode has to be different from that of level ground walking control, to address the functional needs of stair descent. During stair descent, in order to make sure the ankle joint is plantarflexed before the next step landing, plantarflexor actuation would start in the second half of swing. The torque would remain until the late-stance phase of the next cycle so that the weight impact from stair descent could be absorbed. This actuation strategy was also chosen because it was impossible to fully match the torque needed in Figure 19 using only a set of solenoid valves. A revised actuation strategy provided plantarflexor torque of 10 Nm during 0-50% and 80% to 100% of gait cycle.

3.2.10 Experimental Protocol

A preliminary training session was conducted to collect vertical position and orientation data for threshold tuning. One subject wore the PPAFO without actuation, and walked for five trials in five different modes (level, stair ascent/descent, ramp ascent/descent). Training data were collected and processed to compute the thresholds for both stairs and ramps. The thresholds were made available to the microcontroller and remained the same for rest of the study.

Experimental tests were conducted to assess the accuracy of the gait mode recognition algorithms and effectiveness of gait mode control. At the beginning of each trial, 5 seconds of calibration data were collected while the subject stood upright while wearing the PPAFO.

Five healthy male subjects were tested (average age: 23.4yrs, weight: 82.0kg, height 178.6cm). Approval was received from the University of Illinois Institutional Review Board (IRB#12825).

Four scenarios were tested to examine different challenging walking environments: outdoor stairs - one stair traverse (h=14cm, the smallest stair rise), outdoor stairs - two stair traverse (h=28cm), indoor stair - two stair traverse (h=34cm, larger stair rise compared to outdoor), and indoor ramp (6 degrees grade). In each stair (ramp) scenario, the subjects walked over a mixture of level ground, stair (ramp) ascent and descent to test the performance in each mode.

To evaluate the effectiveness of the gait mode controller, three actuation conditions were implemented in each scenario: passive (no actuation), mode controller (stair descent was controlled to have plantarflexion during swing, actuation specific for stair descent) and level controller (always provide dorsiflexor actuation regardless the gait mode, generic actuation used during level walking). The level controller condition was added to examine what would happen if the gait mode was not recognized during stair descent (it would be controlled as level ground instead).

The overall robustness of the algorithm was examined by combining the performance in all the trials of all five subjects. The success rate was defined as,

$$\text{Success Rate} = \frac{\#\text{ of Correctly Recognized Steps}}{\#\text{ of Total Steps}} \times 100\% \tag{29}$$

3.3 RESULTS AND DISCUSSION

3.3.1 EXPERIMENTAL OBSERVATIONS

The gait mode recognition algorithm was able to track vertical position changes at each step and used the optimized thresholds to determine stair modes. In Figure 25, on the left, the tracked vertical position was plotted versus time. Position was reset to zero at every step. The estimated change in vertical position (symbols) showed excellent agreement with the true stair rise. In the figure, if an estimated vertical position difference was greater (less) than the threshold value, the algorithm would consider the step to be stair ascent (descent).

Similarly, an illustrative case (Figure 26) demonstrated that the ramp modes could be recognized by sampling the foot pitch angle when both the heel and toe sensors were simultaneously activated (about 25% of gait cycle). On the right, where the foot pitch angle was plotted against gait percent, it can be observed that around the sample time (~25% GC), the two ramp modes could be clearly distinguished from level walking mode.

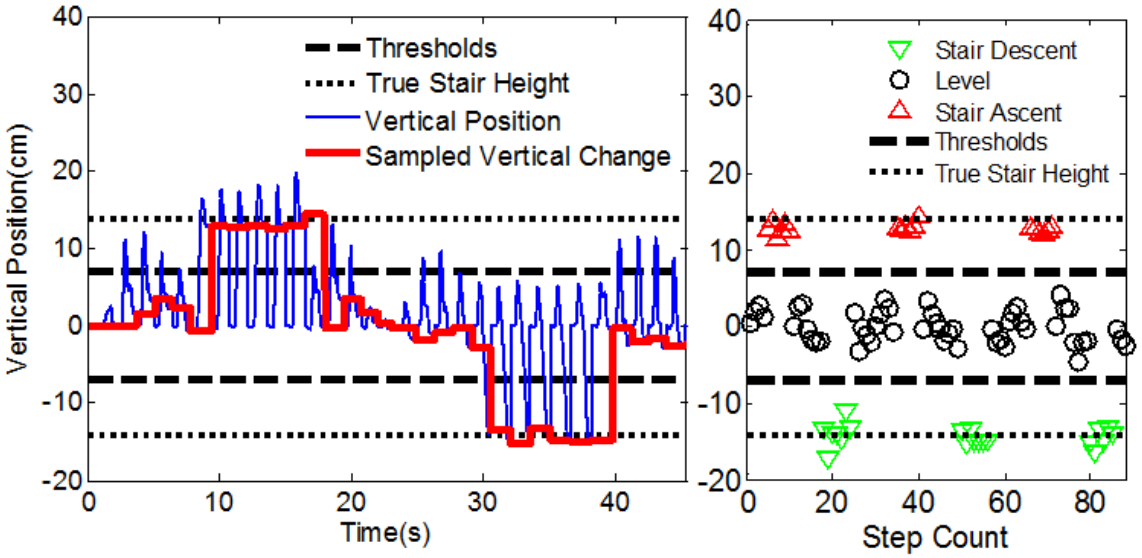

Figure 25 Illustrative case of gait mode recognition of stair ascent/descent mode (indoor, one stair traverse).

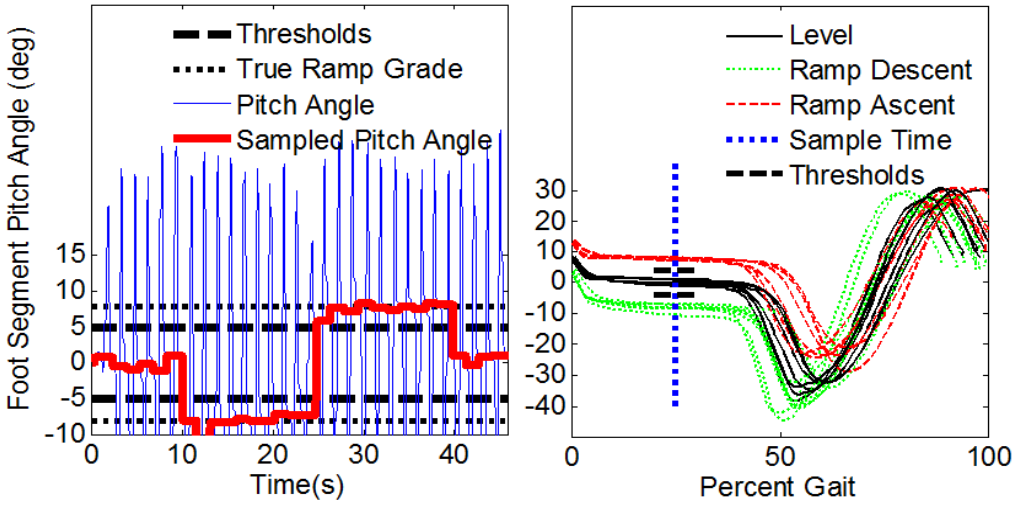

Figure 26 An illustrative case of detecting ramp mode (passive, indoor ramp)

The results of the success rate of different subjects in different scenarios are found in Table 3. The mode recognition algorithm successfully detected the correct mode in at least 92% of the trials. The

correct mode was detected in 4 of 5 subjects for 96% of the trials. One subject (subject 2) showed lower success rates than other subjects. For the ramps, although no subjects reached 100% in all trials, the consistently high success rate of over 98.5% illustrated that ramp recognition was in general more robust compared to stair recognition.

Table 3 Success Rate for Different Scenarios and Subjects

Subject	**Success Rate (%)**			
	Outdoor One Stair Traverse	**Outdoor Two Stair Traverse**	**Indoor Two Stair Traverse**	**Ramp**
1	100.0	100.0	100.0	99.0
2	94.7	92.2	97.4	98.5
3	99.6	97.6	100.0	99.3
4	98.5	96.0	100.0	99.0
5	98.8	100.0	100.0	99.6
Avg	98.3	97.2	99.5	99.1

Differences in gait kinematics and kinetics among the three controller conditions were found during stair descent mode (Figure 27). The passive condition represented the natural gait pattern for healthy normal subjects. The mode controller condition represented the result when the stair descent gait mode was correctly recognized and the actuation matched the mode, while the level controller condition described the outcome when the level ground controller was used even during stair descent mode. It was observed from the figure that the ‘toe strike’ phenomenon in passive condition

(significant toe force at the beginning of the cycle) was reproduced by the mode controller. The level controller, however, failed to do so. Compared to the level controller condition, the angle joint angle pattern for the passive condition was also more similar when using the mode controller condition. This incorrect behavior occurred in the level controller condition because when using the level walking controller, the AFO held the toes up during swing, which allowed very little range of motion. Whereas for stair descent, it was preferred to plantarflex the foot to prepare for contact with the next stair.

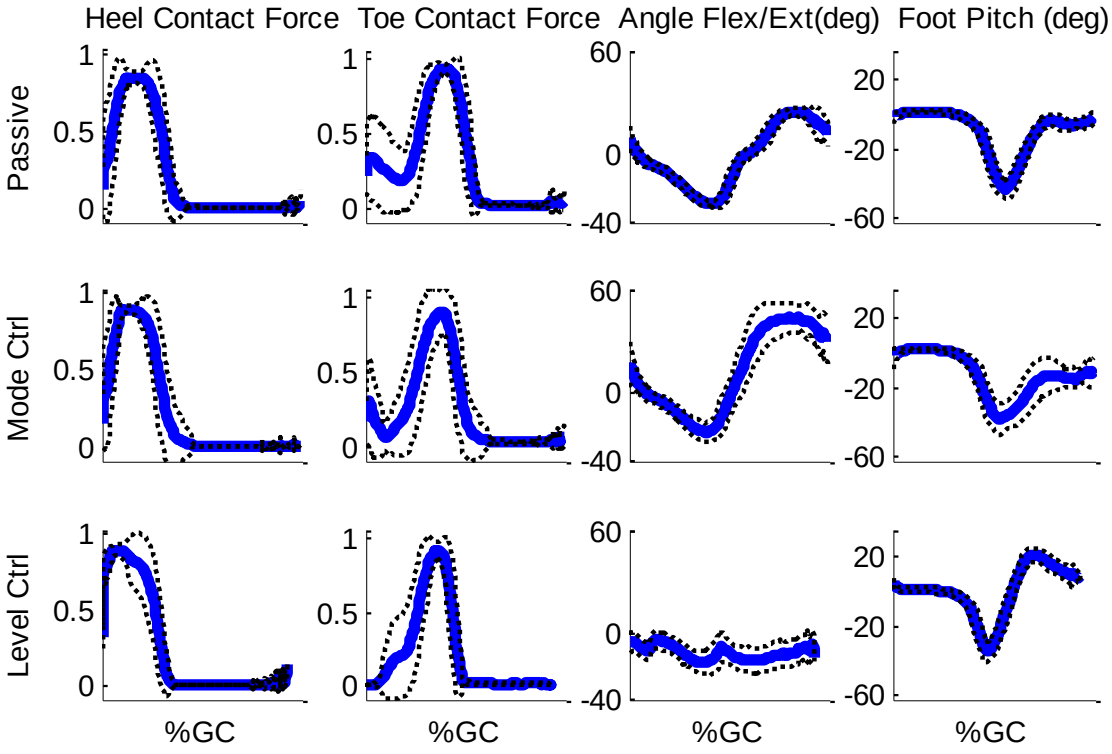

Figure 27 Kinematic and kinetic comparison during stair descent mode (outdoor, one stair traverse) for three controller conditions. The mode controller was better able to reproduce the gait patterns of the passive mode; while the level controller was not appropriate for stair descent.

3.3.2 LIMITATIONS

Although the mode recognition scheme showed promising success rates and was able to demonstrate that it could produce a more natural gait pattern during stair descent compared without having any mode recognition, it suffered from several limitations, such as one step delay and fall risks that were not accounted for in the cost function. These limitations will be discussed separately in rest of this section.

3.3.2.1 ONE STEP DELAY

We made the assumption that the gait mode identified from the immediate past step would stay the same for the current step. Therefore, the actuation could be controlled based on the identified mode as described above. One drawback of this approach is the delay during the mode transition. Due to hardware limitations, the current IMU based scheme could only switch modes no earlier than the end of the first step. In other words, the first step transitioning into a new mode was always unrecognized. This problem could be critical in the scenarios when the subjects have trouble stabilizing themselves. Misfiring in the beginning of a transition can result in a trip or fall. As minimizing the user's risk is the highest priority of the PPAFO design, to address this issue future studies will explore options to allow for zero-delay, such as instrumenting the contralateral limb, infrared (IR) distance sensing, etc.

3.3.2.2 Defining Weighted Cost Function

We currently use the higher error probability as the cost function. The underlying assumption is to treat the importance of correctly identifying each mode equally. In reality, this simplistic approach might not be the best choice.

Some modes have smaller risk when misidentified. For example, when choosing the threshold for descent/level walking, incorrectly detecting actual level mode as descent mode has a much smaller risk compared to the opposite scenario. For safety concerns, instead of minimizing the chance of error equally, the best solution would be to minimize the expected risk and the potential danger that can be caused by mode switching. Consequently, it would be desirable to redefine the cost function, where the greater risk mode can be emphasized and penalized. Future work will address this weighting.

3.3.2.3 Actuation Control

Currently, as a simplified approach, we have only changed the actuation control scheme for stair and ramp descent modes. It is desirable to customize the control specific to each of the gait mode based on their kinetic characteristics. Ideally, the controller would have an embedded library of kinetic profiles of different modes, and the mode recognition scheme would be able to select a control scheme from the library using real-time recognition results.

3.3.2.4 JUSTIFICATION AND COMPARISON ON RECOGNITION RELIABILITY

In this study, the success rate for recognizing the gait mode was demonstrated to be at least 92% with an average of 97% for all users. In the current literature for human assist devices (prostheses and orthoses), no standardized procedure has been established to validate the success rate in the mode or intent recognition reliabilities. Most intent recognition studies only report success rate numbers without discussing whether the rate is a satisfactory result with regard to operational reliability (Table 4).

3.3.2.5 VALIDATION ON IMPAIRED SUBJECTS

In this study, only five healthy subjects were tested to examine the accuracy and robustness of this algorithm. While the promising results demonstrated the controller's ability to recognize modes in real time, further experiments are needed to validate the performance on impaired subjects. As we learned from Study 1, the force patterns from impaired subjects could significantly differ from healthy normal subjects, depending on the types of gait disabilities. Since our current gait mode recognition scheme used contact forces to identify when the foot was on the ground for calibration purposes, this reduction in force pattern could potentially result in reduced reliability in gait mode recognition. The current method of identifying ground contact might need to be revised to accommodate different types of gait patterns.

Table 4 Intent Recognition Success on Different Human Assist Devices

Device Type	Sensors	Recognized Types	Success Rate	Authors	Year	Comments
Transtibial Prosthesis	EMG	Level Stair Descent	100%	Au et al. [110, 137]	2008	Only one Trial
Transfemoral Prosthesis	EMG + Mechanical	Ramps, Stairs, Level, Obstacle	95% - 99%	Huang et al. [118]	2011	
Transfemoral Prosthesis	Mechanical Sensors	Walking, Sitting, Standing	94%	Goldfarb et al. [70]	2010	0.5s delay
Transfemoral Prosthesis	EMG	Ramps Level, Stairs	84% - 98%	Jin et al. [111]	2006	Intact & amputees
Walking Recognition	IMU + Laser + EMG	Ramps Level, Stairs	95.5%	Wang et al. [112]	2013	0.5-1s delay
Arm Recognition	EMG	7 motions	90%	Englehart et al. [138]	2012	Intact & amputees
Arm Recognition	EMG	Wrist Down/Right/Twist	92.7%	Momen et al. [114]	2007	
Arm Recognition	EMG	Wrist, Finger Flexion	94% - 99%	Ajiboye et al. [115]	2005	
Arm Prosthesis	EMG	Elbow/Wrist Extension/Flexion	95.5%	Soares et al. [36]	2003	
Hand Prosthesis	EMG	5 Types of Grip	90.4%	Wojtczak et al. [116]	2009	
Instrumented Glove	Position, Orientation	15 types of grasp	97%	Ekvall et al. [117]	2005	65% for other users*

* Success rate was based on a trial, where the same user was trained and tested. If the model for one user was applied on others, the success rate dropped to 65%

There appears to be two main reasons why such a standard has not been established:

A. Across different types of human assist devices, there are no standardized types of intent or mode that the majority of the researchers agree on. As a result, categorization of mode types varies significantly among different schemes, depending on the sensor availabilities and identified necessary modes. The lack of mode standards adds to the difficulties of establishing a procedure to justify reliability rate, due to its limited applicability.

B. The concept 'success' itself is challenging to define: it is often specifically related to the targeted application, user acceptance, and liability in the case of a failure. For example, whether a misfire is acceptable depends on many other application specific conditions: How likely will it cause a trip of fall? What is the user's own ability to maintain balance? Is it a partial or full power assistance? Does the user have enough experience and expectation on such type of failure?

1) Comparison to Other Human Assist Devices

To better understand and compare the results from different algorithms on intent recognition, reliability results across different human assist devices were collected and reported (Table 4). Similar to our intent/mode recognition scheme, the success rate in those studies were defined as the ratio between the number of successfully recognized trials and the total number of trials.

For powered lower-limb prostheses (transfemoral and transtibial), different gait modes were recognized by EMG, mechanical sensors or the combinations of both. The success rate ranged

from 84% to 99%, with an exception of one illustrative trial of 100% correctness [137]. It was difficult to reach 100% for lower-limb prostheses because the available time allowed for the controller to recognize gait mode was often limited (less than 1s). Additionally, because users had to voluntarily keep balance and compensate for imperfect actuation during the trials, perturbations were further introduced back to the system and added to the difficulty of perfect mode recognition.

For powered upper-limb prostheses (arms and hands), since there was no need to keep the balance of gait, the perturbation and noise from human's locomotion compensation had minimal effect. However, mostly EMG based algorithms suffer from not having well defined tasks: in most studies, the training model came from one initial user and were applied to the rest of the test subjects. Due to the complexity and variability of different hand and arm positions between different users, the repeatability and reliability of the pattern recognition algorithms were greatly impacted.

In summary, the 98% success rate of the PPAFO mode recognition scheme reported in this study was ranked reasonably high among the surveyed human assist devices, considering the full range of recognizable modes and minimal invasion to the human body.

3.4 SUMMARY

One of the challenges that powered orthotic or prosthetic devices must address is the ability to recognize gait modes (i.e. level ground walking, stairs, ramps, etc.) and adapt to mode changes promptly with proper control actuations. In this study, an inertial measurement unit (IMU) based scheme was proposed to track the real-time 3D position and orientation of the PPAFO for gait mode recognition. A compensation scheme using inertial sensors and force sensors was implemented to correct long-term drift problems. An optimal threshold method was used to minimize error in mode recognition. In different gait modes, actuation control schemes were applied to meet the different functional needs. The experimental results showed that during stair descent, compared to a controller without mode recognition, using the proper mode recognition and actuation scheme to control the device can provide more natural gait patterns (i.e. closer to healthy normal subjects). A brief discussion on how to evaluate the reliability results from this study examined literature on other human assist devices as reference.

.

Chapter 4 System Efficiency Analysis and Energy Recycling of a Portable Pneumatically Powered Ankle-Foot Orthosis[3]

Abstract

Fluid power systems show potential as enabling technology for human assistive devices. This potential is particularly true for mechanical devices designed to assist gait: a high-force, low-velocity application. The key advantages of fluid power over purely electromechanical systems are the high force-to-weight and force-to-volume ratios of the actuator and the ability to actuate a joint without a transmission. As such, a novel, pneumatically powered, portable ankle-foot orthosis has been developed and tested to assist individuals with below-the-knee muscle weakness. Currently, the device has a limited duration of use due to its inefficient utilization of pneumatic power. This study separated the overall system efficiency into system operational efficiency and system component efficiency. An improved pneumatic operation was implemented to recycle the exhaust energy from a previous actuation and to power the subsequent one. The overall system efficiency was improved from 20.5% to 29.7%, saving 31% of fuel for each actuation. The work losses across different pneumatic components and the solutions to improve them are also discussed.

[3] This work was presented in conferences [90, 91].

4.1 INTRODUCTION

Ankle-foot orthoses are important in improving gait function of people with lower leg neuromuscular dysfunction and muscle weakness. An ankle-foot orthosis (AFO) is an external device worn on the lower leg and foot that provides mechanical assistance at the ankle joint. In the US alone, more than one million people experience functional limitations in activities of daily living as a result of stroke [93]. These numbers will continue to increase in numbers as the population ages. The use of AFOs can help many populations (including stroke survivors) to regain mobility. Current technologies available to assist gait focus predominately on passive AFOs. A passive AFO is capable of motion control, but unable to provide torque assistance at the ankle [7-12, 15]. Powered AFO systems are able to provide torque assistance as well as motion control; however the current systems are limited in portability due to the need to be tethered to the power source [19, 26, 139].

We have developed an untethered powered AFO system - the portable powered ankle foot orthosis (PPAFO) [54]. Our system uses fluid power in the form of pneumatics to supply torque at the ankle and provide motion control. The portable power source is a small tank of compressed carbon dioxide (CO_2) that can be worn at the waist. The pressurized gas is used to drive a bi-directional actuator, which is capable of providing both dorsiflexion (toes up) and plantarflexion (toes down) assistance. Embedded sensors and micro-controller unit are used to determine the timing for needed assistance during the gait cycle. The portable power source and onboard electronics afford the PPAFO the freedom to be used in a variety of settings (clinic, laboratory, hospital, or even home).

One of the limitations of the PPAFO system is limited usage time due to the power available in the small tank of compressed CO_2. The tank is approximately the size of a one liter beverage container. Larger tanks could not be worn at the waist and would require either a backpack or rolling cart (e.g. oxygen tank). The current configuration of the PPAFO is only capable of ~20 minutes of continuous walking assistance out of a tank that contains 567 g of compressed CO_2. In order to improve the run time without increasing the size of the power source, an energy efficiency analysis was conducted and solutions to enhance the overall efficiency were proposed and implemented.

The body of this paper presents the systematic energy efficiency analysis of the PPAFO system. First, the PPAFO system will be introduced in detail, including the pneumatic circuits and control system used for testing. Second, the system efficiency will be separated and analyzed in two independent categories: operational efficiency and component efficiency. The operational and component efficiency analyses combine for a completed system analysis that allows for insight into future modifications that will improve the overall function of the system.

4.2 METHODS

4.2.1 SYSTEM DESCRIPTION

4.2.1.1 PPAFO SYSTEM

The PPAFO system provides portable powered assistance to an ankle joint. We built a pneumatic system to provide assistive torque using a rotary pneumatic actuator (Figure 28 and Figure 29). A tank and pressure regulator of compressed CO_2 (JacPac J-6901-91, 20 oz capacity; Pipeline Inc., Waterloo, ON, Canada) worn at the user's waist allows for untethered power assistance [54]. The rotary actuator at the ankle joint is a dual-vane, bidirectional pneumatic actuator (PRN30D-90-45, Parker Hannifin, Cleveland, OH) rated for a maximum of 150 psig and 90 degrees of rotation. The actuator can generate about 11.4 Nm of torque at 100 psig. The pressure regulator on the tank controls the pressure supply for the plantarflexor actuation at 100 psig, while a second regulator (LRMA-QS-4; Festo Corp-US, Hauppauge, NY) further reduced the pressure for dorsiflexor assistance (~3.1 Nm of torque at 30 psig). The reduced dorsiflexor pressure was set to 30 psig based on the functional need to allow toe clearance during swing while ensuring that the dorsiflexor muscles were not overpowered. Excessive applied dorsiflexor torque is unnecessary to support the foot during swing and can result in user discomfort. Two solenoid valves (VOVG 5V; Festo Corp-US, Hauppauge, NY) were used to control the actuation. The exhaust gas at the end of both plantarflexion and dorsiflexion actuation was released to atmosphere. Three actuation states could be achieved through the combinations of the solenoid valves: 30 psig in dorsiflexion, 100

psig in plantarflexion, and passive (no actuation) (Figure 30). Actuation was controlled by an embedded micro-controller (TMS320F28335, CPU: 150MHz, Sampling Rate: 1kHz. Texas Instruments, Dallas, TX), reading from two force resistive sensors located at the heel and the toe of the foot plate (403, 2" square; Interlink Electronics Inc., Camarillo, CA, USA) and a rotary potentiometer at the ankle joint (53 Series, Honeywell, Golden Valley, MN).

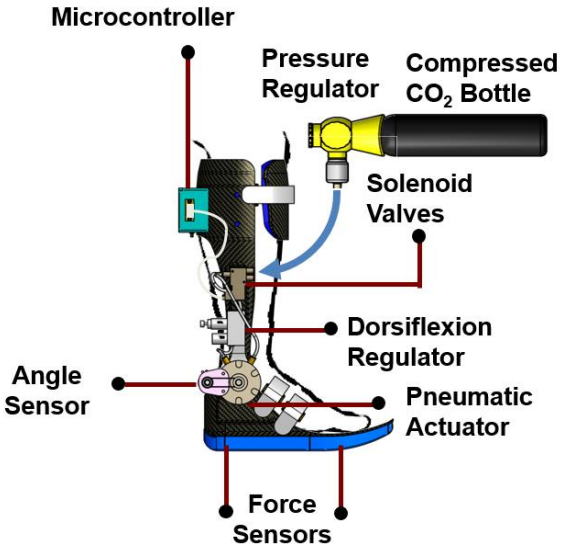

Figure 28 The portable powered ankle foot orthosis (PPAFO). The actuator is powered by a tank of compressed CO_2, which is worn at the user's waist.

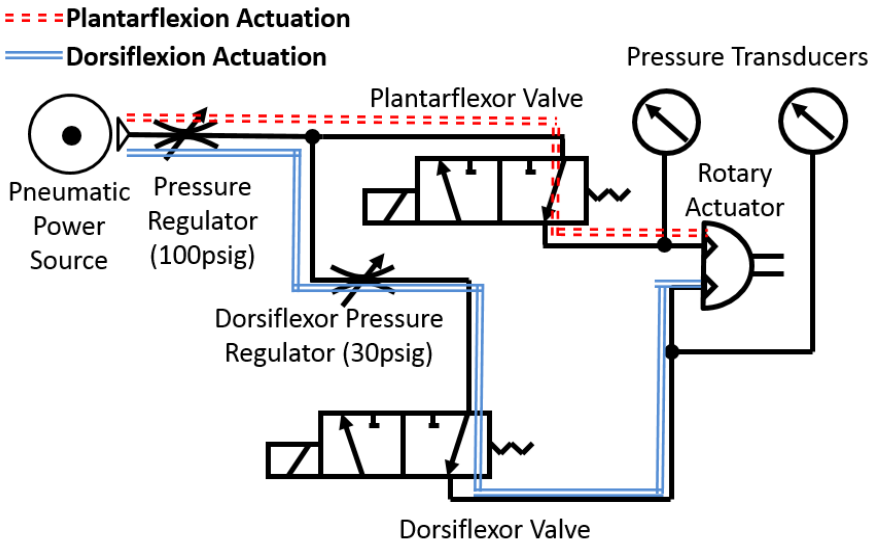

Figure 29 Schematic of the original pneumatic circuit for the PPAFO. The pressures in the chambers of the rotary actuator were controlled by the combination of the two solenoid valves. The additional pressure regulator was used to reduce dorsiflexor torque to avoid user discomfort.

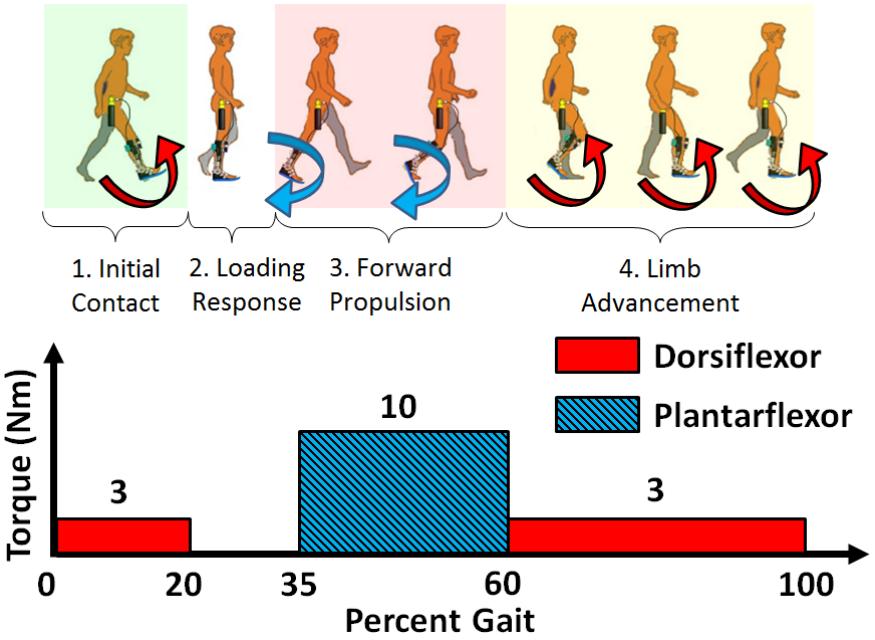

Figure 30 Assistive dorsiflexor and plantarflexor torque at approximate times in a gait cycle of a normal healthy adult during level walking.

4.2.1.2 Gait State Estimation and Actuation Control

The PPAFO can only provide all on/off actuation due to the nature of the solenoid valves. The switching timings for the valves were determined by a state estimation controller that used the sensor readings and microcontroller [85]. The PPAFO provided assistive torque during three regions of the gait cycle (Figure 30): (1) dorsiflexor assistance to control foot motion during loading response (0%-20% of gait cycle), (2) plantarflexor assistance during late stance (terminal stance and pre-swing) to provide propulsive torque (35%-60% of gait cycle), and (3) dorsiflexor assistance during swing to maintain foot clearance (60%-100% of gait cycle). In this study, the three-region actuation strategy was wrapped around a 100% gait cycle to form a two-region equivalent actuation strategy for ease of analysis.

4.2.1.3 Hardware Modification for the Energy Experiment

For system efficiency data collection purposes, the pneumatic components of the PPAFO were mounted to a fixed test bench. All the pneumatic components were kept the same (valves, lines and actuator) with the exception that the pneumatic power supply was replaced by shop air with a regulator. The use of compressed shop air in place of CO_2 was assumed to have little impact on the efficiency results, because using the orifice flow equation [140], the pressure drops across a component was only a function of the upstream and downstream pressure, regardless the gas molecular weight. In order to have a test bench assembly that best matched the working condition of a PPAFO, the mechanical system was modified as following: the rotary actuator was statically mounted to wood blocks onto the testing bench with an inertial load (a steel inertial bar) that

matched the moment of inertial of a foot for an average person of 75 kg [141]. Range of motion was limited to 46 degrees by padded mechanical stops on either side of the bar, matching the full range of normal human ankle joint (28 ºplantarflexion, 18 ºdorsiflexion, [1]). The shaft angle was recorded by the PPAFO potentiometer.

To collect pressure data, two transducers with maximum ratings of 150 psig and 100 psig, respectively, (AST4000A00150P3B1000, AST4000A00100P3B0000, American Sensor Technologies, Inc.) were used to measure the pressure differentials at different locations of the pneumatic circuits. The pressure transducers were calibrated at 24 V.

On the test bench, a data acquisition system (Q8, Quanser Corp. Ontario. Canada) was used as the data logging and real-time controller to interface with the solenoid valves in the place of the TMS320F28335 microcontroller. The system was operated at 500 Hz. MATLAB and Simulink (Mathworks, Natick, MA) were used for valve control signal timing, data recording, and data post processing.

4.2.2 Overall System Efficiency

In this study, the overall PPAFO system efficiency was analyzed by examining two categories based on the primary causes of energy loss, operational efficiency and component efficiency. The overall system efficiency was therefore defined as the product of the component efficiency and operational efficiency. Theoretical and empirical analyses and solutions to improve each category will be discussed respectively.

The system operational efficiency was defined as the ratio between ideal case work output and the available energy in the consumed fuel. Operational efficiency accounted for inevitable wasted energy during pneumatic operations such as exhaust and pressure regulating. Since the ideal case work output can only be obtained through theoretical calculation, operational efficiency could not be directly evaluated through experimental data. Instead, it was a theoretical projection. In the operational efficiency calculation, because all the components were considered ideal, the energy losses were independent from the specific components that make up the system.

In contrast, the system component efficiency was the ratio between the actual work output at the actuator and the ideal case work output. Energy losses in system component efficiency were due to pressure drops across different pneumatic components (e.g., valves, lines, actuator connectors). The pressure drops depended on the choice of flow rate through each individual pneumatic component. As a result, an effective way to increase component efficiency was through hardware improvements (e.g., better diameter to length ratio for transport lines, and valves with higher flow ratings).

4.2.3 Operational Efficiency

In conventional applications of pneumatically powered systems, system efficiency consideration is often neglected for other design factors such as complexity of the overall system. Consequently, very few attempts have been made to enhance system efficiency because most pneumatic applications in industry are not constrained by finite power supplies. Huang et al. proposed a pneumatic energy harvesting scheme for a hybrid pneumatic vehicle to recycle and store excessive

actuation energy into a storage tank, increasing the system efficiency by about 20% [142-144]. EARS (Exhausted Air Recycling Systems) had implemented the same harvesting idea on small hand tools that can reduce the compressor runtime by 50% as well as the noise by 20 dB [145]. A similar approach was used by PET [146] for industrial applications. However, these methods were designed for specific industrial devices with different design limitations than the PPAFO, which could not be directly applied to our current system.

In the literature, few studies have focused on increasing pneumatic system efficiencies and so, there is little consensus on how to quantify the energy available in pneumatic systems [147, 148]. Alternatively, studies have used fuel consumption (mass) or volumetric flow rate in place of a direct quantification of energetic cost [147, 149, 150]. These are effective metrics for overall system comparisons, but do not provide insight on how and where energy is lost inside the system during operation.

To address this issue, Cai et al. [147] derived available pneumatic energy contained in a finite amount of gas. The available energy describes the work-producing potential energy that can be extracted from the fuel. In pneumatic systems under isothermal conditions, available energy represents the maximum mechanical work that the compressed gas can output before reaching its equilibrium atmospheric pressure state in which the gas cannot be utilized any more.

In the following sections, the available energy and the operational efficiency of pneumatic systems will be derived first for a general pneumatic system and then specifically for the PPAFO system.

A recycling scheme will be proposed and the available energy will be recalculated to identify the operational efficiency of the recycling scheme.

4.2.3.1 Derivation of Available Energy in a System

Available energy was used as a measurement of the gas' ability to output work and defined as a function of pressure. Therefore, available energy would peak at the power source and gradually decrease to zero when exhausted to the atmosphere. In this section, the generalized relationship between the available energy and pressure is derived using a simplified two-step procedure, following that proposed by Cai et al. [147].

A few assumptions were made before deriving the available energy in the pneumatic system:

1) All the processes were considered slow enough to allow heat exchange, which can be assumed as an isothermal process (constant temperature).
2) No leakage in the pneumatic system.
3) All system components were assumed ideal (i.e., no pressure drop across lines and valves). This assumption was valid because operational efficiency is independent of the mass flow rate.

A simplified two-step procedure was used to estimate the available energy of the gas. In this derivation, the available energy was equal to the total work output by the gas that entered into, say, one side of a pneumatic linear cylinder and drove the piston until the pressure reached atmosphere

(Figure 31). The total work output in this two-step procedure could be calculated. A linear cylinder actuator was used for demonstration purposes, but the thermodynamics equations are the same for a rotary actuator, and the end result pressure-energy relationship also holds.

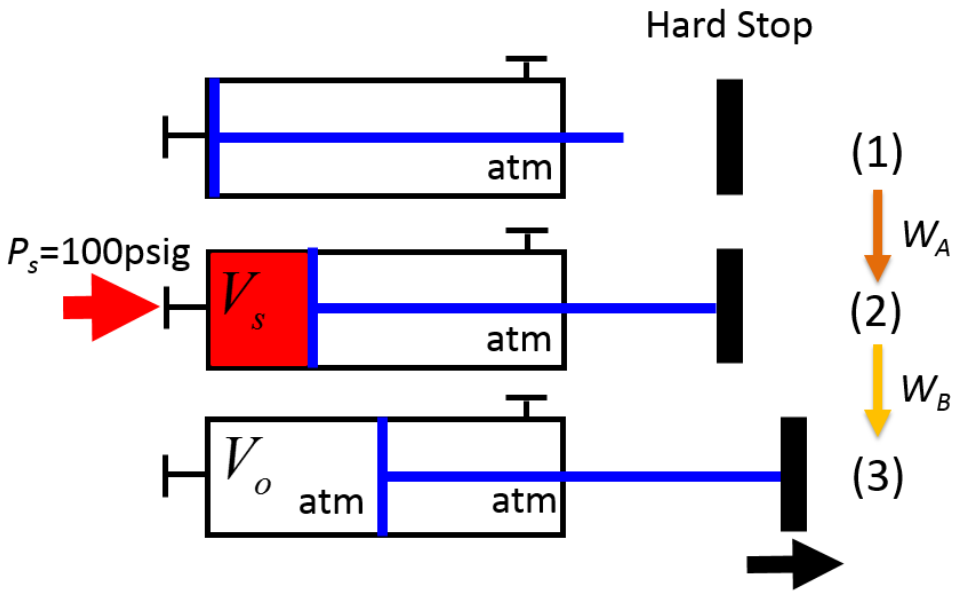

Figure 31 The two-step procedure to calculate the available energy contained in the compressed gas as illustrated by a pneumatic linear cylinder.

Step A (States 1-2) Consider compressed gas at a source pressure of P_s and a volume of V_s. When the gas entered the cylinder, the piston was pushed to the right (Figure 31). During this initial gas intake, the volume on the left side of the cylinder was increased from 0 to V_s until the piston was stopped at a hard stop (vertical solid line). This expansion resulted in an output of mechanical work W_A:

$$W_A = (P_S - P_O)V_S \tag{30}$$

where P_O is the atmospheric pressure.

Step B (States 2-3) After the gas intake, the port to the source was closed. If the hard stop was slowly moved to the right to allow for quasi-steady-state expansion. The sealed compressed gas then can expand from V_S to V_O with a corresponding pressure drop. Assuming the process was slow enough to allow effective heat transfer, the temperature of the gas can be assumed as a constant at room temperature. Therefore the process can be considered as isothermal. The work output W_B in this step can be represented as

$$W_B = \int_{V_S}^{V_O} (P - P_O)dV\ . \tag{31}$$

The pressure (P) and volume (V) have to follow the ideal gas law,

$$PV = \frac{m}{\mu}RT \tag{32}$$

where P was the pressure inside the cylinder, V was the volume of the cylinder that contained pressurized gas, m was the total mass of the gas insider the cylinder, R was the universal gas constant and T was the room temperature, which was also a constant since all the processes were isothermal.

From the conservation of mass in step B, the pressure and volume relationship before and after the step can be expressed as,

$$P_O V_O = P_S V_S \tag{33}$$

The work output is therefore the sum of the work in the two steps, Equation (30) and Equation (31),

$$W = W_A + W_B = P_S V_S ln \frac{P_S}{P_O} \tag{34}$$

In summary, while the compressed gas went through a two-step process, the available energy E_A of the compressed gas decreased to 0 (available energy was zero when compressed gas equalized with atmosphere), as shown in Figure 31. Therefore, E_A consisted of two parts: W_A was the work done when the compressed gas entered the system, and W_B was the additional work done when the volume was allowed to expand until that the pressure of the compressed gas goes to atmosphere (Figure 32). The result can be generalized to calculate the available energy E_A at any given point in the pneumatic circuit, where m_o was the existing gas before intake and m was the mass of gas intake.

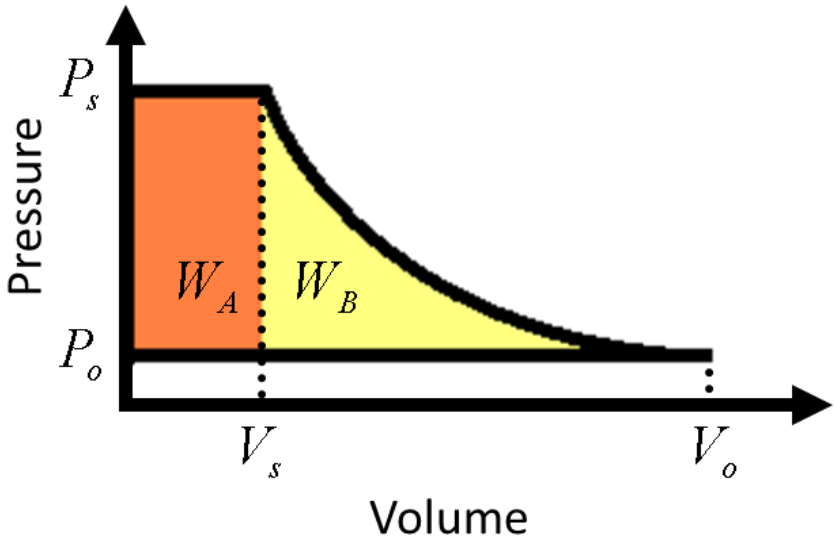

Figure 32 The two-step decomposition of the available energy in compressed gas: work from gas intake (W_A) and the work from isothermal expansion (W_B).

$$E_A = W = P_S V_S ln\frac{P_S}{P_O} = \frac{m + m_O}{\mu} RT ln\frac{P_S}{P_O} \tag{35}$$

In conventional operation of a pneumatic device, the compressed gas will be exhausted to atmosphere right after step A during the return stroke of the actuator, and step B never occurs. In this case, the existing available energy in the exhaust gas is wasted. This wasted exhaust energy E_e is the same as W_B. This exhaust energy E_e can also be expressed as,

$$E_e = W - W_A \tag{36}$$

To improve operational efficiency, this lost energy could be captured (or harvested) and recycled for use in a second lower-pressure actuation cycle, such as a device with two actuators. The PPAFO,

which has only one actuator that can operate bi-directionally, has an actuation strategy (high pressure plantarflexion and low pressure dorsiflexion) that is also ideal for use of a recycling scheme.

In the next section, we will compute the operational efficiency for the original PPAFO system. We will then explore an energy harvesting and recycling scheme to improve the operational efficiency of the PPAFO.

4.2.3.2 Operational Efficiency for the Original PPAFO System

The operational efficiency of the PPAFO system (Figure 29) was analyzed using the available energy expressions derived in the previous section. Since operational efficiency is an idealized concept, only pressure and volume measurements were needed to obtain the operational efficiency results. The parameters were obtained from the actual PPAFO system and used to compute the operational efficiency (Table 5).

Table 5 Parameters used in operational efficiency calculations

Parameter	**Value**	**Source**
Room temperature (T)	300 K	
Regulated Plantarflexion Pressure (P_P)	791 kPa (100 psig)	
Regulated Plantarflexion Pressure (P_D)	308 kPa (30 psig)	
Atmospheric pressure (P_O)	101325 Pa	
Universal Gas Constant (R)	8.314 J/mol K	
Molecular Weight for CO_2 (μ_c)	0.044 kg/mol	
Molecular Weight for air (μ_a)†	0.029 kg/mol	
Full Volume for Actuator (V)‡	34.0 cm^3	From actuator
Actuator Full Range of Motion (ROM_F)	90.0 deg	From actuator
Actual actuator ROM (ROM_A)	46.0 deg	From actuator

† In the analyses in this study, air will be used whenever molecular weight is needed since it was the actual power source in the experimental setup (see section 4.2.1.2).

‡ Since the PPAFO actuator had two vanes, this design has two chambers; however, this volume is for both chambers.

The inertial bar system limited the system range of motion from its full 90 degrees down to the 46 degrees. As a result, the minimum and maximum volume for each chamber in the actuator was also changed. Therefore, the minimum volume for one side of the actuator was,

$$V_B = \frac{V}{2}\left[1 - \frac{ROM_A}{ROM_F}\right] = 8.31\ cm^3 \tag{37}$$

when the opposite side was at its maximum,

$$V_A = V - V_B = 26.0\ cm^3. \tag{38}$$

We defined that the cycle began with the plantarflexor chamber volume was at its minimum. At this point, the pressure in the plantarflexor chamber was atmospheric pressure. The total mass in the chamber was,

$$m_O = \frac{P_O V_B \mu_a}{RT} = 0.0098\ g. \tag{39}$$

During plantarflexor actuation, the chamber was filled with air at the source pressure (100 psig). The added mass of air during this intake was,

$$m_P = \frac{P_P V_A \mu_a}{RT} - m_O = 0.23\ g. \tag{40}$$

The work output during this plantarflexor actuation was computed from Equation (30),

$$W_P = (P_P - P_O)(V_A - V_B) = 12.0\,J. \tag{41}$$

The total available energy contained in the fuel for plantarflexor actuation, from Equation (35), was

$$E_{A,P} = P_P V_A ln\frac{P_P}{P_O} = 41.7\,J. \tag{42}$$

Similarly, for dorsiflexor actuation, the added air to the dorsiflexion side at 30 psig was,

$$m_D = \frac{P_D V_A \mu_a}{RT} - m_O = 0.082\,g. \tag{43}$$

The work output during this dorsiflexor actuation was computed from Equation (30),

$$W_D = (P_D - P_O)(V_A - V_B) = 3.6\,J. \tag{44}$$

The total available energy contained in the fuel for dorsiflexor actuation was determined from Equation (35), to be,

$$E_{A,D} = W = P_P V_A ln\frac{P_P}{P_O} = 16.3\,J. \tag{45}$$

Total available energy theoretically contained in the compressed air before it entered the system, is the sum of Equation (42) and Equation (45),

$$E_A = E_{A,P} + E_{A,D} = 58.0\,J. \tag{46}$$

And the total projected work output is the sum of work output in both directions,

$$W_{pj} = W_P + W_D = 12 + 3.6 = 15.6\,J. \tag{47}$$

Therefore, the theoretic operational efficiency for this system can be computed by the ratio between work output and total energy available,

$$\eta_o = \frac{W_{pj}}{E_A} = 26.9\%. \tag{48}$$

4.2.3.3 Recycling Scheme to Improve Operational Efficiency

As mentioned at the end of 4.2.3.1, conventional pneumatic circuits exhaust any residual compressed gas upon the return stroke of an actuator. This exhaust energy E_e can be calculated from Equation (36). For plantarflexion, this exhaust energy was,

$$E_{e,P} = E_{A,P} - W_P = 41.7J - 12.0J = 29.7\,J. \tag{49}$$

For dorsiflexion, the exhaust energy was,

$$E_{e,D} = E_{A,D} - W_D = 16.3J - 3.6J = 12.7\,J. \quad (50)$$

Two observations were made by examining the results from the operational efficiency: first, for dorsiflexor actuation, although the work output was only 3.6 J (Equation (44)), it cost 16.3 J of fuel available energy from the power source (Equation (45)), because the compressed air that could have been used at 100 psig was regulated down to 30 psig before it entered the actuator. Significant energy was lost at the second (dorsiflexor) regulator. Second, by comparing Equation (45) and (49), it can be noted that the exhaust from plantarflexion (29.7 J, Equation (49)) contained more energy than what was needed (including wasted energy) for dorsiflexor actuation (16.3 J, Equation (45)). This energy distribution can allow opportunities for the compressed exhaust from plantarflexion to be directly recycled for powering the dorsiflexion actuation.

A recycling scheme was proposed to take the advantage of the compressed exhaust air, as shown in Figure 33. An additional solenoid valve (three-way, five-port, VUVG 5V; Festo Corp-US, Hauppauge, NY) and an accumulator were added into the system to recycle the energy in the exhaust of the previous plantarflexor actuation. The valve was chosen for its bidirectional flow switch ability that was specifically required for this particular pneumatic circuit. A duplicate rotary actuator was used as a fixed volume accumulator (PRN30D-90-45, Parker Hannifin Corp). The captured exhaust was then used to power the subsequent dorsiflexor actuation to fully replace the dorsiflexor power supply. The fuel taken from the main power source previously needed for the dorsiflexor actuation was then saved.

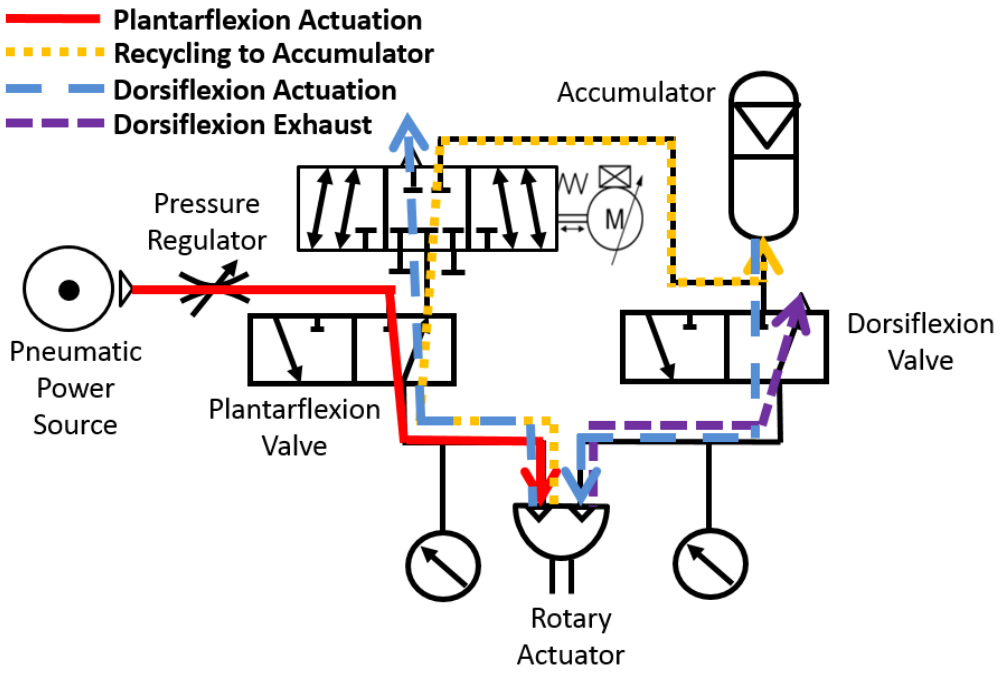

Figure 33 PPAFO energy regeneration scheme using an accumulator and three solenoid valves to recycle exhaust air from plantarflexion actuation. The legends in sequence indicated the pneumatic flow in the four different phases of the cycle.

Here are the four phases of the recycling scheme (Figure 33):

Phase 1: Pressurize one chamber of the rotary actuator at 100 psig for plantarflexor actuation (red solid line). The actuator also moved from one end position to the opposite side.

Phase 2: Connect the pressurized actuator chamber to the accumulator allowing the pressure to reach equilibrium, so that the compressed exhaust from plantarflexor actuation could be harvested into the accumulator and partially recycled (yellow dashed line).

Phase 3: Connect pressurized accumulator to the dorsiflexion side of actuator (blue dashed line). Switch the plantarflexor actuation chamber to atmosphere and ventilate the chamber (blue dashed line). The net pressure direction would be then reversed, and the actuator would move back to the original position during dorsiflexion actuation.

Phase 4: Switch the dorsiflexor actuation chamber to atmosphere and ventilate the chamber (purple dashed line). By now both chambers are at atmospheric pressure. This is the end of the cycle. Repeat Phase 1.

The four-phase procedure allowed the compressed exhaust air from plantarflexor actuation to be partially stored at the accumulator and released later to power the actuator in the reverse direction. This approach guaranteed the same level of work output in both configurations, while significantly reduced the fuel consumption. The valve switching scheme is illustrated in Figure 34 and Table 6.

Table 6 Phase definition for one gait cycle actuation of the pneumatic system

Phase	**Start**	**% gait cycle**	**Plantarflexion**	**Accumulator**	**Dorsiflexion**
1.	0.0 sec	0-30	On	Off	Off
2.	0.3 sec	30-40	Off	On†	Off
3.	0.4 sec	40-90	Off	Off	On
4.	0.9 sec	90-100	Off	Off	Off

† For the non-recycling scheme, the accumulator valve did not exist and therefore did not turn on at 0.3s.

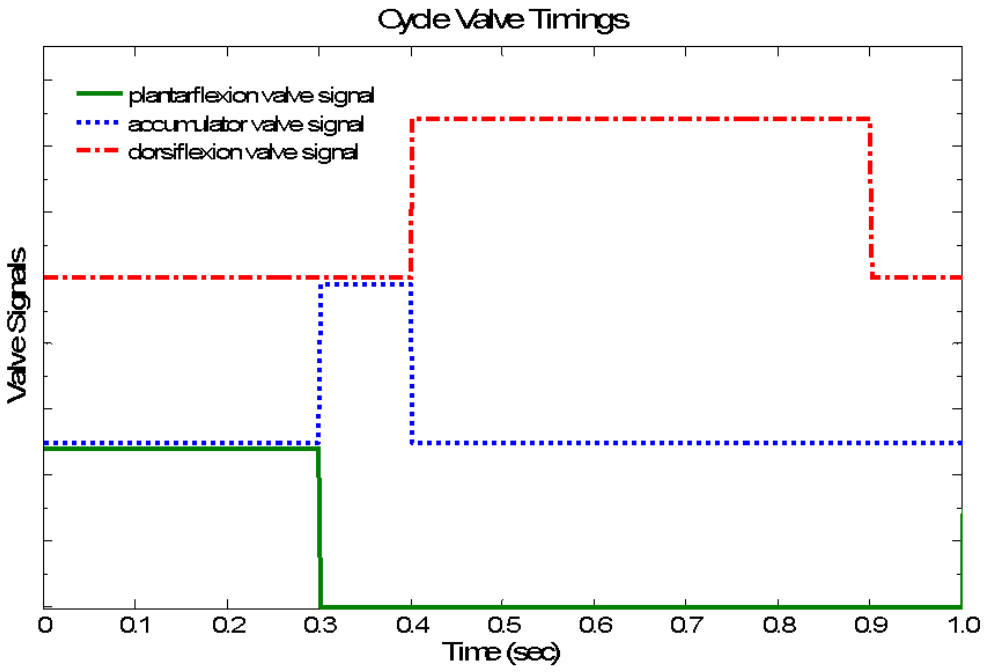

Figure 34 Valve signal timing for one actuation cycle. For the non-recycling scheme, there is no accumulator valve signal.

4.2.3.4 Operational Efficiency for the Recycling Scheme

In the recycling scheme, fuel consumption and work output for plantarflexor actuation remained the same. The fuel needed for dorsiflexor actuation was saved, while the work output was considered to remain approximately the same level since the recycled dorsiflexor pressure stayed about 30 psig (this assumption is verified later in section 4.3.1). To compute the available energy for the reduced fuel consumption, only the fuel used in plantarflexor actuation was used. Similar to Equation (46), the total available energy theoretically contained in the compressed air before it entered the system was

$$E_A' = E_{A,P} = 42\ J. \tag{51}$$

As a result, the theoretic operational efficiency for the system with recycling was improved due to fuel saving from dorsiflexor actuation,

$$\eta_o' = \frac{W_{pj}}{E_A{}'} = 37.3\%. \tag{52}$$

4.2.4 Component Efficiency

The ideal of system component efficiency was to compare pneumatic system actual work output (mechanical work output at the actuator), to the ideal case work output (where all the components were assumed to have no pressure drops). The system component efficiency served as an indicator of how much energy was lost in total along the pneumatic path in an actuation. Additionally, the work losses analyses presented in this section break down the total work loss onto different pneumatic components, helping to identify where the most energy was lost.

The system component efficiency and total work loss accounted for energy losses due to pressure drops across different components (converted into heat). For example, for tubing, shorter length and larger inner diameter should increase component efficiency because it creates less resistance to the flow. Thus, in order to identify work losses across a component, the pressure differential and mass flow rate had to be obtained.

There are a number of ways to measure the pressure drops within a pneumatic system. Mi et al. [151] and Sanchez et al. [152] used empirical equations to estimate the pressure drops where the flow rate was known. A similar approach was taken by Hettiaratchi et al. [153] for vertical and horizontal conveying pipelines. Laouar et al. [154] used direct pressure measurement to develop a set of equations that could predict pressure drops, but the reliability was subject to flow conditions. All aforementioned methods required additional knowledge (e.g., flow rate), which was not available in our experiment. As a result, in our component efficiency and work loss study, we adopted the direct measurement approach by repeating the actuation cycle and measuring the absolute pressures at different locations in the pneumatic circuit.

Thus, it is important that the component efficiency and component work loss were identified in the improved operation – the recycling scheme – such that the identified system efficiency would represent the optimized final system configuration. Therefore, the theoretical derivation and experiments for the component efficiency and component work loss were all designed based on the recycling scheme.

In order to estimate the energy losses across different components and simplify the thermodynamics derivation, we made the following assumptions:

1) All the processes were considered slow enough to allow heat exchange and therefore assumed as isothermal process (constant temperature). This assumption was valid due to the large ratio between surface area and the total amount of compressed gas contained in the actuator and valves. It remains unclear whether this assumption will hold for a portable CO_2 power source

(e.g., during prolonged use the CO_2 tank will cool substantially). Since only shop air was used in this study, this assumption was considered valid.

2) No leakage in the pneumatic system.

3) The pressure drops across each component were small compared to the source pressure, which allowed the use of average pressure across a component to estimate the flow rate.

4) Except for the accumulator and actuator, other pneumatic components were considered of negligible volume. Thus, according to conservation of mass, the mass flow rate into and out of a component was considered a constant at any given moment.

4.2.4.1 Calculation of System Component Efficiency

The actual work output at the pneumatic actuator could be expressed as the integral of net pressure differential over actuator volume change,

$$W_{actual} = \int (P_P - P_D) dV, \tag{53}$$

where P_P and P_D were the pressure measurement from plantarflexor and dorsiflexor sides of the actuator, and V was the actuator chamber volume at plantarflexor side.

The chamber volume at the plantarflexor side could be further expressed as a function of the actuator angle measurement,

$$V = A(\theta - \theta_O)\,, \tag{54}$$

where A was the constant for the actuator's volume/angle ratio, and θ_O was the angle when volume was zero. Thus the total work output could be expressed as functions of measurements,

$$W_{actual} = \int (P_P - P_D) A d\theta. \tag{55}$$

The discretized form of the actuation for computation would be,

$$W_{actual} = \sum A\big(P_P(n) - P_D(n)\big)\,(\theta(n) - \theta(n-1) \tag{56}$$

where $P_D(n)$, $P_P(n)$, $\theta(n)$, were the sampled pressures and angular position at $t = nT$, and T was the sampling period.

The system component efficiency could then be defined as,

$$\eta_c = \frac{W_{actual}}{W_{pj}} \tag{57}$$

W_{actual} is the projected work output when all the components are ideal. W_{pj} is the total projected work output for the system (Equation (47)).

4.2.5 Overall System Efficiency Calculation

Considering the definition of system overall efficiency was its actual work output over the available energy contained in the fuel,

$$\eta_{overall} = \frac{W_{actual}}{E_A}. \tag{58}$$

The overall efficiency could be decomposed to the product of Equations (48) and (57),

$$\eta_{overall} = \frac{W_{actual}}{E_A} = \frac{W_{actual}}{W_{pj}} \frac{W_{pj}}{E_A} = \eta_c \eta_o. \tag{59}$$

Naturally, the overall system efficiency was expressed as the product of operational efficiency and component efficiency.

4.2.6 Calculation of Work Loss Across Different Components

Considering in reality, from Equation (57), the system component efficiency will always be below 1.0, and the difference between W_{actual} and E_A was how much energy was lost (turned into heat, and no leakage assumed) within the pneumatic system. It was important to break down the total energy lost into the energy losses across each of the pneumatic components (valves, tubing, etc.). In this section, equations were derived to use experimental measurements to estimate work losses across each of the pneumatic component along the path.

The work loss when air flows across a pneumatic component can be calculated using volume and pressure measurements. Assuming we know the pressure on both sides, for a controlled volume of air, the work loss was defined as

$$W = \int (P_3 - P_2) dV \tag{60}$$

where P_3 and P_2 were the pressure measurement across the component (Figure 35), and dV could be approximated if the mass flow was known. The pressure was approximated as the average of upstream and downstream pressure of the valve:

$$dV = \frac{RT}{P\mu} dm \approx \frac{2RT}{(P_2 + P_3)\mu} dm. \tag{61}$$

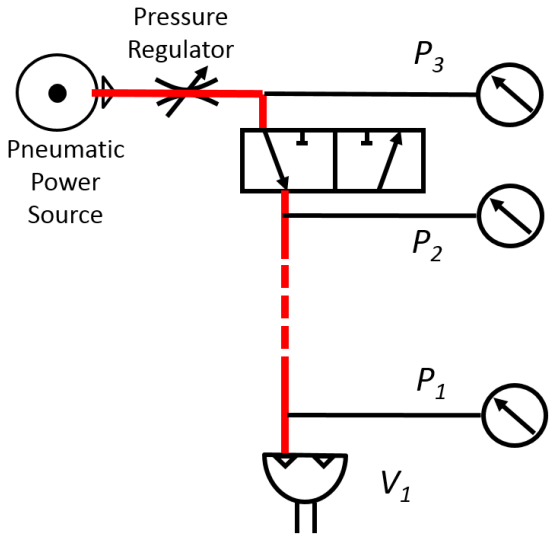

Figure 35 Calculating the work loss across a solenoid valve: pressure drops could be directly measured by the pressure transducers, and the mass flow rate had to be traced down from the actuator, where the volume and pressure were known.

Therefore,

$$W = \frac{2RT}{\mu} \int \frac{P_3 - P_2}{P_2 + P_3} dm. \tag{62}$$

In our experimental setup, the mass flow rate was not directly measured due to the low flow rate compared to the accuracy of the available flow meters. Alternatively, assuming the volumes in the connecting tubing were negligible, the mass flow rate at any given time was considered a constant unless the air flow entered or exited the system (Figure 35).

The best approach to capture the mass flow rate was when the air flow entered or exited a pneumatic component, in which its total mass could be monitored and inversely calculated to find the mass flow rate. For example, when there was mass flow entering one chamber of the rotary actuator, the volume of the actuator was always known,

$$V_1 = A(\theta - \theta_O) \tag{63}$$

where A was the constant for the actuator's volume/angle ratio, and θ_O was the angle when volume was zero. The pressure measurement at the end of the actuator was P_1. The mass flow into the chamber over any time increment could be obtained by differentiating the total mass in the chamber over time,

$$dm = \frac{\mu}{RT} d(P_1 V_1) \tag{64}$$

Combining Equations (62) and (64) would yield the work loss across any given component over a certain time interval,

$$W = \frac{2RT}{\mu}\int \frac{P_3 - P_2}{P_2 + P_3}\frac{\mu}{RT}d(P_1V_1) = 2A\int \frac{P_3 - P_2}{P_2 + P_3}d(P_1\theta_1). \quad (65)$$

The discretized form of the work loss equation for computation from experimental data,

$$W = \sum_n 2A\frac{P_3(n) - P_2(n)}{P_3(n) + P_2(n)}[\theta_1(n)P_1(n) - \theta_1(n-1)P_1(n-1)] \quad (66)$$

where $P_1(n)$, $P_2(n)$, $P_3(n)$, $\theta_1(n)$, were the sampled pressure and angular position at $t = nT$, and T was the sampling period.

Another scenario was when the flow path included an accumulator, where the mass flow rate became the sum of the two paths (Figure 36),

$$dm = dm_A + dm_1. \quad (67)$$

m_A was the mass inside the accumulator, which could be expressed from its pressure measurement (because it had fixed volume V),

$$dm_A = \frac{\mu V_A}{RT}dP_A, \quad (68)$$

where the accumulator internal pressure was P_A.

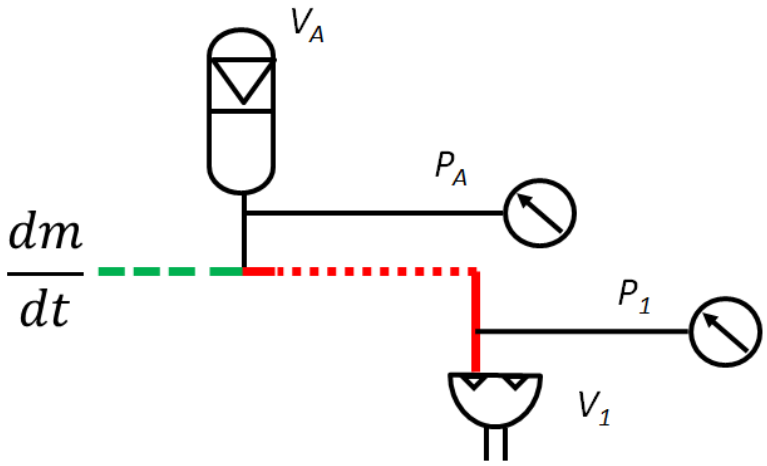

Figure 36 Deriving the mass flow rate when the flow path involved both the accumulator and the actuator.

Therefore, instead of Equation (65), the work loss expression can be rewritten as,

$$W = \frac{2RT}{\mu}\int \frac{P_3 - P_2}{P_2 + P_3}\frac{\mu V_A}{RT}dP_A = 2V_A\int \frac{P_3 - P_2}{P_2 + P_3}dP_A. \tag{69}$$

The discretized form of the work loss equation for computation from experimental data,

$$W = \sum_n 2V_A \frac{P_3(n) - P_2(n)}{P_3(n) + P_2(n)}[P_A(n) - P_A(n-1)] \tag{70}$$

where $P_A(n)$, $P_2(n)$, $P_3(n)$, were the sampled pressures at $t = nT$, and T was the sampling period. V_A was the fixed volume accumulator volume.

4.2.6.1 Components to Examine in Component Work Loss

Six crucial pneumatic components were identified in the circuit as shown in Figure 37 and Table 7). Other components were neglected in the experiment for two main reasons: negligible pressure drops (e.g., short tubing connecting valves and actuator), or components that were impossible to measure (e.g., connector for the actuator, would need a pressure sensor inside the actuator to analyze). Note that component 3 and 4 were only used to harvest energy into the accumulator. Since they had no impact on total harvested energy, they would not account for the losses in work output at the actuator. The two regulators were not included in this analysis because the energy loss across a regulator did not indicate the efficiency of it.

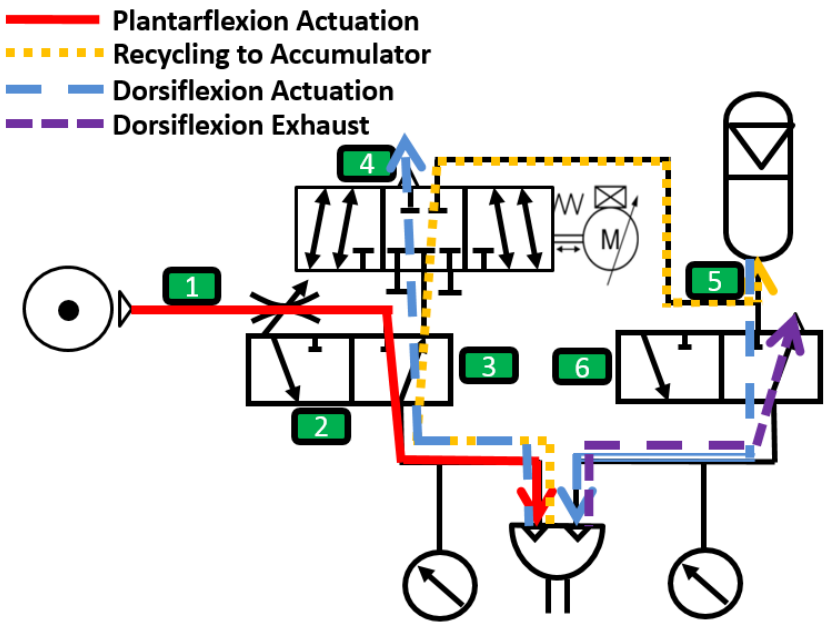

Figure 37 Component efficiency: the numbers indicate the identified the components to analyze.

Table 7 Components tested in component efficiency

#	**Component Description**	**Impacts Work**
1	Inlet Line	Yes
2	Plantarflexion Valve In	Yes
3	Plantarflexion Valve Out	No
4	Accumulator Valve	No
5	Accumulator T-Junction	Yes
6	Dorsiflexion Valve	Yes

4.2.7 EXPERIMENTAL PROCEDURE

To experimentally validate the performance and the fuel saving for the proposed recycling scheme, two schemes were tested: the non-recycling scheme and the recycling scheme.

For the recycling scheme, the valves were controlled to complete a single cycle (plantarflexion and dorsiflexion) in 1 second (Table 6 and Figure 34). Pressure data at all connecting nodes of the pneumatic circuit were collected for component work loss breakdown analysis because this was the improved configuration. For the experiment, data from 12 actuation cycles were collected for each component, after allowing for 5 cycles to allow the accumulator to reach a constant operating pressure.

In the non-recycling scheme for the operational efficiency, the same timing controlled the plantarflexion and dorsiflexion valves such that nothing happened during the second phase of the cycle, and in the third phase of the cycle, the pneumatic power was obtained from the power source

instead of the accumulator (Table 6). The fuel consumption for each actuation could be determined from Equations (40) and (43).

4.3 RESULTS

4.3.1 FUEL SAVINGS AND WORK OUTPUT

Using pressure measurement from the transducers, the fuel consumption for two schemes could be computed. The non-recycling scheme consumed 0.31g of compressed air per cycle, while the recycling scheme consumed 0.23g of compressed air per cycle, from Equations (40) and (43). This result was equivalent to a fuel saving of 28%.

Total work output depended on pressure profiles for the actuation. During dorsiflexor actuation, while the non-recycling scheme pressure was regulated by the regulator, the recycling scheme relied on the accumulator to return pressure. The recycled scheme was able to reproduce the desired pressure and torque output profile fairly well, compared to the non-recycling scheme (Figure 38 and Figure 39). The recycled dorsiflexor actuation pressure was around 30 psig, which is the desired amount needed for assisting dorsiflexion. As assumed in section 4.2.3.4, the actual total work output W_{actual} was found to change little between the non-recycling and recycling schemes, 11.9 J and 12.4 J, respectively.

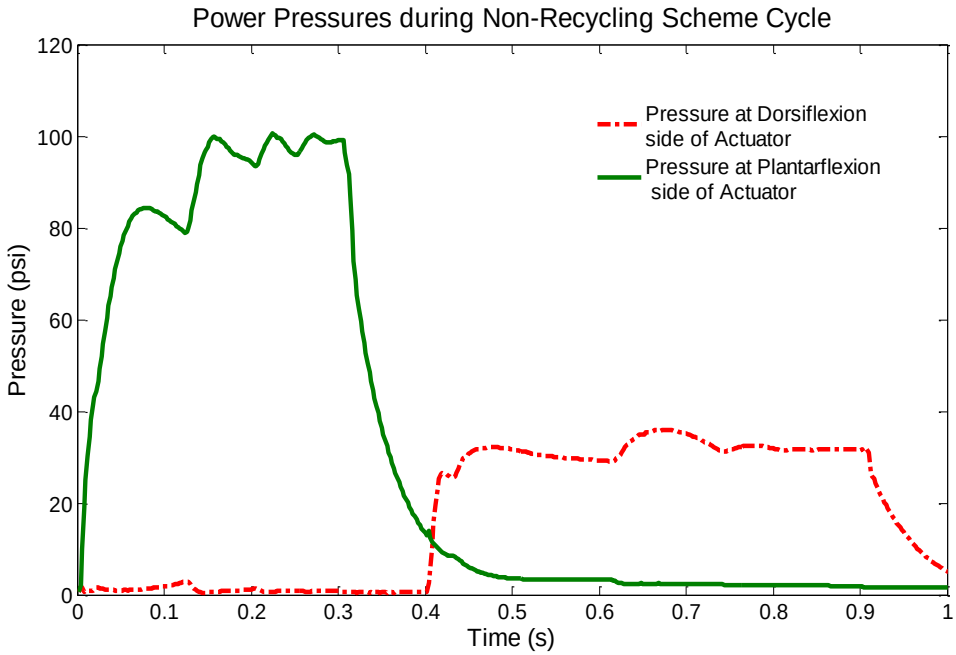

Figure 38 Pressure profiles at the actuator for a non-recycling scheme cycle. Both plantarflexion and dorsiflexion were powered from the compressed air line as the source.

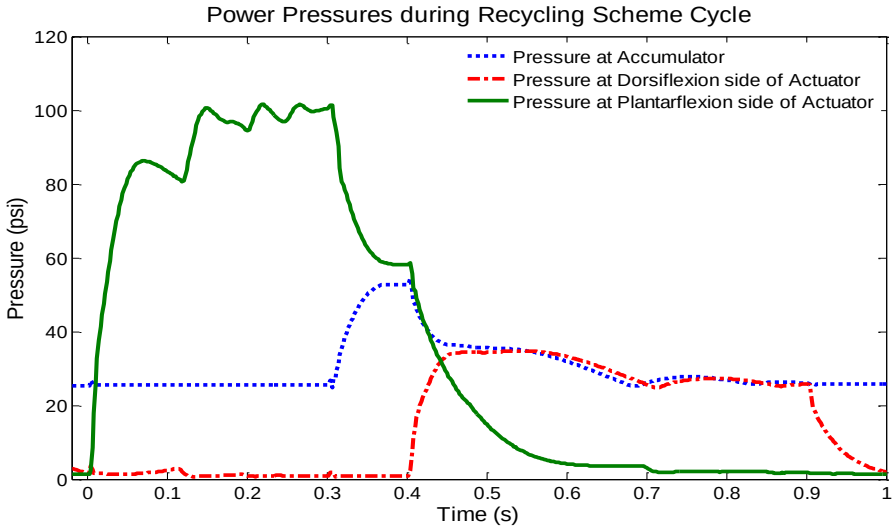

Figure 39 Pressure profiles at the actuator for a recycling scheme cycle. Plantarflexion was powered from the compressed air line as the source while dorsiflexion was powered from recycled energy from the accumulator.

4.3.2 Operational Efficiency and Component Efficiency

The ideal case work output (W_{pj}) could be calculated from measured source pressure using Equations (41), (44) and (47). For both recycling and non-recycling, the W_{pj} was 15.6 J.

For non-recycling scheme, the operational efficiency as from Equation (48),

$$\eta_o = \frac{W_{pj}}{E_A} = \frac{15.6}{58} = 26.9\%. \tag{71}$$

The component efficiency was,

$$\eta_c = \frac{W_{actual}}{W_{pj}} = \frac{11.9\,J}{15.6\,J} = 76.2\%\,. \tag{72}$$

Overall system efficiency could be expressed as the product of the two,

$$\eta_{overall} = \eta_c \eta_o = 76.2\% \times 26.9\% = 20.5\%\,. \tag{73}$$

For recycling scheme, the operational efficiency as from Equation (52),

$$\eta_o = \frac{W_{pj}}{E_A} = \frac{15.6}{42.0} = 37.3\%. \tag{74}$$

The component efficiency was,

$$\eta_c = \frac{W_{actual}}{W_{pj}} = \frac{12.4\,J}{15.6\,J} = 79.5\%\,. \tag{75}$$

Overall system efficiency could be expressed as the product of the two,

$$\eta_{overall} = \eta_c \eta_o = 79.5\% \times 37.3\% = 29.7\%\,. \tag{76}$$

4.3.3 Work Losses Breakdown on Components

The component efficiency for the recycled scheme also provided us with the breakdown of the energy losses across each component that would impact the work output (Table 8). Identified total work loss by components was found to be 3.3J, which was sum of the No.1, 2, 5, and 6 components. The total energy loss from the difference between W_{actual} and W_{pj} was 3.2J, which closely matched the breakdown from the components.

Table 8 Work loss totals across each component. The work loss values were computed during the phase(s) of the cycle in which that component was active. The loss values are the average over 12 actuation cycles.

#	Component	Loss (J)	Impacts Work Output?
1	Inlet Line	2.09	Yes
2	Plantarflexion Valve In	0.32	Yes
3	Plantarflexion Valve Out	1.76	No
4	Accumulator Valve	0.23	No
5	Accumulator T-Junction	0.43	Yes
6	Dorsiflexion Valve	0.49	Yes
	Total Work Loss (that impacts work output)	3.3	

4.4 DISCUSSION

4.4.1 OPERATIONAL EFFICIENCY

It was illustrated from the results that the majority of the pneumatic energy was lost in the compressed exhaust due to low operational efficiency (non-recycling operational efficiency of 26.9%), even with improved recycling scheme (37.3%). Persistent low operational efficiency is considered one of the biggest drawbacks of pneumatic technology when it comes to improving system efficiency. One important result of this study is that, for a given control volume, pneumatic systems that operate at higher pressures will have reduced operational efficiency compared to lower pressure systems, because more energy is contained in the exhaust gas, from Equation (36). Therefore, when designing a pneumatic system, harvesting exhaust air will help to improve efficiency.

In this study, it was also demonstrated that recycling scheme theoretically improved the operational efficiency from 26.9% to 37.3%. We have recently performed an experimental study that compares the work output and fuel consumption without and with recycling and while using two different control schemes [91]. This study found that the energy improvement can be even more enhanced by using a pneumatic strain energy accumulator. The concept of a pneumatic strain energy accumulator is adopted from a hydraulic strain energy accumulator [155]. Some of the energy of the fluid that enters the accumulator is stored in an elastomer that fills like a balloon, while inside a rigid outer cylinder. Due to nature of the elastomer, the stored energy could be

returned at a relatively higher pressure (on average) than from a fixed volume accumulator, thus more energy can be recovered from this experimental setup [91].

The proposed recycling scheme also poses new control challenges. The current state-estimation control algorithm is compatible with the energy recycling scheme because it assumes a repeatable task with fixed timings. Easy cyclic controls might not be the best controller if we need to change the actuation requirement in the future based on the targeted population. For example, if we need to modulate dorsiflexion actuation pressure, the residual pressure in the accumulator might not be enough to actuate the dorsiflexor assistance multiple times before being refilled by the plantarflexor exhaust. To allow for these diverse powering schemes, more complex power management will be warranted, including refilling the accumulator using the source pressure if necessary, or selectively using power source to actuate dorsiflexor assistance when the accumulator is running low in pressure.

From operational efficiency results, it is also worth noticing that since higher pressure always results in lower operational efficiency, due to greater energy lost in the exhaust. If possible, reducing the system input pressure would help enhance operational efficiency. As a certain output force or torque is needed in most applications, having a bigger actuator that could deliver the same level of force under lower pressure could potentially improve the operational efficiency without sacrificing the system performance.

4.4.2 FUEL CONSUMPTION

In the results of fuel consumption estimate, non-recycling scheme consumed 0.31 g of air and recycling consumed 0.23 g of air. This translated to an estimated 28% of fuel saving.

In this study, current approach to calculate fuel consumption was to estimate from Equations (40) and (43) for each actuation cycle from pressure measurement in the actuator chamber and actuator volume from the data sheet. This simplistic projection of fuel consumption was a reasonable estimate for the fuel consumption, but it failed to account for multiple factors in reality: the residual gas left in valves and tubing, change in temperature within an actuation cycle, leaking, etc. A complete fuel consumption experimental analysis was conducted in a follow up study [91], in which the CO_2 bottle was weighted before and after a 3-min trial to precisely calculate how much CO_2 was used.

Nevertheless, the fuel consumption can still give us some insights about our pneumatic power source selection: in order for the PPAFO to be effective for assistance and rehabilitation, one hour of continuous use would be an ideal operating parameter. From these fuel consumption results, assuming a pace of 1 second per step during one-hour of continuous use, it was estimated that with non-recycling scheme the total amount of air needed to be 1116 g (equivalently 1693 g of CO_2). For the recycling scheme, the needed air was 828 g (equivalently 1256 g of CO_2). As a reference, our current CO_2 tank can hold up to 567 g of CO_2 and lasted about 30 min at full actuation with the non-recycling scheme. Therefore, with the current efficiency and configuration of the PPAFO,

twice the amount of CO_2 would be necessary for one hour of continuous operation. Equivalently, with the recycling scheme, current CO_2 tank can run up to 42 min.

4.4.3 COMPONENT EFFICIENCY

The system components efficiency was an indicator of how much energy was turned into heat, as a result of pressure drops across different pneumatic components. In the results, similar levels of component efficiency were found for both non-recycling and recycling schemes (76.2% for non-recycling, and 79.5% for recycling). Note that because component efficiency was separated from operational efficiency, it could be improved by selection of more efficiency pneumatic components (the upper limit for component efficiency is 100%). Our current results of around 80% component efficiency indicated that there was still room for further improvement. Guidelines on how to further component efficiency could be found in the component work loss analysis.

The work loss analysis broke down the total work loss in the component efficiency into the work losses across each individual component. This analysis could serve as a reference and guideline to identify what was the most inefficient pneumatic component, in the sense that the most of the work was lost across it.

Among the four components that impact system component efficiency, the inlet line (No. 1) illustrated the most work loss (~2 J). This observation agreed with our intuition: the port size for

the valves were the same as the inner diameter of the inlet line, but the inlet line had a much longer length (~ 1.5 m), which allowed much larger pressure drops. The big pressure drop across the inlet line reduced the total work output at the actuator because it moved at a lower net pressure. In contrast, the T junction and two valves during actuation consumed comparable amount of energy (< 0.5 J).

In the future, the first and the most effective step would be to improve the inlet line by substituting a shorter length (if possible) and larger inner diameter tubing. In a quick calculation, to reduce the energy losses from 2.1 J to 1 J, the tubing diameter would have to be 5.8 mm, if the length stayed the same.

4.5 CONCLUSION

In this study, the system overall efficiency was separated into two types of efficiency and analyzed respectively. The exhaust gas from plantarflexion actuation was recycled into an accumulator to improve the operational efficiency from 26.9% to 37.3%, saving fuel from 0.31 g to 0.23 g (a 26% fuel saving). The overall efficiency was improved from 20.5% to 29.7% as a result of the new operation scheme. Additionally, the energy losses across different components were identified experimentally to find out which component had the greatest impact on the work output in component efficiency analysis. The total system component efficiency was identified in both recycling and non-recycling scheme (76.2% for non-recycling, and 79.5% for recycling). The total work loss across all the components was broken down onto each individual component, and the inlet line was found to have the biggest work loss (2.09 J out of 3.3 J total).

Chapter 5 CONCLUSIONS AND FUTURE WORK

5.1 GAIT STATE ESTIMATION AND ACTUATION CONTROL (CHAPTER 2)

In Chapter 2, a state estimator was proposed to learn from training models, compare to sensor readings, and predict the system state for actuation control. Currently, the actuation control policy is solely based on the identified gait state. However, it is believed that the system performances from past gait cycles can also be learned and utilized to design control policies in the future. The attempt to incorporate learning control is described in the following section.

5.1.1 LEARNING CONTROL

Gait is considered a quasi-periodic process, which means there is high level of repeatability in the system. For example, if a user has a history of dropping his/her toes during swing phase of gait, it is very likely that when using the AFO, the next step taken is going to illustrate similar behavior. In other words, there are lessons to be learned in the past system behavior in gait, so that it can be compensated in the future (in a feed forward manner).

Iteration learning control has broad implementations in controlling repetitive processes, especially in manufacturing processes control [70]. Considering gait as a quasi-periodic behavior, a similar ILC approach could be taken. In orthotic device control, iterative learning from past cycles of control performance has the equivalent significance of being able to learn from human dynamics

including muscle weakness, neurological behavior, etc. For the intended end users of the AFO, which are the impaired individuals with below-the-knee muscle weakness, a general trend can be learned between different gait cycles of the same subject. Using information from past experience to control has the potential to make the device capable of predicting human behavior, and responding to the gait events as needed even before it happens.

For pneumatic systems, one major drawback is its delay and slow response time. Mechanical valves take a relatively longer time to drive compared to electromechanical systems. Additionally, the pressure has to build up before the rotary actuator starts to generate desired torque. This compound effect deteriorates the system performance. The ILC can potentially solve this problem by anticipating what is needed and sending in the desired control signal before an event occurs.

However, ILC suffers from several limitations when applied to human assist devices: the ILC is based on the assumption of the repeatability and continuity of gait. While this assumption holds true for therapeutic walking conditions (e.g., continuous treadmill walking), it might not be able to address unpredictable changes while being used as an assist device. For example, the ILC is expected to suffer in a scenario where the user constantly changes paces, stops or turns, when the previous knowledge of the system can no longer help assist the next step. Further investigation is warranted to examine how ILC can be paired with feedback controllers, so that their functionalities will compliment each other.

5.1.2 Stability Analysis

Both DE and LSE controllers function in a feedback loop. The stability of the system has not been systematically analyzed. It has not been a critical issue in designing the current control policy, because the level of assistance that the current actuator can generate (up to 10 Nm) is very modest compared to what the human ankle is able to provide (up to 70 Nm at peak). As a result, with the current experimental setup, only partial assistance is provided. Thus, the human ankle is very likely to dominate the motion and stabilize it.

A system stability analysis will become critical when the PPAFO system is able to generate much more torque (at least 30 Nm). The controller will have to make sure that the actuator is not overpowering the ankle joint, causing instability at the ankle joint. A modelling approach could be taken as a start, where the non-linear models of the PPAFO (previously developed by Shorter et al. [156]) would be coupled with a human dynamics model to mimic gait dynamics, including human motor control.

5.2 GAIT MODE RECOGNITION (CHAPTER 3)

5.2.1 REDUCING THE DELAY IN RECOGNITION

The main drawback for the IMU based mode recognition scheme of Chapter 3 was the one step delay. Since the algorithm tracked the vertical position difference in the past step and assumes continuity, the earliest time to recognize a new gait mode was after the first step in this mode. Moreover, since up to now we have only instrumented the right side with an AFO, the 'first step' has to be on the right side.

For example, in Figure 40, an illustrative case of transiting from level ground mode to stair descent mode is shown. The subject took the first step in stair descent mode with the right foot, but it was not until the end of this first step when the recognition eventually detects a vertical position change. The actuation control scheme for stair descent can then be triggered.

Figure 40 Ankle joint angle (positive for dorsiflexion) as a function of percent gait cycle in three gait modes [125].

Therefore, a zero-delay algorithm is desired to reduce the user's risk. However, given the current hardware setup, it is very difficult for the microcontroller to detect the stair descent intent with no significant delay. Comparing a step of level walking to a step of stair descent, the ankle joint remains about the same range of 10 degrees (Figure 41) for the first half of the gait cycle in both cases. Although the stair descent has a significantly lower starting ankle angle (plantarflexed for landing), it only happens in the repeated cycle therefore not suitable for transition detection. In other words, knowing the kinematic measurement of first half step of a transitional step into stair descent mode does not provide us enough insight to properly detect the new gait mode and modify the controller to accommodate for the new mode.

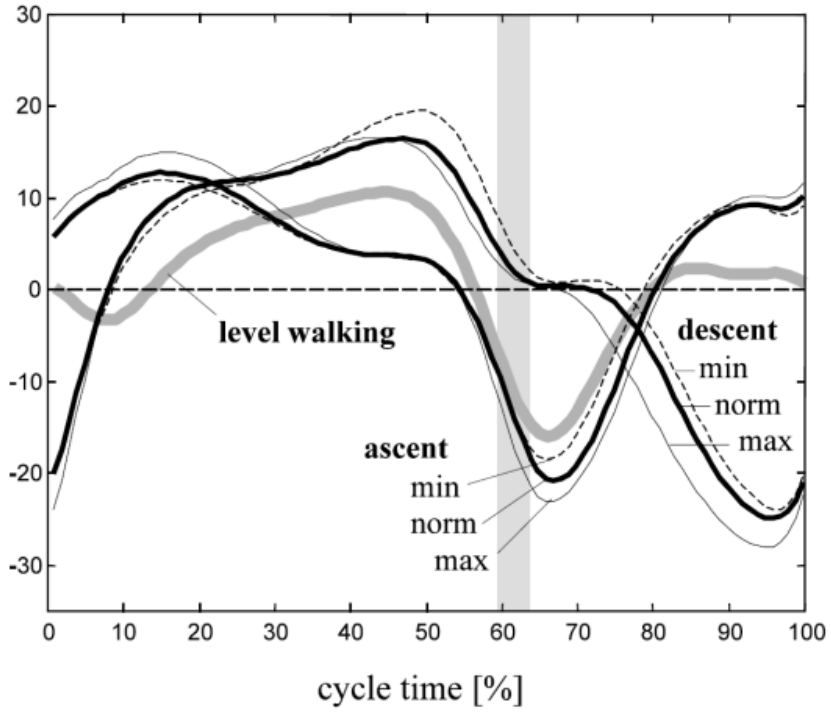

Figure 41 Ankle joint angle (positive for dorsiflexion) as a function of percent gait cycle in three gait modes [125].

Possible solutions include instrumenting the contralateral leg (or foot), adding EMG sensor(s), or looking at other algorithms (such as frequency domain sensor measurement data analysis) to promptly detect gait mode changes.

Alternatively, one-step delay could be eliminated by recognizing a 'transitional state', using any virtual sensors. We could construct a stair (or ramp) environment in the motion capture lab and record the full set of kinetic and kinematic data. With the help of the rich dataset, we will be able to identify what are the most relevant variables to recognize the transitional state between two gait modes. The most relevant variables can then be obtained from different sensors (e.g., thigh segment angle could be measured by an IMU). This is an idealistic approach that could help identify the best sensor array that we need to recognize gait mode transitions in an ideal set-up.

5.2.2 Exploring Faulty Recognition

As discussed in Chapter 3, it is very important for us to establish methods to evaluate how well our current mode recognition system works. In order to answer this question, two related problems need to be further explored: what types of faulty recognition are most undesirable (misrecognizing which two modes), and how likely is it for a faulty recognition to result in a trip (or fall).

5.2.2.1 Consequences in Different Types of Faulty Mode Recognition

In Chapter 3, an optimized threshold was selected to make sure the algorithm would not be biased to favor one gait mode or another. This selection was based on the assumption that all modes were equally important, and misrecognizing any two modes would have equal impact on the

consequence for the device. However, this assumption needs to be further examined: intuitively, misrecognizing stair descent as level ground walking has greater risk than the opposite. Thus, an experimental study is warranted to explore the levels of consequences in different combinations of faulty mode recognition. In this future study, gait mode recognition and control would be implemented with intentional faulty recognition and misfire at random steps to perturb gait and examine the consequence (whether the subject falls as a result). All combinations of actual gait mode and incorrectly identified gait mode would be tested (Figure 42).

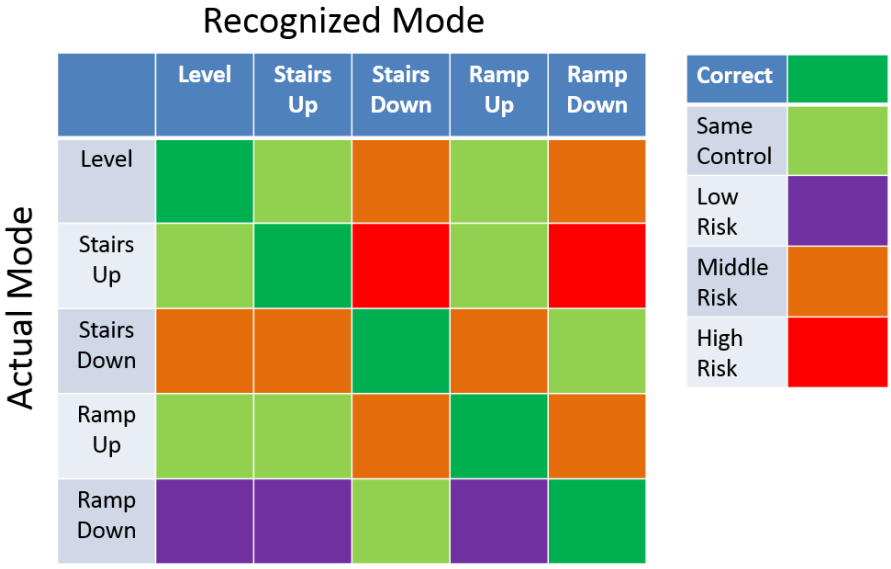

Figure 42 Preliminary expected level of consequences in different faulty mode recognition combinations

5.2.2.2 Probability of Trip and Fall Caused by Faulty Mode Recognition

As described in the discussion section of Chapter 3, it was of interest to understand the likelihood of a trip or a fall in the event of a faulty recognition. These type of data can only be obtained by testing a large number of trials, during which the actuation control was randomly and intentionally set to the wrong gait mode. The end result will be an expected ratio between the number of actual

falls and the total number of faulty mode recognitions. This indicator will help identify the requirement of mode recognition success rate in order to match certain probability of trips and falls (e.g., the requirement for a gait assistance device could be maximum one fall per 100, 000 steps of actuation).

There are two main difficulties in conducting this experiment: First, from a safety standpoint, it is very risky to set up an experiment to intentionally make people fall. Considering that multiple locations will have to be tested (stairs and ramps), the only choice of protection is to have multiple spotters moving next to the subject. It remains unclear whether such a setup will change the perceptions of users and affect the results of this study. Second, since we are trying to estimate the probability of a 'rare event', the consistency between different users can not be guaranteed and requires further investigation.

5.3 Energy Efficiency Analysis and Energy Harvesting (Chapter 4)

5.3.1 Harvesting Human Energy

One of the biggest differences between human walking dynamics and how a human assist devices function is how energy enters and exists the system. Given that human gait is almost an energy neutral process [72], during normal unassisted walking most of the kinetic energy during gait is harvested by the soft musculoskeletal tissues and restored back. As a bio-mimicking approach, efforts to incorporate such energy harvesting mechanisms have been made to human assist devices [27, 30, 73, 74], using regenerative mechanisms (e.g. springs).

Similar concepts can potentially be applied to our pneumatic system to take the advantage of the compressibility of the system. Instead of engaging and disengaging gears or springs, a set of valves can redirect the gas flow into or out of the actuator, and store it into an accumulator, at times when there actuator is supposed to output negative work to human [157] (i.e., human kinetic energy can be absorbed and used as a compressor for gas), as in Figure 43. This solution enjoys the benefits of both minimal addition of hardware (only a set of valves and tubing), and optimized energy harvesting ability.

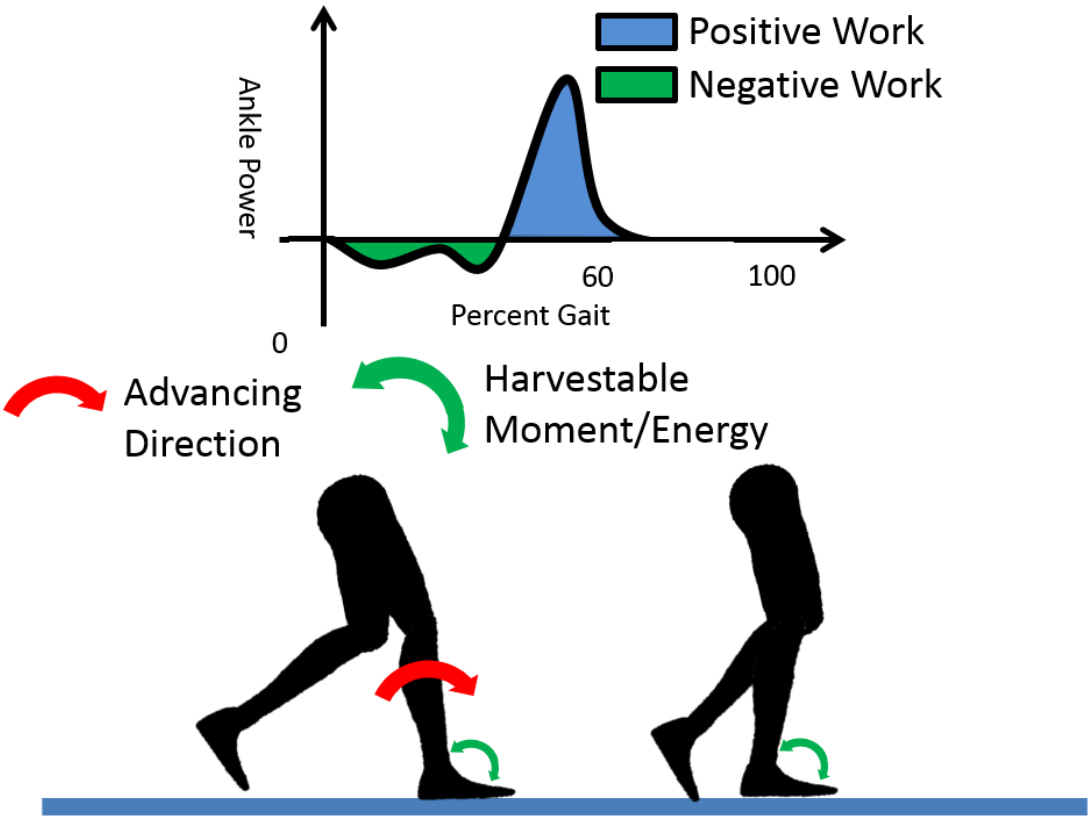

Figure 43 Demonstration of the energy harvestable zone for the ankle during gait

REFERENCES

[1] J. Perry, *Gait analysis: normal and pathological function*. Thorofare, NJ: Slack INC., 1992.

[2] A. M. Dollar and H. Herr, "Lower extremity exoskeletons and active orthoses: challenges and state-of-the-art," *Robotics, IEEE Transactions on,* vol. 24, pp. 144-158, 2008.

[3] T. C. Turin, Y. Kokubo, Y. Murakami, A. Higashiyama, N. Rumana, M. Watanabe, and T. Okamura, "Lifetime risk of stroke in Japan," *Stroke,* vol. 41, pp. 1552-1554, 2010.

[4] D. J. Farris and G. S. Sawicki, "The mechanics and energetics of human walking and running: a joint level perspective," *Journal of The Royal Society Interface,* vol. 9, pp. 110-118, 2012.

[5] D. Ferris, G. Sawicki, and M. Daley, "A physiologist's perspective on robotic exoskeletons for human locomotion," *International Journal of Humanoid Robotics,* vol. 4, pp. 507 - 528, 2007.

[6] K. A. Shorter, J. Xia, E. T. Hsiao-Wecksler, W. K. Durfee, and G. F. Kogler, "Technologies for Powered Ankle-Foot Orthotic Systems: Possibilities and Challenges," 2010.

[7] S. Yamamoto, M. Ebina, et al. , "Development of a New Ankle-Foot Orthosis with Dorsiflexion Assist, Part 1: Desirable Characteristics of Ankle-Foot Orthosis for Hemiplegic Patients," *Journal of Prosthetics and Orthotics,* vol. 9, pp. 174-9, 1997.

[8] H. B. Kitaoka, X. M. Crevoisier, K. Harbst, D. Hansen, B. Kotajarvi, and K. Kaufman, "The effect of custom-made braces for the ankle and hindfoot on ankle and foot kinematics and ground reaction forces," *Archives of Physical Medicine and Rehabilitation,* vol. 87, pp. 130-135, January 2006.

[9] G. K. Rose, *Orthotics: Principles and Practice*. London: Williams Heinemann, 1986.

[10] C. E. Buckon, S. S. Thomas, S. Jakobson-Huston, M. Moor, M. Sussman, and M. Aiona, "Comparison of three ankle–foot orthosis configurations for children with spastic diplegia," *Developmental Medicine & Child Neurology,* vol. 46, pp. 590-598, Aug 2004 2004.

[11] C. Bulley, J. Shiels, K. Wilkie, and L. Salisbury, "User experiences, preferences and choices relating to functional electrical stimulation and ankle foot orthoses for foot-drop after stroke," *Physiotherapy,* vol. 97, pp. 226-233, 2011.

[12] J. C. Patzkowski, R. V. Blanck, J. G. Owens, J. M. Wilken, K. L. Kirk, J. C. Wenke, and J. R. Hsu, "Comparative effect of orthosis design on functional performance," *The Journal of Bone & Joint Surgery,* vol. 94, pp. 507-515, 2012.

[13] J. B. Redford, *Orthotics etcetera.* Baltimore, MD: Williams and Wilkins, 1986.

[14] R. Jiménez-Fabián and O. Verlinden, "Review of control algorithms for robotic ankle systems in lower-limb orthoses, prostheses, and exoskeletons," *Medical Engineering & Physics,* vol. 34, pp. 397-408, 2012.

[15] J. Bakker, I. De Groot, H. Beckerman, B. De Jong, and G. Lankhorst, "The effects of knee-ankle-foot orthoses in the treatment of Duchenne muscular dystrophy: review of the literature," *Clinical rehabilitation,* vol. 14, pp. 343-359, 2000.

[16] J. Furusho, T. Kikuchi, M. Tokuda, T. Kakehashi, K. Ikeda, S. Morimoto, Y. Hashimoto, H. Tomiyama, A. Nakagawa, and Y. Akazawa, "Development of shear type compact MR brake for the intelligent ankle-foot orthosis and its control; research and development in NEDO for practical application of human support robot," in *IEEE 10th International Conference on Rehabilitation Robotics, 2007*, Noordwijk, the Netherlands, 2007, pp. 89-94.

[17] W. Svensson and U. Holmberg, "Ankle-foot-orthosis control in inclinations and stairs," in *2008 IEEE International Conference on Robotics, Automation and Mechatronics*, Chengdu, China, 2008, pp. 301-306.

[18] T. Kikuchi, S. Tanida, K. Otsuki, T. Yasuda, and J. Furusho, "Development of third-generation intelligently Controllable ankle-foot orthosis with compact MR fluid brake," in *Robotics and Automation (ICRA), 2010 IEEE International Conference on*, 2010, pp. 2209-2214.

[19] J. A. Blaya and H. Herr, "Adaptive control of a variable-impedance ankle-foot orthosis to assist drop-foot gait," *Neural Systems and Rehabilitation Engineering, IEEE Transactions on,* vol. 12, pp. 24-31, 2004.

[20] A. W. Boehler, K. W. Hollander, T. G. Sugar, and S. Dosun, "Design, implementation and test results of a robust control method for a powered ankle foot orthosis (AFO)," in *Robotics and Automation, 2008. ICRA 2008. IEEE International Conference on*, 2008, pp. 2025-2030.

[21] D. Ferris, G. Sawicki, and A. Domingo, "Powered lower limb orthoses for gait rehabilitation," *Topics in Spinal Cord Injury Rehabilitation,* vol. 11, pp. 34 - 49, 2005.

[22] S. Hwang, J. Kim, and Y. Kim, "Development of an active ankle-foot orthosis for hemiplegic patients," in *Proceedings of the 1st international convention on Rehabilitation engineering & assistive technology: in conjunction with 1st Tan Tock Seng Hospital Neurorehabilitation Meeting* Singapore 2007.

[23] G. A. Pratt and M. M. Williamson, "Series elastic actuators," in *IEEE International Conference on Intelligent Robots and Systems*, 1995, pp. 399-406.

[24] A. Roy, H. I. Krebs, D. J. Williams, C. T. Bever, L. W. Forrester, R. M. Macko, and N. Hogan, "Robot-Aided Neurorehabilitation: A Novel Robot for Ankle Rehabilitation," *Robotics, IEEE Transactions on,* vol. 25, pp. 569-582, 2009.

[25] A. Roy, H. I. Krebs, S. L. Patterson, T. N. Judkins, I. Khanna, L. W. Forrester, R. M. Macko, and N. Hogan, "Measurement of human ankle stiffness using the Anklebot," in *IEEE 10th International Conference on Rehabilitation Robotics, 2007. ICORR 2007*, Noordwijk, The Netherlands, 2007, pp. 356-363.

[26] K. W. Hollander, R. Ilg, T. G. Sugar, and D. Herring, "An efficient robotic tendon for gait assistance," *J. Biomech. Eng. ,* vol. 128, pp. 788-792, October 2006.

[27] J. Hitt, A. M. Oymagil, T. Sugar, K. Hollander, A. Boehler, and J. Fleeger, "Dynamically Controlled Ankle-Foot Orthosis (DCO) with Regenerative Kinetics: Incrementally Attaining User Portability," in *Robotics and Automation, 2007 IEEE International Conference on*, 2007, pp. 1541-1546.

[28] A. W. Boehler, K. W. Hollander, T. G. Sugar, and D. Shin, "Design, implementation and test results of a robust control method for a powered ankle foot orthosis (AFO)," in *IEEE International Conference on Robotics and Automation, 2008. ICRA 2008*, 2008, pp. 2025-2030.

[29] D. W. Robinson, J. E. Pratt, D. J. Paluska, and G. A. Pratt, "Series elastic actuator development for a biomimetic walking robot," in *Advanced Intelligent Mechatronics, 1999. Proceedings. 1999 IEEE/ASME International Conference on*, 1999, pp. 561-568.

[30] J. A. Ward, T. G. Sugar, and K. W. Hollander, "Using the translational potential energy of springs for prosthetic systems," in *Control Applications (CCA), 2011 IEEE International Conference on*, 2011, pp. 1461-1467.

[31] J. Ward, T. Sugar, J. Standeven, and J. R. Engsberg, "Stroke survivor gait adaptation and performance after training on a Powered Ankle Foot Orthosis," in *Robotics and Automation (ICRA), 2010 IEEE International Conference on*, 2010, pp. 211-216.

[32] J. Xia and W. K. Durfee, "Analysis of Small-Scale Hydraulic Actuation Systems," *Reviews of Microfluidics Components* vol. 9, p. 11, 2013.

[33] A. Wolczowski and M. Kurzynski, "Control of artificial hand via recognition of EMG signals," in *Biological and Medical Data Analysis*, ed: Springer, 2004, pp. 356-367.

[34] A. Wolczowski and M. Kurzynski, "Control of dexterous hand via recognition of EMG signals using combination of decision-tree and sequential classifier," in *Computer Recognition Systems 2*, ed: Springer, 2007, pp. 687-694.
[35] J. Hitt, T. Sugar, M. Holgate, R. Bellman, and K. Hollander, "Robotic transtibial prosthesis with biomechanical energy regeneration," *Industrial robot,* vol. 36, pp. 441-447, 2009.
[36] A. Soares, A. Andrade, E. Lamounier, and R. Carrijo, "The development of a virtual myoelectric prosthesis controlled by an EMG pattern recognition system based on neural networks," *Journal of Intelligent Information Systems,* vol. 21, pp. 127-141, 2003.
[37] F. Sup, A. Bohara, and M. Goldfarb, "Design and Control of a Powered Transfemoral Prosthesis," *The International Journal of Robotics Research,* vol. 27, pp. 263-273, February 1, 2008 2008.
[38] S. M. M. Rahman and R. Ikeura, "A Novel Variable Impedance Compact Compliant Ankle Robot for Overground Gait Rehabilitation and Assistance," *Procedia Engineering,* vol. 41, pp. 522-531, 2012.
[39] M. R. Eicholtz and S. H. Collins, "Two-dimensional parameter study to characterize performance of ankle-foot orthosis joint impedance control," 2012.
[40] G. S. Sawicki and D. P. Ferris, "Mechanics and energetics of level walking with powered ankle exoskeletons," *The Journal of Experimental Biology,* vol. 211, pp. 1402-1413, 2008.
[41] S. Cain, K. E. Gordon, and D. P. Ferris, "Human motor adaptation during walking with a powered ankle-foot orthosis depends on control method," *Journal of NeuroEngineering and Rehabilitation,* vol. 4, p. 48, 2007.
[42] D. P. Ferris, K. E. Gordon, G. S. Sawicki, and A. Peethambaran, "An improved powered ankle-foot orthosis using proportional myoelectric control," *Gait and Posture,* vol. 23, pp. 425-428, 2006.
[43] G. S. Sawicki and D. P. Ferris, "A pneumatically powered knee-ankle-foot orthosis (KAFO) with myoelectric activation and inhibition," *Journal of neuroengineering and rehabilitation,* vol. 6, p. 23, 2009.
[44] D. Ferris, J. Czerniecki, and B. Hannaford, "An ankle-foot orthosis powered by artificial pneumatic muscles," *Journal of Applied Biomechanics,* vol. 21, pp. 189 - 197, 2005.
[45] V. Nekoukar and A. Erfanian, "Adaptive terminal sliding mode control of ankle movement using functional electrical stimulation of agonist-antagonist muscles," in *Engineering in Medicine and Biology Society (EMBC), 2010 Annual International Conference of the IEEE*, 2010, pp. 5448-5451.
[46] D. Popovic and T. Sinkjaer, "Improved control for functional electrical stimulation to restore walking," *Hong Kong Physiotherapy Journal,* vol. 18, pp. 12-20, 2000.
[47] D. Popovic, "Externally Powered and Controlled Orthotics and Prosthetics," *The Biomedical Engineering HandBook. Boca Raton: CRC Press LLC,* 2000.
[48] H. A. Quintero, R. J. Farris, W. K. Durfee, and M. Goldfarb, "Feasibility of a hybrid-FES system for gait restoration in paraplegics," in *Engineering in Medicine and Biology Society (EMBC), 2010 Annual International Conference of the IEEE*, 2010, pp. 483-486.
[49] W. K. Durfee and M. Goldfarb, "Design of a controlled-brake orthosis for regulating FES-aided gait," in *Engineering in Medicine and Biology Society, 1992 14th Annual International Conference of the IEEE*, 1992, pp. 1337-1338.
[50] M. Goldfarb, K. Korkowski, B. Harrold, and W. Durfee, "Preliminary evaluation of a controlled-brake orthosis for FES-aided gait," *Neural Systems and Rehabilitation Engineering, IEEE Transactions on,* vol. 11, pp. 241-248, 2003.
[51] T. Sugar, O. Kameyama, R. Ogawa, M. Matsuura, and H. Oka, "Newly designed computer controlled knee-ankle-foot orthosis (Intelligent Orthosis)," *Prosthetics and Orthotics International,* vol. 22, pp. 230-239, 1998.
[52] T. G. Sugar, K. W. Hollander, and J. K. Hitt, "Walking with springs," pp. 797602-797602, 2011.
[53] M. A. Holgate, A. W. Bohler, and T. G. Sugar, "Control algorithms for ankle robots: A reflection on the state-of-the-art and presentation of two novel algorithms," in *Biomedical Robotics and*

Biomechatronics, 2008. BioRob 2008. 2nd IEEE RAS & EMBS International Conference on, 2008, pp. 97-102.

[54] K. A. Shorter, E. T. Hsiao-Wecksler, G. F. Kogler, Loth, E., and W. K. Durfee, "A Portable-Powered-Ankle-Foot-Orthosis for rehabilitation," *Journal of Rehabilitation Research & Development,* vol. 48, pp. 459-472, Nov 4 2011.

[55] M. A. Holgate, T. G. Sugar, and A. W. Bohler, "A novel control algorithm for wearable robotics using phase plane invariants," in *Robotics and Automation, 2009. ICRA '09. IEEE International Conference on*, 2009, pp. 3845-3850.

[56] M. A. Holgate, A. W. Bohler, and T. G. Sugar, "Control Algorithms for Ankle Robots: A Reflection on the State-of-the-Art and Presentation of Two Novel Algorithms," presented at the 2008 IEEE International Conference on Biomedical Robotics and Biomechatronics, Scottsdale, Arizona, USA, 2008.

[57] M. F. Eilenberg, H. Geyer, and H. Herr, "Control of a Powered Ankle–Foot Prosthesis Based on a Neuromuscular Model," *Neural Systems and Rehabilitation Engineering, IEEE Transactions on,* vol. 18, pp. 164-173, 2010.

[58] H. Geyer and H. Herr, "A muscle-reflex model that encodes principles of legged mechanics produces human walking dynamics and muscle activities," *Neural Systems and Rehabilitation Engineering, IEEE Transactions on,* vol. 18, pp. 263-273, 2010.

[59] M. F. Eilenberg, "A neuromuscular-model based control strategy for powered ankle-foot prostheses," Master of Science, Massachusetts Institute of Technology, 2009.

[60] J. M. Wang, D. J. Fleet, and A. Hertzmann, "Gaussian process dynamical models for human motion," *Pattern Analysis and Machine Intelligence, IEEE Transactions on,* vol. 30, pp. 283-298, 2008.

[61] H. A. Varol, F. Sup, and M. Goldfarb, "Multiclass Real-Time Intent Recognition of a Powered Lower Limb Prosthesis," *Biomedical Engineering, IEEE Transactions on,* vol. 57, pp. 542-551, 2010.

[62] J. Yoon, B. Novandy, C.-H. Yoon, and K.-J. Park, "A 6-DOF gait rehabilitation robot with upper and lower limb connections that allows walking velocity updates on various terrains," *Mechatronics, IEEE/ASME Transactions on,* vol. 15, pp. 201-215, 2010.

[63] W. C. Flowers and R. W. Mann, "An Electrohydraulic Knee-Torque Controller for a Prosthesis Simulator," *Journal of Biomechanical Engineering,* vol. 99, pp. 3-8, 1977.

[64] M. Arazpour, A. Chitsazan, M. A. Bani, G. Rouhi, F. T. Ghomshe, and S. W. Hutchins, "The effect of a knee ankle foot orthosis incorporating an active knee mechanism on gait of a person with poliomyelitis," *Prosthetics and orthotics international,* 2013.

[65] H. Krebs, L. Dipietro, S. Levy-Tzedek, S. Fasoli, A. Rykman-Berland, J. Zipse, J. Fawcett, J. Stein, H. Poizner, A. Lo, B. Volpe, and N. Hogan, "A paradigm shift for rehabilitation robotics," *Engineering in Medicine and Biology Magazine, IEEE,* vol. 27, pp. 61-70, July-Aug. 2008.

[66] S. HosseinNia, F. Romero, I. Tejado, F. Alonso, and B. Vinagre, "Controller Design for A Stance-Control Knee-Ankle-Foot Orthosis Based on Optimization Techniques," *arXiv preprint arXiv:1206.1626,* 2012.

[67] X. Zhang, X. Kong, G. Liu, and Y. Wang, "Research on the walking gait coordinations of the lower limb rehabilitation robot," in *Robotics and Biomimetics (ROBIO), 2010 IEEE International Conference on*, 2010, pp. 1233-1237.

[68] D. J. J. Bregman, M. M. van der Krogt, V. de Groot, J. Harlaar, M. Wisse, and S. H. Collins, "The effect of ankle foot orthosis stiffness on the energy cost of walking: A simulation study," *Clinical Biomechanics,* vol. 26, pp. 955-961, 2011.

[69] M. B. Wiggin, G. S. Sawicki, and S. H. Collins, "An exoskeleton using controlled energy storage and release to aid ankle propulsion," in *Rehabilitation Robotics (ICORR), 2011 IEEE International Conference on*, 2011, pp. 1-5.

[70] K. L. Barton and A. G. Alleyne, "A cross-coupled iterative learning control design for precision motion control," *Control Systems Technology, IEEE Transactions on,* vol. 16, pp. 1218-1231, 2008.
[71] C. Yang, G. Ganesh, S. Haddadin, S. Parusel, A. Albu-Schaeffer, and E. Burdet, "Human-like adaptation of force and impedance in stable and unstable interactions," *Robotics, IEEE Transactions on,* vol. 27, pp. 918-930, 2011.
[72] A. D. Winter, *Biomechanics and Motor Conbtrol of Human Movement*. New York: John Wiley & Sons, 1990.
[73] A. M. Oymagil, J. K. Hitt, T. Sugar, and J. Fleeger, "Control of a Regenerative Braking Powered Ankle Foot Orthosis," in *Rehabilitation Robotics, 2007. ICORR 2007. IEEE 10th International Conference on*, 2007, pp. 28-34.
[74] S. H. Collins and A. D. Kuo, "Recycling energy to restore impaired ankle function during human walking," *PLoS one,* vol. 5, p. e9307, 2010.
[75] G. Sawicki, K. Gordon, and D. Ferris, "Powered lower limb orthoses: applications in motor adaptation and rehabilitation," *Proceedings of the IEEE International Conference on Rehabilitation Robotics; Chicago, IL,* 2005.
[76] K. Gordon, G. Sawicki, and D. Ferris, "Mechanical performance of artificial pneumatic muscles to power an ankle-foot orthosis," *Journal of Biomechanics,* vol. 39, pp. 1832 - 1841, 2006.
[77] K. H. Ha, H. A. Varol, and M. Goldfarb, "Volitional Control of a Prosthetic Knee Using Surface Electromyography," *Biomedical Engineering, IEEE Transactions on,* vol. 58, pp. 144-151, 2011.
[78] C. M. Kim and J. J. Eng, "The Relationship of Lower-Extremity Muscle Torque to Locomotor Performance in People With Stroke," vol. 83, ed, 2003, pp. 49-57.
[79] D. J. Weber, R. B. Stein, K. M. Chan, G. Loeb, F. Richmond, R. Rolf, K. James, and C. Su Ling, "Bionic WalkAide for correcting foot drop," *Neural Systems and Rehabilitation Engineering, IEEE Transactions on,* vol. 13, pp. 242-246, 2005.
[80] J. M. Hausdorff and H. Ring, "Effects of a new radio frequency–controlled neuroprosthesis on gait symmetry and rhythmicity in patients with chronic hemiparesis," *American Journal of Physical Medicine and Rehabilitation,* vol. 87, pp. 4-13, January 2008.
[81] S. E. Irby, K. A. Bernhardt, and K. R. Kaufman, "Gait changes over time in stance control orthosis users," *Prosthetics and Orthotics International,* vol. 31, pp. 353-361, December 1, 2007 2007.
[82] R. J. Farris, H. A. Quintero, and M. Goldfarb, "Preliminary Evaluation of a Powered Lower Limb Orthosis to Aid Walking in Paraplegic Individuals," *Neural Systems and Rehabilitation Engineering, IEEE Transactions on,* vol. 19, pp. 652-659, 2011.
[83] A. B. Zoss, H. Kazerooni, and A. Chu, "Biomechanical design of the Berkeley lower extremity exoskeleton (BLEEX)," *Mechatronics, IEEE/ASME Transactions on,* vol. 11, pp. 128-138, 2006.
[84] A. Hamid, M. N. A. A. Patar, and M. A. Ayub, "Force Sensor Detection and Performance Evaluation of New Active System Ankle Foot Orthosis," *Procedia Engineering,* vol. 41, pp. 510-515, 2012.
[85] D. Li, A. Becker, K. A. Shorter, T. Bretl, and E. A. Hsiao-Wecksler, "Estimating System State During Human Walking With a Powered Ankle-Foot Orthosis," *Mechatronics, IEEE/ASME Transactions on,* vol. 16, pp. 835-844, 2011.
[86] E. A. Morris, K. A. Shorter, Y. Li, E. T. Hsiao-Wecksler, G. F. Kogler, T. Bretl, and W. K. Durfee, "Actuation Timing Strategies for a Portable Powered Ankle Foot Orthosis," *ASME Conference Proceedings,* vol. 2011, pp. 807-814, 2011.
[87] Y. Li, Hsiao-Wecksler, E., "Gait Mode Recognition Using an Inertial Measurement Unit to Control an Ankle-Foot Orthosis During Stair Ascent and Descent," in *Dynamic Systems and Controls Conference*, Fort Lauderdale, FL, 2012.
[88] Y. Li, Hsiao-Wecksler, E., "Gait Mode Recognition using An Inertia Measurement Unit on A Powered Ankle-Foot Orthosis " presented at the American Society of Biomechanics., Gainesville, FL, 2012.

[89] Y. Li and E. Hsiao-Wecksler, "Gait Mode Recognition and Control for a Portable-Powered Ankle-Foot Orthosis," in *IEEE 13th International Conference on Rehabilitation Robotics, 2013*, Seattle, USA, 2013.

[90] Y. Li, E.A. Morris, K. A. Shorter, E.T. Hsiao-Wecksler, "Energy Efficiency Analysis of A Pneumatically-Powered Ankle-Foot Orthosis," presented at the 52nd National Conference on Fluid Power, Las Vegas, NV, 2011.

[91] M. Boes, M. Islam, Y. Li, and E. Hsiao-Wecksler, "Fuel Efficiency of a Portable Powered Ankle-Foot Orthosis," in *IEEE 13th International Conference on Rehabilitation Robotics, 2013*, Seattle, USA, 2013.

[92] R. R. Neptune, S. A. Kautz, and F. E. Zajac, "Contributions of the individual ankle plantar flexors to support, forward progression and swing initiation during walking," *Journal of Biomechanics,* vol. 34, pp. 1387-1398, November 2001.

[93] V. L. Roger, A. S. Go, D. M. Lloyd-Jones, E. J. Benjamin, J. D. Berry, W. B. Borden, D. M. Bravata, S. Dai, E. S. Ford, and C. S. Fox, "Heart Disease and Stroke Statistics—2012 Update A Report From the American Heart Association," *Circulation,* vol. 125, pp. e2-e220, 2012.

[94] M. C. Dalakas, "The post‐polio syndrome as an evolved clinical entity," *Annals of the New York Academy of Sciences,* vol. 753, pp. 68-80, 1995.

[95] G. Rosati, "The prevalence of multiple sclerosis in the world: an update," *Neurological sciences,* vol. 22, pp. 117-139, 2001.

[96] M. Bernhard, A. Gries, P. Kremer, and B. W. Böttiger, "Spinal cord injury (SCI)—prehospital management," *Resuscitation,* vol. 66, pp. 127-139, 2005.

[97] J. Baio, "Prevalence of Autism Spectrum Disorders: Autism and Developmental Disabilities Monitoring Network, 14 Sites, United States, 2008. Morbidity and Mortality Weekly Report. Surveillance Summaries. Volume 61, Number 3," *Centers for Disease Control and Prevention,* 2012.

[98] B. Orthopedic, ed. Troy, Michigan: Becker online catalog.

[99] S. Yamamoto, M. Ebina, M. Iwasaki, S. Kubo, H. Kawai, and T. Hayashi, "Comparative Study of Mechanical Characteristics of Plastic AFOs," *Journal of Prosthetics & Orthotics,* vol. 5, April 1993.

[100] D. J. Weber, R. B. Stein, K. M. Chan, G. Loeb, F. Richmond, R. Rolf, K. James, and S. L. Chong, "BIONic WalkAide for correcting foot drop," *IEEE Transactions on Neural Systems and Rehabilitation Engineering,* vol. 13, pp. 242-246, June 2005.

[101] R. Chin, E. T. Hsiao-Wecksler, E. Loth, G. Kogler, S. D. Manwaring, S. N. Tyson, K. A. Shorter, and J. N. Gilmer, "A pneumatic power harvesting ankle-foot orthosis to prevent foot-drop," *Journal of NeuroEngineering and Rehabilitation,* vol. 6, 2009.

[102] A. Forner-Corderoa, H. J. F. M. Koopman, and F. C. T. van der Helma, "Describing gait as a sequence of states " *Journal of Biomechanics,* vol. 39, pp. 948-957, 2006.

[103] A. V. S. Oppenheim, Ronald W. (1975). Digital Signal Processing. Prentice Hall. p. 5. . *Digital Signal Processing*. Upper Saddle River, New Jersey: Prentice Hall, 1975.

[104] R. T. Collins, R. Gross, and J. Shi, "Silhouette-based human identification from body shape and gait," in *Automatic Face and Gesture Recognition, 2002. Proceedings. Fifth IEEE International Conference on*, 2002, pp. 366-371.

[105] J. Mantyjarvi, M. Lindholm, E. Vildjiounaite, S.-M. Makela, and H. Ailisto, "Identifying users of portable devices from gait pattern with accelerometers," in *Acoustics, Speech, and Signal Processing, 2005. Proceedings.(ICASSP'05). IEEE International Conference on*, 2005, pp. ii/973-ii/976 Vol. 2.

[106] R. Kram, T. M. Griffin, J. M. Donelan, and Y. H. Chang, "Force treadmill for measuring vertical and horizontal ground reaction forces," *Journal of Applied Physiology* vol. 85, pp. 764-769, 1998.

[107] W. S. Cleveland and S. J. Devlin, "Locally weighted regression: an approach to regression analysis by local fitting," *Journal of the American Statistical Association,* vol. 83, pp. 596-610, 1988.

[108] C. Bishop, *Pattern Recognition and Machine Learning*. Berlin: Springer, 2006.
[109] D. Ferris, K. Gordon, G. Sawicki, and A. Peethambaran, "An improved powered ankle-foot orthosis using proportional myoelectric control," *Gait Posture.,* vol. 23, pp. 425 - 428, 2006.
[110] S. Au, M. Berniker, and H. Herr, "Powered ankle-foot prosthesis to assist level-ground and stair-descent gaits," *Neural Networks,* vol. 21, pp. 654-666, 2008.
[111] D. Jin, J. Yang, R. Zhang, R. Wang, and J. Zhang, "Terrain identification for prosthetic knees based on electromyographic signal features," *Tsinghua Science & Technology,* vol. 11, pp. 74-79, 2006.
[112] D. Wang, L. Du, and H. Huang, "Terrain recognition improves the performance of neural-machine interface for locomotion mode recognition," in *Computing, Networking and Communications (ICNC), 2013 International Conference on*, 2013, pp. 87-91.
[113] P. Parker, K. Englehart, and B. Hudgins, "Myoelectric signal processing for control of powered limb prostheses," *J Electromyogr Kinesiol.,* vol. 16, pp. 541 - 548, 2006.
[114] K. Momen, S. Krishnan, and T. Chau, "Real-time classification of forearm electromyographic signals corresponding to user-selected intentional movements for multifunction prosthesis control," *Neural Systems and Rehabilitation Engineering, IEEE Transactions on,* vol. 15, pp. 535-542, 2007.
[115] A. B. Ajiboye and R. F. Weir, "A heuristic fuzzy logic approach to EMG pattern recognition for multifunctional prosthesis control," *Neural Systems and Rehabilitation Engineering, IEEE Transactions on,* vol. 13, pp. 280-291, 2005.
[116] P. Wojtczak, T. G. Amaral, O. P. Dias, A. Wolczowski, and M. Kurzynski, "Hand movement recognition based on biosignal analysis," *Engineering Applications of Artificial Intelligence,* vol. 22, pp. 608-615, 2009.
[117] S. Ekvall and D. Kragic, "Grasp recognition for programming by demonstration," in *Robotics and Automation, 2005. ICRA 2005. Proceedings of the 2005 IEEE International Conference on*, 2005, pp. 748-753.
[118] H. Huang, F. Zhang, L. J. Hargrove, Z. Dou, D. R. Rogers, and K. B. Englehart, "Continuous Locomotion-Mode Identification for Prosthetic Legs Based on Neuromuscular–Mechanical Fusion," *Biomedical Engineering, IEEE Transactions on,* vol. 58, pp. 2867-2875, 2011.
[119] OttoBock. (2002). *The Electronic C-Leg® Knee Joint System: Instructions for Use* [Cited 2013 http://www.ottobockus.com].
[120] F. Sup, H. A. Varol, and M. Goldfarb, "Upslope Walking With a Powered Knee and Ankle Prosthesis: Initial Results With an Amputee Subject," *Neural Systems and Rehabilitation Engineering, IEEE Transactions on,* vol. 19, pp. 71-78, 2011.
[121] B. E. Lawson, H. A. Varol, F. Sup, and M. Goldfarb, "Stumble detection and classification for an intelligent transfemoral prosthesis," in *Engineering in Medicine and Biology Society (EMBC), 2010 Annual International Conference of the IEEE*, 2010, pp. 511-514.
[122] B. E. Lawson, H. A. Varol, and M. Goldfarb, "Ground adaptive standing controller for a powered transfemoral prosthesis," in *Rehabilitation Robotics (ICORR), 2011 IEEE International Conference on*, 2011, pp. 1-6.
[123] Z. Fan, F. Zheng, L. Ming, and H. He, "Preliminary design of a terrain recognition system," in *Engineering in Medicine and Biology Society,EMBC, 2011 Annual International Conference of the IEEE*, 2011, pp. 5452-5455.
[124] B. Coley, B. Najafi, A. Paraschiv-Ionescu, and K. Aminian, "Stair climbing detection during daily physical activity using a miniature gyroscope," *Gait & posture,* vol. 22, pp. 287-294, 2005.
[125] R. Riener, M. Rabuffetti, and C. Frigo, "Stair ascent and descent at different inclinations," *Gait & Posture,* vol. 15, pp. 32-44, 2002.

[126] A. Protopapadaki, W. I. Drechsler, M. C. Cramp, F. J. Coutts, and O. M. Scott, "Hip, knee, ankle kinematics and kinetics during stair ascent and descent in healthy young individuals," *Clinical Biomechanics,* vol. 22, pp. 203-210, 2007.

[127] B. J. McFadyen and D. A. Winter, "An integrated biomechanical analysis of normal stair ascent and descent," *Journal of Biomechanics,* vol. 21, pp. 733-744, 1988.

[128] S. Nadeau, B. J. McFadyen, and F. Malouin, "Frontal and sagittal plane analyses of the stair climbing task in healthy adults aged over 40 years: what are the challenges compared to level walking?," *Clinical biomechanics (Bristol, Avon),* vol. 18, pp. 950-959, 2003.

[129] D. Gates, "Characterizing ankle function during stair ascent, descent, and level walking for ankle prosthesis and orthosis design," Master of Science, Boston University, 2002.

[130] H. Luinge and P. Veltink, "Measuring orientation of human body segments using miniature gyroscopes and accelerometers," *Medical and Biological Engineering and Computing,* vol. 43, pp. 273-282, 2005.

[131] E. R. Bachmann, Y. Xiaoping, D. McKinney, R. B. McGhee, and M. J. Zyda, "Design and implementation of MARG sensors for 3-DOF orientation measurement of rigid bodies," in *Robotics and Automation, 2003. Proceedings. ICRA '03. IEEE International Conference on*, 2003, pp. 1171-1178 vol.1.

[132] E. Foxlin, "Inertial head-tracker sensor fusion by a complementary separate-bias Kalman filter," in *Virtual Reality Annual International Symposium, 1996., Proceedings of the IEEE 1996*, 1996, pp. 185-194, 267.

[133] J. L. Marins, Y. Xiaoping, E. R. Bachmann, R. B. McGhee, and M. J. Zyda, "An extended Kalman filter for quaternion-based orientation estimation using MARG sensors," in *Intelligent Robots and Systems, 2001. Proceedings. 2001 IEEE/RSJ International Conference on*, 2001, pp. 2003-2011 vol.4.

[134] A. Gallagher, Y. Matsuoka, and A. Wei-Tech, "An efficient real-time human posture tracking algorithm using low-cost inertial and magnetic sensors," in *Intelligent Robots and Systems, 2004. (IROS 2004). Proceedings. 2004 IEEE/RSJ International Conference on*, 2004, pp. 2967-2972 vol.3.

[135] E. Foxlin, "Pedestrian tracking with shoe-mounted inertial sensors," *Computer Graphics and Applications, IEEE,* vol. 25, pp. 38-46, 2005.

[136] X. Yun, E. R. Bachmann, H. Moore, and J. Calusdian, "Self-contained Position Tracking of Human Movement Using Small Inertial/Magnetic Sensor Modules," in *Robotics and Automation, 2007 IEEE International Conference on*, 2007, pp. 2526-2533.

[137] S. K. Au, P. Bonato, and H. Herr, "An EMG-position controlled system for an active ankle-foot prosthesis: an initial experimental study," in *Rehabilitation Robotics, 2005. ICORR 2005. 9th International Conference on*, 2005, pp. 375-379.

[138] L. Liu, P. Liu, E. A. Clancy, E. Scheme, and K. B. Englehart, "Whitening of the electromyogram for improved classification accuracy in prosthesis control," in *Engineering in Medicine and Biology Society (EMBC), 2012 Annual International Conference of the IEEE*, 2012, pp. 2627-2630.

[139] D. P. Ferris, G. S. Sawicki, and A. R. Domingo, "Powered lower limb orthoses for gait rehabilitation," *Topics in Spinal Cord Injury Rehabilitation,* vol. 11, pp. 34-49, 2005.

[140] B. R. Munson, Donald F. Young, and T. H. Okiishi, *Fundamentals of Fluid Mechanics*, 4th ed. vol. 1. New York: Wiley, 2002.

[141] R. Isman, V. Inman, and P. Poor, "Anthropometric studies of the human foot and ankle," *Bull Prosthet Res,* vol. 11, pp. 97-108, 1969.

[142] K. D. Huang and S.-C. Tzeng, "Development of a hybrid pneumatic-power vehicle," *Applied Energy,* vol. 80, pp. 47-59, 2005.

[143] K. D. Huang, S.-C. Tzeng, and W.-C. Chang, "Energy-saving hybrid vehicle using a pneumatic-power system," *Applied Energy,* vol. 81, pp. 1-18, 2005.

[144] K. David Huang, K. V. Quang, and K.-T. Tseng, "Study of recycling exhaust gas energy of hybrid pneumatic power system with CFD," *Energy Conversion and Management,* vol. 50, pp. 1271-1278, 2009.
[145] E.A.R.S. *The Compressed Air Revolution (H ed.)* [Cited 5/20/2013 http://www.ears-europe.eu/index%20engl.html].
[146] PET. *PET Blowmolding Air Recycling Systems* [Cited 5/20/2013 http://www.connell-ind.com/recycling.html].
[147] M. Cai, "Power assessment of flowing compressed air," *Journal of fluids engineering,* vol. 128, p. 402, 2006.
[148] M. Cai, T. Kagawa, and K. Kawashima, "Energy conversion mechanics and power evaluation of compressible fluid in pneumatic actuator systems," in *Energy Conversion Engineering Conference, 2002. IECEC '02. 2002 37th Intersociety*, 2002, pp. 438-443.
[149] J. Ke, J. Wang, N. Jia, L. Yang, and Q. H. Wu, "Energy efficiency analysis and optimal control of servo pneumatic cylinders," in *Control Applications, 2005. CCA 2005. Proceedings of 2005 IEEE Conference on*, 2005, pp. 541-546.
[150] A. Yang, J. Pu, C. B. Wong, and P. Moore, "By-pass valve control to improve energy efficiency of pneumatic drive system," *Control Engineering Practice,* vol. 17, pp. 623-628, 2009.
[151] B. Mi and P. W. Wypych, "Pressure drop prediction in low-velocity pneumatic conveying," *Powder Technology,* vol. 81, pp. 125-137, 1994.
[152] L. Sanchez, N. A. Vasquez, G. E. Klinzing, and S. Dhodapkar, "Evaluation of models and correlations for pressure drop estimation in dense phase pneumatic conveying and an experimental analysis," *Powder Technology,* vol. 153, pp. 142-147, 2005.
[153] K. Hettiaratchi, S. R. Woodhead, and A. R. Reed, "Comparison between pressure drop in horizontal and vertical pneumatic conveying pipelines," *Powder Technology,* vol. 95, pp. 67-73, 1998.
[154] S. Laouar and Y. Molodtsof, "Experimental characterization of the pressure drop in dense phase pneumatic transport at very low velocity," *Powder Technology,* vol. 95, pp. 165-173, 1998.
[155] A. Pedchenko and E. J. Barth, "Design and validation of a high energy density elastic accumulator using polyurethane," in *ASME/Bath Fluid Power Symposium: Pump Design, Analysis and Appliation*, 2009.
[156] K. A. Shorter, Y. Li, T. Bretl, and E. T. Hsiao-Wecksler, "Modeling, control, and analysis of a robotic assist device," *Mechatronics, IEEE/ASME Transactions on,* vol. 22, pp. 1067-1077, 2012.
[157] J. Donelan, Q. Li, V. Naing, J. Hoffer, D. Weber, and A. Kuo, "Biomechanical energy harvesting: generating electricity during walking with minimal user effort," *Science,* vol. 319, pp. 807-810, 2008.